ADDIS ABABA UNIVERSITY

SCHOOL OF GRADUATE STUDIES

ADDIS ABABA INSTITUTE OF TECHNOLOGY

ENERGY CENTRE

PREDICTION OF PERFORMANCE PARAMETERS AND DETERMINATION OF AERODYNAMIC CHARACTERISTICS OF WIND TURBINE AIRFOIL USING CFD MODELING:

A CASE STUDY OF ADAMA I WIND TURBINE BLADE AIRFOIL SECTION

BY

MILLION MERID

AUGUST 2014

ADDIS ABABA, ETHIOPIA

DECLARATION

I, the under signed, declare that this thesis is my original work and has not been presented for a degree in any other University, and that all sources of materials used for the thesis have been duly acknowledged.

Name **Million Merid**

Signature ___________

Date of submission ___________

Place **Addis Ababa**

This thesis has been submitted for Examination with my approval as university Advisor

Name **Dr.-Ing. Abebayehu Assefa**

Signature ___________

ADDIS ABABA UNIVERSITY
ADDIS ABABA INSTITUTE OF TECHNOLOGY

SCHOOL OF GRADUATE STUDIES
ENERGY CENTRE

Prediction of Performance Parameters and Determination of Aerodynamic Characteristics of Wind Turbine Airfoil Using CFD Modeling:

A Case Study of Adama I Wind Turbine Blade Airfoil Section

A Thesis Submitted to the Addis Ababa Institute of Technology, School of Graduate Studies, Addis Ababa University

In partial fulfillment of the Requirement for the Degree of Masters of Science in Energy Technology

By

Million Merid

Advisor: Dr. - Ing. Abebayehu Assefa

August, 2014

ADDIS ABABA UNIVERSITY

ADDIS ABABA INSTITUTE OF TECHNOLOGY

SCHOOL OF GRADUATE STUDIES

ENERGY CENTRE

Prediction of Performance Parameters and Determination of Aerodynamic Characteristics of Wind Turbine Airfoil Using CFD Modeling:

A Case Study of Adama I Wind Turbine Blade Airfoil Section

Million Merid

GSR/0570/04

Approval by Board of Examiners

Dr.-Ing. Abebayehu Assefa	____________
Chairman Department of Graduate Committee	**Signature**
Dr.-Ing. Abebayehu Assefa	____________
Advisor	**Signature**
Dr.-Ing. Demiss Alemu	____________
Internal Examiner	**Signature**
Dr.Tesfaye Dama	____________
External Examiner	**Signature**

Abstract

In the current situation of global energy crisis, generation of energy derived from renewable energy resource has grown a significant attention. Wind energy is a very interesting due to the fact that fuel is free of cost. The most important aspect of wind energy technology is the wind turbine and its aerodynamic characteristics of the airfoil forming the blade. Thus predicting the performance parameters and determining aerodynamic characteristics of airfoil section are important. However, this requires continued experimental wind tunnel test and validation tools such as computational fluid dynamics (CFD).

The primary objective of this study was learning the CFD software and its applications. Secondly, this study was focused on predicting aerodynamic characteristics of an airfoil for varying angles of attack (AOAs). Simulation was done to deduce aerodynamic parameters (lift, drag, lift to drag ratio, contour plot of velocity and pressure distribution over the airfoil section). This can reduce dependence on wind tunnel testing. The simulation was done on airflow over a two – dimensional NACA 63-415 airfoil using FLUENT (version 6.3.26) at various angles of attack varied from -5^0 *to* 20^0 *using two turbulence models (S-A and SST k- ω) with the aim of selecting the most suitable model. Domain discretization was carried out using structured quadrilateral grid generated with GAMBIT (version 2.3.16), the fluent pre-processing tool.*

Comparisons and validation were made with available experimental data for NACA 63-415 airfoil with numerical results. Accordingly, it was found that the two turbulence models achieved a reasonable and a good agreement in predicting the coefficients especially for angle of attacks prior to stall. Among the model, studied the most appropriate turbulence model for the simulations were the SST k- ω two equation models, which had good agreement with the experimental data than S-A one equation model. As a result, it was decided to use the SST k- ω turbulence model for the main analysis with acceptable deviations in results (9.028% for lift and 12.203 % for drag coefficients).

This study concluded that CFD simulation provides sufficiently accurate results for a majority of AOAs. The discrepancy in calculating the lift and drag values comes from limitations in the turbulence model behavior. However, the majority of the lift and drag curves match the experimental data. Finally, this study includes simulation results of Adama I wind turbine airfoil section and predicted results was complied.

Acknowledgments

My heartfelt thanks go to my thesis advisor **Dr. - Ing. Abebayehu Assefa** for all the guidance, advice and support that he has provided during this thesis undertaking. I am especially thankful for his valuable insights, and all his endurance in encouraging me throughout .The completion of thesis would never be possible but for his help.

Specially, I would like to thank Mr. Takele Merid for his valuable suggestions and providing me help whenever needed. I would also like to thank Mr. Daniel Tesfaye for his positive response in providing some important information regarding the turbine specification.

I extend my acknowledgment to AAiT, department of Mechanical Engineering staff members for their kindness in providing countless suggestions. Last but not least, I would like to thank my dearly beloved friends for their valued comments and support along the way.

Lastly, it is impossible to describe in words the love, encouragement and support that I received from my family.

Table of contents

List of Tables

List of Figures

Abbreviations

2ddp	Two –dimensional with double precision
2D	Two dimensional
3D	Three dimensional
AOA (α)	Angle of attack
CFD	Computational fluid dynamics
FDM	Finite difference methods
FEM	Finite element methods
FVM	Finite volume methods
GW	Giga Watts
GWEC	Global wind energy council
HAWT	Horizontal axis wind turbine
kW	Kilo watts
LE	Leading edge
MW	Mega Watts
NACA	National Advisory Committee for Aeronautics
NSE	Navier Stokes Equations
PBS	Pressure- based solver
RANS	Reynolds –Average Navier Stokes
SA	Spalart- Allmaras in turbulence model
SST k−ω	Shear-Stress-Transport k−ω in turbulence model
SPBS	Segregated pressure based- solver
TE	Trailing edge
WTG	Wind turbine generator
VAWT	Vertical axis wind turbine

Nomenclature

A	Axial force
C	Chord length
D	Drag force
Cl	Lift coefficients
Cd	Drag coefficient s
Cm	Moment coefficients
Cp	Pressure coefficient
Cl_{max}	Maximum lift coefficient
f_x, f_y	Model-dependent source terms i.e. Porous-media & user-defined sources
L	Lift force
M	Pitching moments
N	Normal force
Re	Reynolds number
U_{wind}	Incoming stream velocity
U	Velocity
P_∞	Free stream reference pressure
ρ_∞	Fluid density
q_∞	free stream dynamic pressure
μ_∞	Fluid viscosity at free steam condition
k	Turbulence kinetic energy in SST - $k-\omega$ turbulence model
ω	Specific dissipation rate in SST - $k-\omega$ turbulence model
$\tilde{\nu}$	Spalart-Allmaras variable
ε	Turbulence dissipation rate in $k - \varepsilon$ turbulence model

CHAPTER 1

INTRODUCTION

1.1 Background

Global demands for renewable energy resources have been exponentially increasing in the 21st century. This is due to continuous expansion of industrial development, depletion of fossil fuels and emerging environmental consciousness. Above all, this increasing in energy demand and growing recognition of global warming and environmental pollution, has become an integral and cross cutting issue for development of economies of many countries of the world. However, to respond to the energy demand and environmental problem, more and more countries have prioritized renewable energy sources such as wind, solar, hydropower, biomass, geothermal, etc., as the replacements for nonrenewable sources such as, fossil fuels **[1].**

As compared to other renewable energy sources, wind has long been glorified as the ultimate solution to the world's energy and environmental problems. Wind energy provides virtually cheap, clean, inexhaustible, and above all environmentally friendly energy source. In addition to the above, application of wind energy improves air quality, reduces greenhouse gases and diversifies the global electricity supply **[1].** However, even if renewable energy's overall fortunes declined, development of one particular renewable energy technology, the wind turbines, continued to make important progress with continuous improvements in reliability, efficiency and reductions in capital cost**.** Thus, as the most promising renewable energy source, wind energy is believed to play a critical role in global power supply in the 21st century **[1].** As a result, wind energy prices in the 21st century have become roughly comparable in many cases against conventional forms of electricity generation **[2].**

According a report received from Global Wind Energy Council (GWEC) shows that the total amount of wind energy installed capacity has reached **282.5 (GW)** by the end of 2012 around the world. Moreover, its fast growth ensures that the wind power will be an important part of electricity generation in the close future according to the latest annual market report of Global Wind Energy Council (GWEC) Report, 2012 **[3].** According to the report installed capacity of wind power shows a cumulative increase of almost 19 % as compared to 2011. Likewise, new global installations of wind power reached **44.8 GW** in 2012, which indicate 10 % increase from the new installations recorded in 2011, GWEC Report, 2012 **[3]**.

Moreover, record installations in the United States (US) were noted by the wind association, with the western country once again regaining the number one spot for global markets. This is the first time the US has managed to do that since released the spot to China in 2009. China remained strong in 2012, with over 75 GW of installed capacity. The country intends to have around 18 GW of new installations in 2014 **[3] [4].** Likewise, Asian countries such as India, Asia, Pakistan, Mongolia, the Philippines and Thailand are expected to see significant installations and market growth in 2013. In Latin America, Brazil continues to lead the pack and may surpass the goal of 2 GW of annual installations in 2013 **[3]**.

Africa's wind resource is best around the coasts and in the eastern highlands, but it is in North Africa that wind power has been developed at scale. This is where current national policies are set to grow the sector further. At the end of 2011, over 98% of the continent's total wind installations of just over 993 (MW) were to be found across four countries - Egypt (550 MW), Morocco (291 MW), Tunisia (114 MW) and Cape Verde (24 MW) **[5].**

In South Africa, the World Wind Energy Conference held in November 2003 in Cape Town emphasized the imperative role of wind energy for future power generation especially in Africa. For example, the west coast of South Africa has been identified as a viable location for wind farms. In the meantime, South Africa is also experiencing in solar power projects already under construction **[3].**

Furthermore, recent wind power developments in east Africa with a total of **171 MW** (Adama I **51 MW** and Ashegoda **120 MW)** projects completed and **153 MW** Adama II wind project under development in Ethiopia and a **300 MW** project under development in Kenya are to be mentioned. Hopefully, these early projects will make a substantial contribution to the total generating capacity in each of these countries. If successful, they will herald a much broader uptake of wind on the continent in the coming few years [**5].**

According to statistics estimates, the installed capacity of large wind park in Ethiopia is about **2005MW** with wind speed of more than 8.8 m/s at the height of 50m. The country is rich in wind resource and development of wind power generation is considered as one of the important measures for solving the energy crisis in Ethiopia. The Ethiopian Electric Power Corporation (EEPCo) has planned to build **200 MW** of wind park projects in the country by the end of 2012/2013 **[6].**

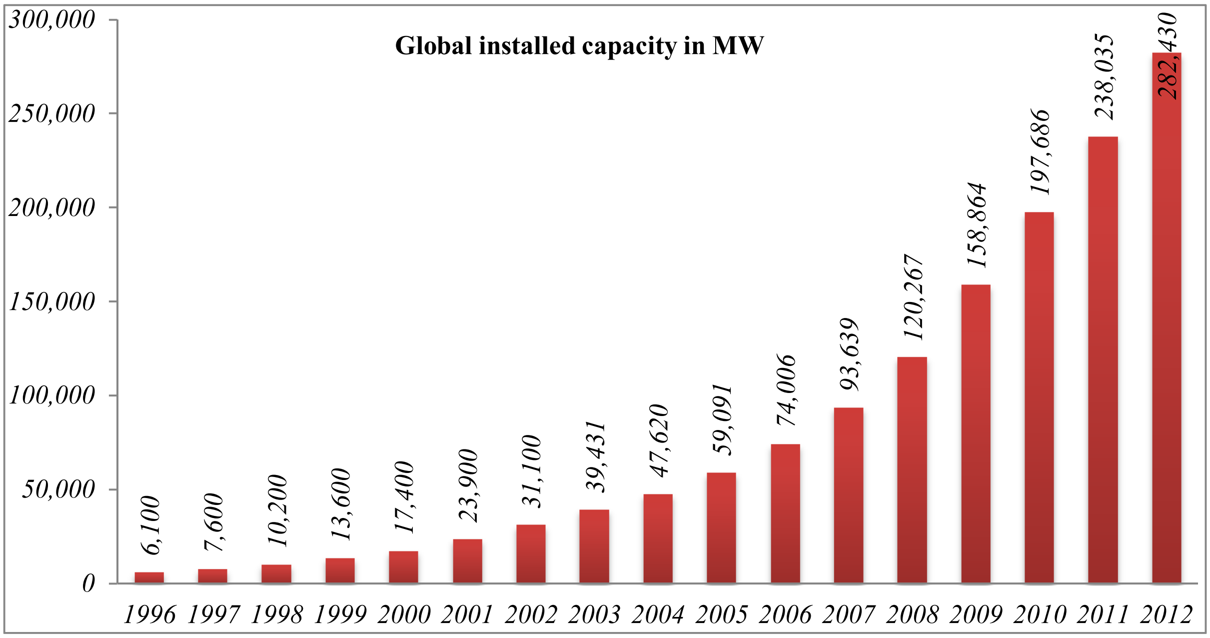

Figure 1-1: Global cumulative installed wind capacity 1996-2012 [Source: GWEC]

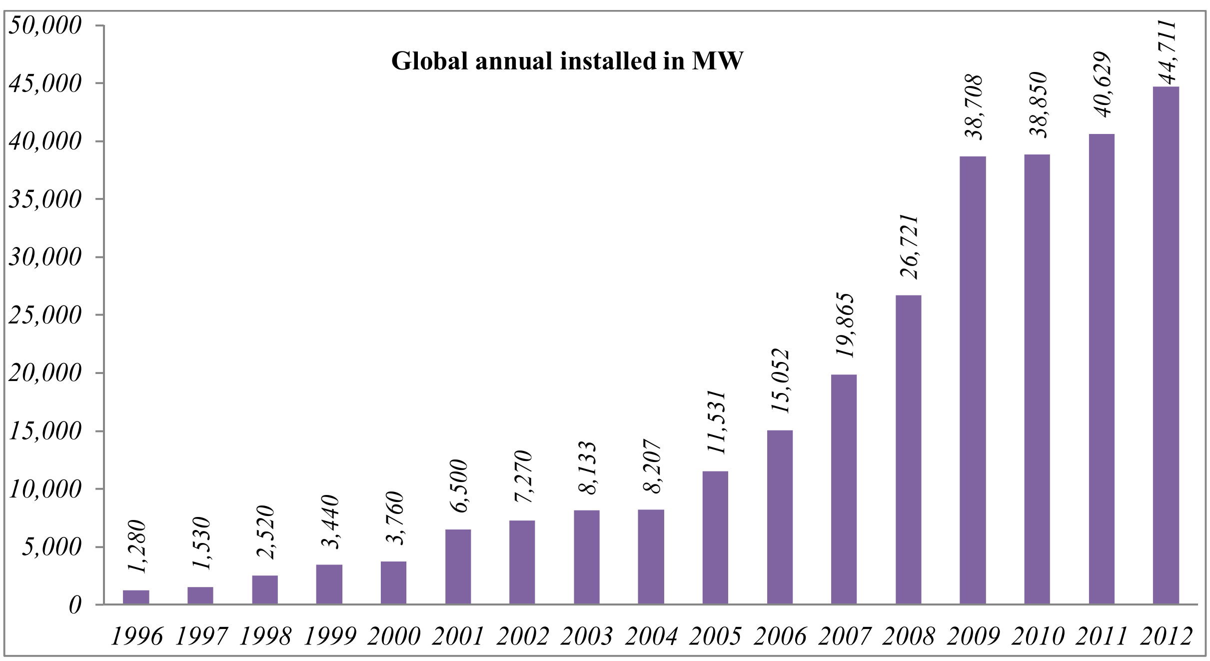

Figure 1-2: Global annual installed wind capacity 1996-2012 [Source: GWEC]

Generally, wind energy could meet global demand yet only provides small fraction of power consumption **[7].** The wind turbine developed to capture wind power and use it for generating electricity is the technology behind and one of the fastest growing industries within the rural and urban areas of countries all around the world **[7].** Accordingly, the sector started slowly and it is now one of the most advanced renewable energy technology. Therefore, wind energy production with its relatively safer and positive environmental characteristics has developed in the past few decades from a marginal activity into a multi-billion dollar industry.

Horizontal axis wind turbine (HAWT) is the least expensive and clean way to harness this important energy source [**8**]. However, for the design and implementation of more efficient and reliable wind turbine, accurate prediction of aerodynamic behaviour is very crucial, since the interaction of the wind with the blades influences the performance. In the meantime, it affects the lifetime and reliability of the blades as well. Thus, it is important to note that prediction of performance parameters and determination of aerodynamic force coefficients such as lift and drag on a HAWT blade airfoil is an indispensable, but a complex process **[8].**

Accordingly, aerodynamic performance parameters of wind turbine blade airfoils can be determine using computational fluid dynamics (CFD), which is one of the branches of fluid mechanics that uses numerical methods and algorithms to solve and analyze problems of fluid flows [**9] [10].** Prediction of performance parameters in the determination of the aerodynamic force coefficients and the effects of various turbulence models in the determination of these parameters (lift and drag) is crucial. At present; CFD method is almost entirely used as a rationale tool to predict the aerodynamic performance parameters of airfoil and give a massive understanding of the flow physics **[10].** However, CFD method is an attractive solution for performance prediction and determination of aerodynamic characteristics; reliability and accuracy of CFD have become the key factors.

This study addresses issues that are related to prediction of performance parameters and determination of aerodynamic properties; 2D CFD simulations of HAWT airfoil are conducted to give a better understanding of flow physics. In addition, comparison analyses have been done to validate results with experimental data from literature **[36]** and simulation are done to verify the reliability and accuracy of CFD model.

1.2 Problem Description

Despite the plentiful of wind resources, Ethiopia is gifted with the amount utilized to date for power generation is very small and insignificant. It is a well-known fact that growing economy of the country demands sufficient and reliable supply of electric energy and this demand could be fulfilled by increasing the power generation and broadening its capacity. Accordingly, design and development of more efficient and reliable wind turbine is critically significant.

In the design and development of a commercially viable wind turbine, it is very important that an accurate assessment is made on the aerodynamic characteristics of the airfoils employed on the blades and performance prediction of the airfoils. Any miscalculations of these characteristics may result in wrong estimates of the turbine's performance as well as economic projections.

In the past, performance of wind turbine was determined using prototypes and testing their performance in wind tunnel or test labs. This required high capital and running cost of labs, skill required in manufacturing prototypes accurately and in realization of data, interpretation of result etc.

However, modern wind turbine airfoil design process is improved with the implementation of computational fluid dynamics (CFD) software's. CFD enables the analysis of fluid flow through very complex geometry and boundary conditions such as flow over an airfoil. Therefore, if airfoil characteristics cannot be determined by experimental tests, one will rely on computational fluid dynamics (CFD) methods to minimize the problem related with manufacture of prototypes and time spent in wind tunnel or test labs.

1.3 Aims and Objectives of the Study

1.3.1 Aims

The aim of this thesis is to simulate fluid flow over wind turbine airfoils in order to predict the performance parameters and determine aerodynamic characteristics, while ensuring good agreement result with available experimental wind tunnel data. By using the CFD–software, thorough two – dimensional (2D) modeling of the airfoil, prediction of performance parameters were made. Out of the different turbulence models available in the solver two of the models will also be applied to find the most suitable one for the main analysis of this study. FLUENT with CFD package has been employed together with its pre-processor GAMBIT, used for mesh generation and to obtain reliable, at the same time inexpensive simulations. This can be effectively employed as flow analysis tools in the framework of performance prediction and determination of aerodynamic characteristic of the airfoils. Starting from mesh generation, time required to extract aerodynamic parameters of the airfoil behaviour has been shortened by means of some simplification, i.e. structured mesh, reduced grid size, incompressible flow assumption, etc. The whole CFD process (pre–processing, processing, and post-processing) has been used for the analyses and the chosen final settings are the results between numerical accuracy and required solution.

1.3.2 Objectives of the Study

1.3.2.1 General Objective

The general objective of this study is to predict the performance parameters and determine the aerodynamic characteristic of an airfoil through two- dimensional computational fluid dynamics (CFD) modeling.

1.3.2.2 Specific Objectives

The specific objectives include:

- Generation of numerical mesh around two–dimensional (2D) airfoil model using GAMBIT;
- Analyses of the aerodynamic performance parameters of wind turbine blade airfoil and compare with available experimental data;
- Analyses of the lift, drag , moment and lift to drag coefficients employed on the wind turbine blade airfoil;
- Determination of pressure contours, velocity contours and pressure coefficient at various angle of attacks; and
- Analyses of the fluid flow field around the model which are all solved using turbulence model of FLUENT;

1.4 Significance of the Study

Wind turbine blade airfoils need performance test using expensive wind tunnel before installation on the actual size. However, every aerodynamic surface must be tested under an expensive process of testing of its performance in a wind tunnel. This thesis minimizes the need of undertaking costly experiment by introducing numerical simulation modeling, using commercially available software computational fluid dynamics (CFD) solver such as FLUENT. FLUENT is software which is applied for the performance test of several existing airfoils and which is frequently used in many wind turbines industries. In addition to, the determination of the aerodynamic characteristic of the airfoil, the simulation modeling implemented in this study reduces the cost of production of prototypes.

1.5 Scope of the Study

A number of researchers worldwide have been investigating the performance parameters and aerodynamic characteristics of HAWT blade and tried to identify the optimum design which gives better performance compared to VAWTs.

Previously, two - dimensional (2D) airfoil data were determined from test carried out in wind tunnels; even though wind tunnel tests and the airfoil prototypes are expensive. It is not economical to manufacture prototypes from each design and analyze it in wind tunnel; different computational options are available like CFD, even though time consuming. It is the scope of this study to consider the CFD for the simulation and validate the CFD results as well as to show the level of agreement between that of simulation result with experimental data available **[36].**

The other scope of this study is to predict the aerodynamic characteristics of blade airfoil as air flows over the surface of the airfoil. In this case, a horizontal axis wind turbine blade GW77/1500, which is the same as LM 37.3P2 blade type **[6],** the aerodynamic profile of which is the same as the oldest five (5) digit series of NACA 63-4xx airfoil is considered to predict the performance parameters and determine aerodynamic characteristics using two - dimensional (2D) simulation. Because of limited resources available, this study is limited to two CFD code (GAMBIT +FLUENT) and one airfoil section (NACA63-415).

1.6 Organization of the Report

In this thesis some issues related with modeling the aerodynamics of HAWT airfoils are discussed. The main body of the report study deals with determination of performance parameters of an airfoil using computational tools (GAMBIT and FLUENT) which are used for reproducing the aerodynamic characteristics of the airfoil and to compare with experiment in order to validate and verify results which are previously determined by experiment. This section also presents the basic outline of the thesis and offers some description about each chapter.

Chapter 1 is concerned with a brief introduction to the field of renewable energy, global wind energy installation and energy generation, specifically from HAWT. The research problem, aims and objectives, significance of the study as well as the scope of the study are outlined in this chapter. In **Chapter 2** literature review, which includes both theoretical frameworks as well as previous numerical studies by different scholars across time, are described. **Chapter 3** is concerned with discussion of fundamental principles of HAWT aerodynamics including the different types of aerodynamic flows and how to solve an aerodynamics problem. This is followed by a description of airfoils, their aerodynamic properties and the various types of flow phenomena associated with them and some of important performance parameters. This chapter also describes the basics of computational fluid dynamics (CFD) and criteria for CFD selection are discussed besides the structure of a CFD code. The methodologies for CFD analysis of typical HAWT blade airfoil are included. In this chapter mathematical formulation and turbulence modeling is also discussed. In **Chapter 4** the full two - dimensional (2D) airfoil modeling is presented. The next chapter, **Chapter 5** deals with experimental comparison and validation of the 2-D airfoil simulation results. This chapter also provides the results and discussion of the simulation results of the case study. The final chapter of this study is **Chapter 6** which outlines the conclusion drawn from the experiences gained over the course of this study.

CHAPTER 2

LITERATURE REVIEW

2.1 Historical Development of Wind Turbines

The utilization of wind energy is not a new technology; it is the reemerge of a long tradition of wind power. Since long time, people have used the energy of the wind and conversion of wind energy into useful form which has laid the foundations for one of the most significant technological developments of the 21th century **[8].** Wind turbines developed to harness wind power and use it for generating electricity are the technology behind and one of the fastest growing industries for power generation, and are now a common sight within the rural and urban areas of countries all over the world **[7].** Wind energy is a continually growing source of alternative power generation in many countries around the world. It is a clean, renewable energy source that has many inherent advantages when compared with other alternative and even some conventional power generation methods.

The first reliable information about the existence of wind turbine as windmills on record was built by the Persians, present day Iran. Persians used windmills to grind grain into flour approximately in 644 A.D. It is noted that these had vertical axes and were drag type devices. They were characteristically inefficient and particularly susceptible to damage in high winds **[11] [12].** A later description, including a sketch, dates back to the year 945 and depicts a windmill with a vertical axis of rotation. It was obviously used for milling grain. Similar, extremely primitive windmills have survived in Afghanistan up to the present time **[12].** Some centuries later, the first news arrived in Europe that the Chinese were also using wind wheels for draining rice fields. Whether the Chinese knew windmills even before the Persians and whether the European mills might have been only an offshoot of the Chinese invention, can no longer be determined with certainty today. It is remarkable, however, that the Chinese wind wheels were simple structures made of bamboo sticks and fabric sails and that they had a vertical axis of rotation **[12].**

In 11th century, windmills have begun to be used in Europe to grind grain. All windmills had horizontal axes. They were used for mechanical tasks, including water pumping, grinding grain, sawing wood, and powering tools. Although there is no reliable information as to whether the first post and tower windmills could already be yawed into the wind, yawing became a commonly found property of post windmills. The post windmill in its simple and serviceable form remained not in existence right into the 20th century **[12].** These mills normally had four blades **[11].**

In 14th century improvements were slowly made to European windmills to increase the aerodynamic lift of the blades and raise rotor speeds, allowing for superior grinding and pumping. By late 1700s, windmills had become the "electrical motor" of pre-industrial Europe, supplying an estimated 1500 MW of power in Europe, a level not reached again until the late 1980s. This wind power was used for draining lands, grinding grain, milling timber and processing commodities such as spices and tobacco. One of the major players in advancing windmills to create wind turbines was the Danish scientist Poul La Cour, in the year 1891 **[13].** La Cour was one of the first to use wind tunnels to establish guidelines for optimum rotor performance **[13].**

At the end of the 19th century, interest increased in using wind power for electrical generation. At that time, it had to be direct-current (DC) power if only because of the varying speed on the windmill. For example, in 1888 a US scientist and businessman Charles Brush built the first wind turbine to generate electricity in Cleveland, Ohio; it had a capacity of 12 kW of DC power for charging storage batteries. The upwind rotor was a solid wheel type, with its 17 m rotor diameter and 144 blades on a tower of 18 m high. The whole system was operated automatically. It had been operated for 20 years until the rotor was removed in 1908. The Brush wind turbine was a milestone, because it was the first attempt to combine the best developed structural and aerodynamic windmill technology with newly developing electrical technology **[13].**

However, for much of the 20th century there was little interest in using wind energy other than for battery charging for remote dwellings. This is because, wind energy is considered as low-power system which was quickly replaced by electricity grid. This does not mean that all wind energy system had vanished; there were some. For example, one notable exception was the 1250 kW Smith–Putnam wind turbine constructed in the US in 1941. This remarkable machine had a steel rotor 53 m in diameter, full-span pitch control and flapping blades to reduce loads. Although a blade spar failed catastrophically in 1945, it remained the largest wind turbine operated for some 40 years **[13].**

In early 1930's thousands of small wind turbines were built in rural areas across the US with 1 to 3kW in capacity. The turbines were at first installed to provide lighting for farms and to charge batteries for crystal radio sets. Later, their use was extended to power appliances and farm machinery. In late 1970s the interest in wind power generation returned as response to the oil crises in 1973 and 1979 **[3].** The oil crisis of 1973 caused interest in large wind turbines and encouraged government-sponsored renewable energy research programs in Germany, Sweden, Canada, Great Britain and the United States. These programs caused the development and use of new wind turbine designs, helping to cut the cost of wind power significantly over the next two decades. Countries like Germany, US and Sweden developed large-scale wind turbine prototypes in the MW range, others concentrated on creating the right market conditions for deployment of the technology **[13].**

Further advancements in wind power were virtually changed during World War II and would not see change until the fuel crisis of the 1970s **[12].** This renewed interest in wind energy generated new innovative turbine designs, including many variations of the Vertical Axis Wind Turbine (VAWT). More recently, governments all over the world have begun offering incentives to build and operate renewable energy power production facilities, and with the oil crisis as a catalyst, wind turbines once again moved to the forefront of alternative energy production. Advancements made in wind turbine technology through the latter part of the 20^{th} century culminated in the common configuration of wind turbines seen today, known as Horizontal Axis Wind Turbines (HAWTs) **[14].** While the VAWTs designed in the latter part of the 20^{th} century were innovative and provided certain advantages over HAWTs; eventually, they were ignored to be operated in large scale utilities due to their destructive tendencies at high wind speeds and reduced efficiency at low speeds **[14].** It is estimated that by 2008 the U.S had 25,000 MW of wind energy based power generation capability. By 2030, the U.S. hopes to use wind power for 20% of its electrical generation requirements **[14] [15**].

While it is noted that concerns exist regarding the impact of wind turbines on the environment, further research is needed to accurately determine causes and possible solutions for any adverse impacts discovered on local and/or migratory bat and bird species **[15].** The other major concern with wind turbines is the noise. This concern can also be improved by further research into blade design and wind turbine siting, in order to decrease the overall acoustic effects of wind turbines and to keep turbine far enough away from homes remove unnecessary noise **[14][15].**

The wind turbines commonly used for large-scale power generating applications today are typically referred to as utility-scale turbines. The typical size of a utility scale turbine can range from 1 to 6 MW depending on the available wind energy at the location at which the turbine will be installed.

2.2 Previous Numerical Studies

With intensive progress of computer technology in recent time, computational fluid dynamics in the form of steady RANS has made significant improvements in the prediction of airfoil performance. Some of the two-dimensional (2-D) airfoil studies are discussed below.

Eleni et al., (2012) performed the analysis of a two dimensional subsonic flow over a NACA 0012 airfoil at various angles of attack and operating at a Reynolds number of 3×10^6. The flow was obtained by solving the steady-state governing equations of continuity and momentum conservation combined with one of the three turbulence models [Spalart-Allmaras, Realizable and shear stress transport (SST)]. The aim of the work was to validate the models through the comparison of the predictions and the free field experimental measurements for the selected airfoil and to show the behavior of the airfoil and to establish a verified solution method, at the same time. Their work highlighted two areas in computational fluid dynamics (CFD) that require further investigation: transition point prediction and turbulence modeling. The laminar to turbulent transition point was modeled in order to get accurate results for the drag coefficient at various Reynolds numbers **[16].**

Saraf et al., (2011) developed a procedure to numerically model airflow over airfoils using GAMBIT and FLUENT. This model presented the analysis of two - dimensional subsonic flow over NACA 4412 airfoil at various angles of attack and operating at a velocity of 50 m/s. The flow was obtained by solving the steady-state governing equations of continuity and momentum conservation combined with one of the two turbulence models: Spalart Allmaras and k-ω standard. The main attention was to validate those models through the comparison of the predicted results and the free field experimental measurements for the selected airfoil. At the same time the work was to show the behavior of the airfoil and to establish a verified solution method. Calculations were done for constant air velocity altering only the angle of attack for every turbulence model tested. The study highlighted two areas in computational fluid dynamics (CFD) that require further investigation: transition point prediction and turbulence model. The calculations show that the turbulence models used in commercial CFD codes do not give accurate results at high angles of attack **[17].**

Wolfe (1997) is the other researcher who worked on the capabilities and accuracy of a representative CFD code to predict the flow field and aerodynamic characteristics of typical HAWT airfoils. He made comparisons of the computed pressure and aerodynamic coefficients with wind tunnel data. Like other **[16] [17]** , the work indicated two areas in CFD that require further investigation and improvement in order to facilitate accurate numerical simulations of flow about wind-turbine airfoils: transition prediction and turbulence modeling. The result of the studies shows that the laminar-to-turbulent transition point must be modeled correctly to get accurate simulations for attached flow. Calculations also show that the standard turbulence model used in most commercial CFD codes, the k-ε model, is not appropriate at angles of attack with flow separation **[18].**

Rajendran (2011) focused on the potential of an incompressible Navier–Stokes CFD method for aerodynamic performance analysis of horizontal axis wind turbines. The main objective of the analysis was to put side by side the CFD results obtained from the simulation and validated against experimental data of the NREL power performance testing activities. Comparisons were shown for the surface pressure distributions at several stations along the blades as well as for the field domain. The selected case corresponded to 12.5 m/s up-wind wind turbine at zero degree of yaw angle and a rotational speed of 25 rpm. The simulation result obtained suggest that the method can cope well with flows encountered around horizontal axis wind turbines providing useful results for their aerodynamic performance in the meantime revealing flow details near and off the blades **[19].**

Kays (2010) evaluated the performance of three commercially available computational codes to determine the aerodynamic coefficients of airfoils. The methodology followed in the analysis was to select two airfoil models, design codes and apply CFD that solves and evaluates their accuracy and eases reproducing the coefficients of the two wind turbine airfoils, previously determined by wind tunnel experiment. The major conclusion of the work, using CFD was found to be more labour intensive in both the airfoil analysis and design codes. However, it was shown to be more accurate and flexible for determining the behaviour of complex turbulent flows. At the same time three turbulence models were used in the CFD solver to analyse their accuracy for modeling the flow over airfoils. Also it was shown that a turbulence model must be equipped to model the behaviour of adverse pressure gradient flows in order to accurately model the forces experienced by a wind turbine airfoil. The SST k-ω and Spalart-Allmaras models proved to satisfy criterion which makes it the best out of three analysed models. The accuracy of CFD was also shown to be largely dependent on the standard of the mesh used **[7].**

According to the investigation done by **L. X. Zhang et al., (2013**) numerical simulation had become an attractive method to carry out researches on structure design and aerodynamic performance prediction of wind turbines, while the prediction accuracy was the major concern of CFD. The main objectives of the simulation was to develop a two - dimensional CFD model, at the same time a series of systematic investigations were conducted to analyze the effects of computational domain, grid number, near-wall grid and time step on prediction accuracy. Then efforts were devoted into prediction and analysis of the overall flow field, dynamic performance of blades and its aerodynamic forces. The final out came of the results well agrees with experimental data. It demonstrates that RNG k-ε turbulent model is great to predict the tendency of aerodynamic forces, but with a high estimate value of turbulence viscosity coefficients **[20].**

Kandwal et al., (2012) investigated an inviscid flow over an airfoil surface using CFD. The major objective was to deduce the lift and drag properties using computational methods, aimed to reduce the dependency on wind tunnel testing. The study is done on air flow over a two-dimensional NACA 4412 airfoil using ANSYS FLUENT (version 12.0.16), to obtain the surface pressure distribution, from which drag and lift were calculated using integral equations of pressure over finite surface areas. The drag and lift forces can be determined through experiments using wind tunnel testing; the experimental data was taken from Theory of Wing Sections by Abbott et al., for comparison. The CFD simulation results show close agreement with those of the experiments, thus suggesting CFD is a reliable alternative to experimental method in determining drag and lift coefficients **[41].**

CHAPTER 3

MODERN WIND TURBINES AND AERODYNAMICS OF HAWT

3.1 Modern Wind Turbine

From the past, power generated from nonrenewable sources like coal, natural gas, nuclear and fuel was considerably economical than wind power. However, with increased fossil fuel price and improvements in wind turbine technology and environmental problems, the field is starting to increase interest to many countries of the world. As a result of the increased interest for wind turbine technology, modern wind turbines have increased in size and capacity considerably in the last several years. Their power generating capability also varied greatly with some turbines producing just a few kilowatts and others producing a few megawatts **[21].** The size of commercial wind turbines has increased dramatically, from approximately a rated power of 50 kW and a rotor diameter of 10-15 m up to today's commercially available 5-7 MW turbines with a rotor diameter of more than 120 m **[21].**

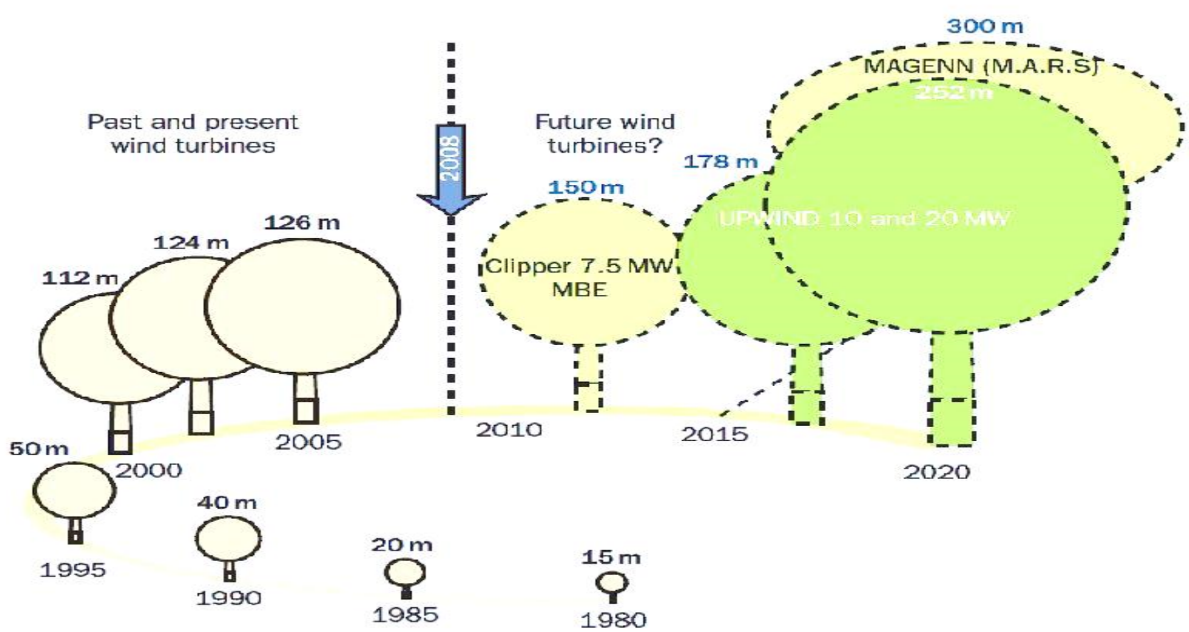

Figure 3-1: Growths in size of commercial wind turbine designs.

[Source: www.intechopen.com]

3.2 Orientation

Modern wind turbines can be classified according to their aerodynamic functions or conceptual design. Whether wind energy converter captures its power exclusively from aerodynamic drag of airstream acting on rotor surfaces, or whether it is able to utilize the aerodynamic lift created by the flow against surfaces characterizes the rotor's aerodynamic function. Accordingly, they are named as drag rotors and rotors which use the aerodynamic lift. Classification according to design aspects is more practicable and common. There are different designs of wind turbines to accommodate different needs. The most common design types are the horizontal-axis design, with the axis of the blades horizontal to the ground and the less common are the vertical-axis turbines: the Savonius and the Darrieus.

3.2.1 Horizontal Axis wind Turbines (HAWTs)

Horizontal axis wind turbines designs are the most common turbine configuration used today. They consist of a tall tower, atop which sits a fan-like rotor that faces into or away from the wind, a generator, a controller, and other components. Most horizontal axis wind turbines built today are two- or three-blades spin upwind of the tower. They sit high atop towers to take advantage of the stronger and less turbulent wind or more aboveground **[22].** Each blade acts like an airplane wing, so when wind blows, a pocket of low-pressure air forms on the downwind side of the blade. The low-pressure air pocket then pulls the blade toward it, which causes the rotor to turn**.** The force of the lift is actually much stronger than the wind's force against the front side of the blade, which is called drag **[22].** The combination of lift and drag causes the rotor to spin like a propeller, and the turning shaft spins a generator to make electricity.

3.2.2 Vertical Axis wind Turbines (VAWTs)

Vertical axis turbines are of two types: Savonius and Darrieus. Neither type is in wide use. The Darrieus turbine was invented in France in the 1920s **[22].** Often described as looking like an eggbeater, it has vertical blades that rotate into and out of the wind. The Giromill and cyclo-turbine are variants on the Darrieus turbine. The Savonius turbine is S-shaped if viewed from above. This drag-type turbine turns relatively slowly but yields a high torque. It is useful for grinding grain, pumping water, and many other tasks, but due to its lower rotational speeds, is not suitable for generating electricity [**22**].

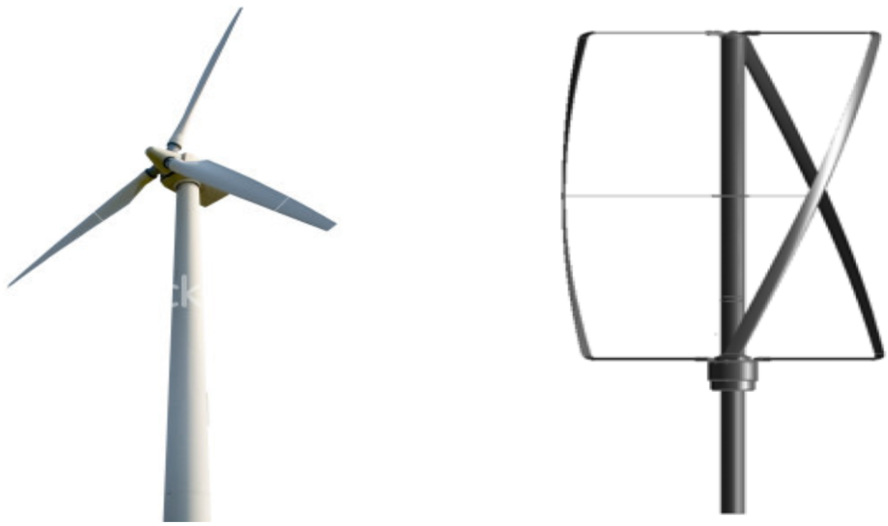

(a) HAWT **(b)** VAWT

Figure 3-2: Horizontal (a) and vertical (b) axis design wind turbines

3.3 HAWT Aerodynamics

Before discussing some of the issues related with modeling HAWT airfoil, it is indispensable to have some thoughts behind the aerodynamics characteristics associated with horizontal axis wind turbine airfoils. Wind turbine power production depends on the interaction between the rotor and the wind. The wind is considered to be a combination of the mean wind speed and turbulent fluctuations about that mean flow. Experience has shown that the major aspects of wind turbine performance are determined by the aerodynamic forces generated by the mean wind speed **[11].** Aerodynamics is a very important aspect of wind turbines and aerodynamics of one wind turbine to the other can be very different. An aerodynamic force generated by the mean wind speed is fundamentally important. The following section will first introduce fundamental concepts behind aerodynamic flows and the mathematical equations used to describe them. It will then provide some insight into airfoils and their applications to wind turbines.

3.3.1 Fundamental Concepts of Aerodynamics

Designing wind turbines starts with basic concepts of the aerodynamic forces acting on the wind turbines. The subject 'Aerodynamics' relates to the study of relative flow of air past an airfoil or any other object of interest **[23].** The term 'air' is used in a common sense. It basically means the flowing fluid medium which could be air, or any other for that fluid matter depending on situation **[24].** An airfoil is a body which is able to rotate because of aerodynamic forces and moments generated by the action of air flowing past it. This flow of air could be due to the motion of an airfoil through air during operation or due to the motion of flowing air past an airfoil model fixed in the test section of a wind tunnel. Aerodynamics is an important branch of fluid dynamics and Aerospace Engineering **[24].**

3.3.2 Components of Modern Aerodynamics

Generally, there are three components in modern aerodynamic studies which include the experimental, theoretical (analytical) and computational fluid dynamics (CFD) approaches respectively. Each approach has its own advantages and disadvantages too. Usually the most effective approach is to combine both experimental and theoretical/ CFD investigation in a most rational manner to solve particular flow problems **[24].**

Experimental studies are conducted in wind tunnels. Wind tunnels are used to conduct aerodynamic measurements on an airfoil surface in scaled down models of prototypes. Usually measurement of pressure on model surface, forces and moments acting on the model, wake survey, flow visualization, etc., are performed to obtain valuable understanding of the flow physics. However, the high capital and running cost of wind tunnels, skill required in manufacturing prototypes accurately and in realization of data, interpretation of results, etc. are the major limitation of this approach. Above all, maintaining simultaneously the Mach number and Reynolds number experienced airfoils under operation is the other problem **[24]**. Mach number is the ratio of relative air velocity and speed of sound through air. Reynolds number is the ratio of inertia force and viscous force which will be discussed in detail later**.** It is a well-known fact that in order to maintain dynamic similarity between the flow past a scaled down model in a wind tunnel and that around an actual prototype under operation needs to maintain equality of the above non dimensional numbers **[24].** If they are not simultaneously satisfied, there would be some differences in the flow character between the two situations and therefore corrections would have to be made in the wind tunnel data before they could be used.

In addition, the theoretical and CFD studies have led to valuable understanding of wide range of flow problems. In opposition, these approaches suffer some limitations too. The basic limitation is in solving governing equation of real viscous compressible or incompressible flow around a body, the Navier-Stokes equations cannot in general be solved theoretically. Navier-Stokes equations, in principle, are capable of giving a totally adequate description of all flow regimes of interest to the aerodynamicist **[24].** However, that needs highly accurate numerical solution of governing equations subject to initial and suitable boundary conditions. Levels of accuracy required make the numerical simulations extremely expensive and therefore unreasonable to practice on a routine basis.

Therefore, very often, instead of solving the full Navier Stokes equations its simplified forms are used. Following this approach, significantly easier to solve numerically as compared to Navier Stokes equations exist that give valuable inputs about certain flow problems. A variety of correction schemes have also been developed to incorporate effects due to viscosity and compressibility in the solution. These 'correction schemes' have played an important role in providing alternative solutions to Navier-Stokes equation and other approaches **[24].**

3.3.3 Forces and Moments Acting on an Airfoil

Airfoils are structures with specific geometric shapes that are used to generate mechanical forces due to the relative motion of the airfoil and a surrounding fluid **[24].** Wind turbine blades use airfoils to develop mechanical power. The cross-sections of wind turbine blades have the shape of airfoils. The width and length of the blade are functions of the desired aerodynamic performance, the maximum desired rotor power and the assumed airfoil properties **[11].**

In general, there are two forces and one moment that act on an airfoil; these being lift, drag and pitching moment **[7].** In aerodynamic studies, the wind velocity is usually designated as free stream velocity which suggests that flow at infinite distance from the turbine blade airfoil is completely unaffected by the presence of the airfoil. As the flow approaches the airfoil, it gets disturbed and the local velocity on the surface of the airfoil is changed. At different points on the surface of the airfoil, different values of velocity will be observed which may be significantly different from the free stream velocity. Consequently the pressure distribution on the surface of the airfoil differs from the undisturbed pressure of the free stream at infinity **[24].**

The two main reasons which are responsible for a body to move through a fluid are pressure and shear stress distribution on its surface **[7] [24].** The main focus of aerodynamics is determination of this pressure and shear stress distribution on a surface and integrating their distribution to obtain the resultant force and moment acting on a surface. Pressure acts normal to the surface of the body while shear stress acts tangential to it. Pressure on the upper surface of the airfoil is usually lower and on the lower surface is higher. This difference in pressure between the upper and lower surfaces provides the necessary lift force which makes the airfoils rotate. Shear stress acts tangential to the body surface and it arises due to the viscous nature of the flow. It acts in the direction of the flow and has an effect on slowing down the relative flow between the body and the fluid **[24] [40].** Due to this stress the relative flow appears as a perfect halt at the body surface, which is comparatively lower than the free stream velocity. The effect of viscous stresses is felt within a small region called the boundary layer where the velocity changes rapidly from zero at the wall to free stream velocity some distance away from the wall in the surface normal direction. Viscous stresses are proportional to coefficient of viscosity and velocity gradients.

In general, the resultant force and moment acting on an airfoil in motion could be resolved into three components each. Resultant force could be resolved into lift, drag and thrust force and resultant moment could be resolved into pitching moment, rolling moment and yawing moment respectively **[24].** Lift force (L) acts upwards perpendicular to the direction of oncoming airflow or undisturbed stream. It is formed as a consequence of the unequal pressure on the upper and lower airfoil surfaces. Drag force (D) acts in parallel direction to oncoming airflow which is in the same direction as the motion of the undisturbed stream **[11].** The drag force is due both to viscous friction at the surface of the airfoil and unequal pressure on the airfoil surfaces facing toward and away from the oncoming flow. It is the force which resists the motion of the airfoil. Trust force acts in the span wise direction of the airfoil. Pitching moment (M) acts in the plane containing the lift and drag forces.

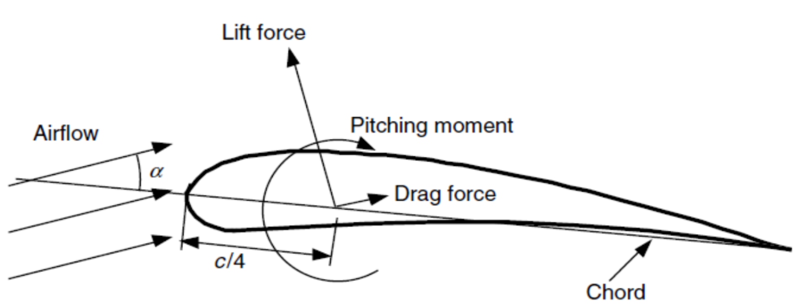

Figure 3-3: Forces and moments on an airfoil section **[13]**

In figure 3-3, α is the angle of attack and c the chord length of the airfoil. The directions of positive forces and moments are indicated by the direction of the arrows **[13].**

The aerodynamic characteristics of wind turbine airfoil strongly depend on its rotor blade. It is evident that certain thickness of the airfoil is disposed equally around the so called ‘mean camber line’ to produce the airfoil shape. The mean camber line is the locus of points halfway between the upper and lower surfaces of the airfoil **[11].** One can also realize that there is a particular location for maximum thickness and camber. When the mean camber line is coincident with the mean chord line a symmetric airfoil is obtained, otherwise called cambered airfoil. Actually the entire airfoil surface is enveloped by a distribution of pressure and shear stress. Note that the free stream is incident on the airfoil surface at an angle of attack **α**; also realize that the airfoil could be extruded along z direction to form an airfoil of finite span which is not shown in **Figure 3-3** above. Flow past an airfoil section is two dimensional (2D) whereas that around a finite airfoil is three dimensional (3D) **[11].** The integrated effect of pressure and shear stress distribution on the airfoil is the formation of a resultant force and a moment which is kwon as force system.

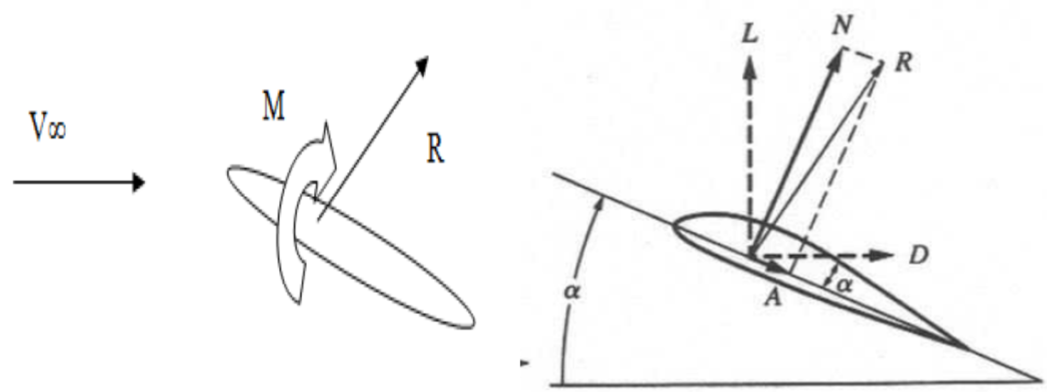

Figure 3-4: Resultant aerodynamic force, moment and force system on typical airfoil **[11]**

M is defined as the pitching moment which is taken about an axis perpendicular to the airfoil cross section **[7];** this is mostly placed at the quarter of chord length (0.25c). Where moments that tend to increase **α** (nose up) are positive, and moments that decrease **α** (nose down) are negative. The pitching moment can be calculated by integrating the net moments acting on the airfoil from the leading to the trailing edge, taking the 25% of chord (0.25c) as the reference axis **[11].**

An expression for M can therefore be determined from equation (3.1) **[7]:**

$$M = \int_{LE}^{TE} dM_{Upper} + \int_{LE}^{TE} dM_{lower} \quad \textbf{(3.1)}$$

Further, the resultant force 'R' could be resolved into a pair of components as shown in **Figure 3-4** above. One pair comprises of lift and drag force, the other pair comprises of normal force (N) and axial force (A).The geometrical relation between these two pair of force components is given by:

$$L = N\cos\alpha - A\sin\alpha \quad \textbf{(3.2)}$$

$$D = N\sin\alpha + A\cos\alpha \quad \textbf{(3.3)}$$

3.3.4 Airfoil Nomenclature

After a century of theoretical research on the subject of airfoil, the final word on the performance of an airfoil depends on wind tunnel testing. The reason for this state of affairs is that the flow field about an airfoil is extremely complicated. The simplifying assumptions that are frequently introduced in order to treat the problem theoretically are much too severe to fail and influence the final results. Many of these assumptions ignore the effects of viscosity, nonlinearities in the equations of motion, three-dimensional effects, non-steady flow, free stream turbulence and airfoil surface roughness. Airfoil geometry can be characterized by the coordinates of the upper and lower surface. It is often summarized by a few parameters such as: maximum thickness, maximum camber, position of max thickness, position of max camber and nose radius **[11].** One can generate a reasonable airfoil section by given these parameters.

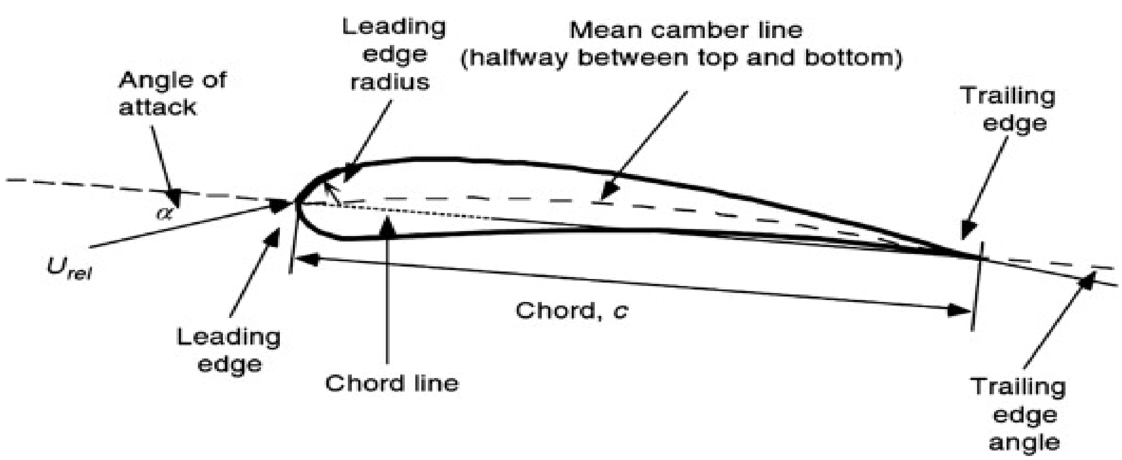

Figure 3-5: Geometric properties of airfoils **[11]**

3.3.5 Types of Flow and Properties of Fluids

Particle of fluid acting on a surface of an airfoil can be categorized as having four distinct variable properties: pressure, density, and temperature and flow velocity **[7].** These are properties of fluid flow over a surface which can vary greatly in the flow field. When solving an aerodynamic problem mathematically, these properties are usually expressed in terms of a three-dimensional coordinate system **[7].**The variation in and presence of these properties throughout a flow field gives rise to the following distinct types of flow, which are summarized in Table 3-1 below.

Table 3-1: Various flow types and a description of their characteristics

Types of Fluid Flow	**Characteristics**
Steady	The various flow parameters and fluid properties at any point do not change with time. Time is a criterion.
Un-steady	Unsteady flow is the type of flow in which the various flow parameters and fluid properties at any point change with time.
Laminar	Laminar flow is a type of flow in which the fluid particles move along well defined paths or stream-lines. The behavior of fluid particles in motion is a criterion.
Turbulent	Turbulent flow is a type of flow in which the fluid particles move in zigzag way in flow field. Reynolds number is a criterion.
Compressible	Compressible flow is the type of flow in which the density of the fluid changes in the flow field. Mach number is a criterion.
Incompressible	Incompressible flow is a type of flow in which the density is constant in the flow field. This assumption is valid for flow Mach number less than in 0.3.

Inviscid	The flow to be an inviscid flow, an approximation in which we neglect viscosity at all, compared to inertial term.
Viscous	Viscous flows are those in which fluid friction has significant effects on the fluid motion. The Reynolds number can be used to evaluate whether viscous or inviscid.

Aerodynamic problems can be classified according to the flow environment. External aerodynamic flow is the study of flow around solid objects of external aerodynamics. Internal aerodynamics is the study of flow through passages in solid objects. Some problems may encounter only very small viscous effects on the solution, in which case viscosity can be considered to be negligible. The approximations to these problems are called inviscid flows. Flows for which viscosity cannot be neglected are called viscous flow **[41].** Generally, flow over a wind turbine airfoil is entirely incompressible and this is due to the low speed of air flow with a constant density over the surface of the airfoil. Depending on the region and regime, the flow can both be inviscid or viscous. For the majority of its operation, the flow through a wind turbine airfoil is steady. However, as a result of certain atmospheric and operational conditions, the flow can become unsteady.

3.3.6 Aerodynamic Performance Parameters and Non-Dimensional Coefficients

The most significant flow factor influencing the behavior of low-speed airfoils is characterized by the Reynolds number and Mach number of the airfoil. When analyzing the aerodynamic forces and moments on an airfoil, it is more common and convenient to express them as their dimensionless coefficients **[7].** The most important non dimensional parameter for defining the characteristics of fluid flow conditions is the Reynolds number and Mach number **[11].** The force and moment coefficients of an airfoil are functions of these important parameters; Reynolds number describes the ratio of the inertial forces to the viscous forces within the flow.

Reynolds number, Re, is defined by

$$Re = \frac{\rho_\infty c\, U_\infty}{\mu_\infty} \tag{3.4}$$

Where ρ_∞ the fluid density, $_\infty$the fluid viscosity, U_∞ and c are velocity and length that characterize the scale of the flow. These might be the incoming stream velocity, U_{wind}, and the chord length of an airfoil.

The free-stream Mach number relates the free-stream velocity, $U\infty$, to the local speed of sound though air, a_∞:

$$Ma = \frac{U\infty}{a\infty} \quad \textbf{(3.5)}$$

where, for a perfect fluid: $a\infty = \sqrt{\frac{\gamma\, P\infty}{\rho\, \infty}}$ **(3.6)**

Where γ is the ratio of specific heats of the fluid, ρ is the density of the fluid, and P_∞ the pressure of the fluid.

For flow over an airfoil, the velocities and chord size are both relatively small, and the flow is characterized by low Mach numbers (<0.3) and low Reynolds numbers. Thus, the flow is nearly incompressible and viscous forces dominate with relatively thick boundary layers. In regions where, Mach number is possibly above 0.3, compressibility effects cannot be completely ignored.

Additional non-dimensional parameters are force and moment coefficients, which are functions of the Reynolds number, which can be defined for two- or three-dimensional objects **[11]**. Force and moment coefficients for flow around two-dimensional objects are usually designated with a lower case subscript. In that case, the forces measured are forces per unit span. Lift and drag coefficients that are measured for flows around three-dimensional objects are usually designated with an upper case subscript. Airfoil design usually uses two-dimensional coefficients, determined for a range of angles of attack and Reynolds numbers, in wind tunnel tests **[11].** Forces and moments by a dimensionless quantity are expressed in terms of the free stream dynamic pressure, expressed in:

$$q_\infty = 0.5\, \rho_\infty U_\infty{}^2 \quad \textbf{(3.7)}$$

For two dimensionless force and moment, coefficients are defined as follows with **S** as some reference area and **c= 1** and *L* as a reference length.

$$Cl = \frac{L}{q_\infty\ s}\ ,\quad Cd = \frac{D}{q_\infty\ s},\quad Cn = \frac{N}{q_\infty\ s}\ , Ca = \frac{A}{q_\infty\ s}\ ,\ Cm = \frac{M}{q_{\infty\, L}\ s} \qquad \textbf{(3.8)}$$

When determining these coefficients for a complete three dimensional body capital letters are employed, e.g. CL, CD CN, CA and CM in above equation.

The other dimensionless coefficients that are important to know is the pressure distribution around an airfoil surface for the purpose of determining the aerodynamic forces is the pressure coefficient which is expressed as:

$$Cp = \frac{\text{static pressure}}{\text{dynamic pressure}} = \frac{p - p_\infty}{q_\infty} \qquad \textbf{(3.9)}$$

Where p the static pressure on the airfoil surface and p_∞ is the free stream pressure.

The other property that depends on the Reynolds number is the boundary layer. Boundary layer is a thin layer of fluid near the surface of an aerodynamic body which is affected by the friction between the surface of the body and the viscous fluid flowing around it. This friction results in the force of skin friction drag. The properties of the boundary layer around an airfoil can be grouped together into three categories:

Attached regime – At low Reynolds's numbers layers of fluid slide smoothly over each other in a thin boundary layer resulting in low skin friction drag. These are the attached regimes which specifically occur for relatively small angle of attack. The flow over an airfoil will usually start off laminar before transitioning into turbulent as it travels away from the leading edge. The position of the transition point is dependent on Reynolds's number and the localized flow conditions.

High-lift or the stall development regime – At this regime the airfoil are characterized with maximum lift coefficients for moderate angle of attack and higher Reynolds's numbers, or after the transition point, the flow near the surface becomes unstable and the boundary layer thickens, leading to higher skin friction drag.

Flat plate or fully – stalled: - At this regime, a high adverse pressure gradient occurring towards the trailing edge of the airfoil can cause the flow to separate. Flow near the surface reverses direction and a large turbulent wake is created from swirling eddy currents that dramatically increases skin friction drag. These are occurring relatively at larger angle of attack.

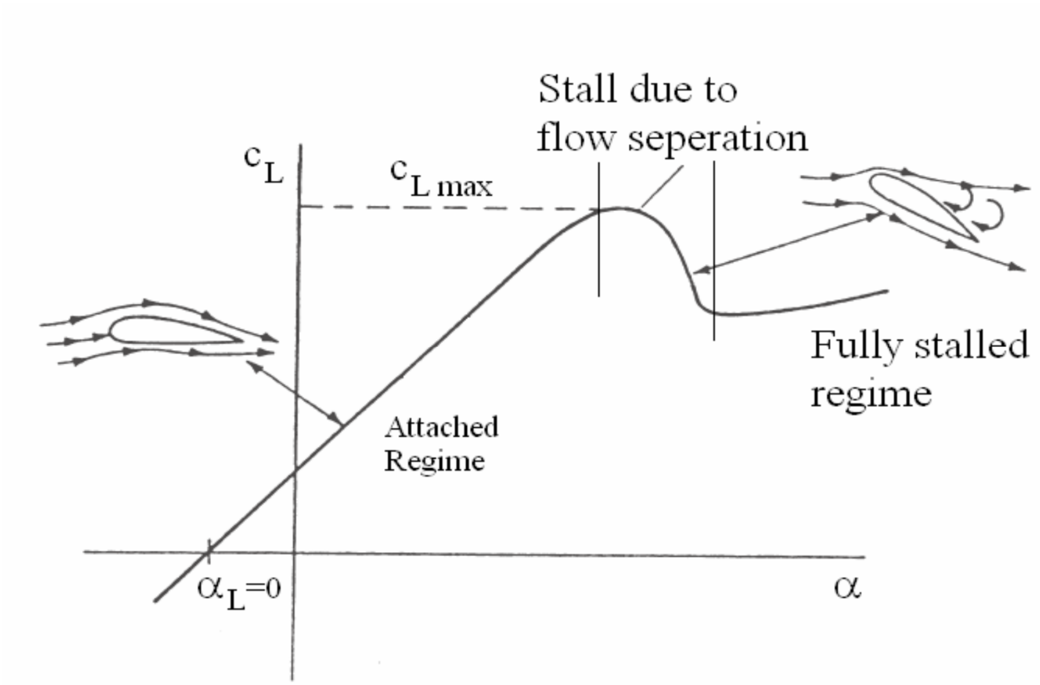

Figure 3-6: Typical airfoil aerodynamic characteristic CL vs. α curve.

3.4 Computational Methodology

In this study, commercially available software, computational fluid dynamics (CFD) package is applied to validate the computational results, to predict the performance parameters and determine aerodynamic characteristic of selected wind turbine blade airfoil. This section gives brief explanation of the computational methods used in this study. It begins with a description of CFD before describing the airfoil modeling.

3.4.1 Computational Fluid Dynamics (CFD)

The importance of CFD in the field of aerodynamics is incomparable. As many researchers have indicated, CFD has been an effective and efficient tool in the field of aerodynamics. Since its introduction in the early 1960's, it has served as a tool for providing exact solutions to many complex aerodynamic flow fields that without it, would never have been solved theoretically **[25].** CFD uses high speed supercomputers to solve the full Navier-Stokes equations for any three or two dimensional, steady, unsteady, incompressible, compressible, inviscid or viscous flow problem.

Generally defined, Computational Fluid Dynamics (CFD) is a branch of fluid mechanics that uses numerical methods and algorithms to solve and analyze problems that involve fluid flows. Computers are used to perform the calculations required to simulate the fluid flow over the aerodynamic surfaces which are defined by boundary conditions **[9]** **[25]**. Ongoing research yields software that improves the accuracy and speed of complex simulation scenarios such as transonic or turbulent flows.

3.4.2 Computational Codes

The CFD package chosen for this study is a product of Fluent, Inc. and consists of a preprocessor called GAMBIT and a suite of flow solvers to various flow situations. The flow solver used in this investigation is FLUENT version **6.3.26**, while version **2.3.16** of the GAMBIT preprocessor was utilized. There were several fundamental reasons for the selection of this CFD package.

3.4.3 Why CFD for the Simulation?

A number of valuable advantages are achieved following a CFD approach to a fluid dynamic problem:

- CFD is faster and positively cheaper. A considerable reduction of time and costs for solving problem involving fluid flow over an airfoil as compared to the experimental wind tunnel test approaches.

- Full-size analysis is difficult to perform for large systems, like modern wind turbines. A CFD study is a favorable choice in these cases.

- In most of the cases solving a fluid dynamic problem does not require a dedicated powerful work station and sometimes a personal computer might be sufficient.
- The CFD analysis of the physical problems have good accuracy and comparable with experimental wind tunnel data, due again to the newest mathematical improvements of solution methods and of turbulence models.

Like most software, CFD is not without its limitations. Its accuracy or validity are dependent on different factors: the quality and appropriateness of the mesh, the degree to which the chosen equations match the type of flow to be modeled, the interpretation of the results, the accuracy of the boundary conditions entered by the user or the level of convergence of the solution, many but to list few. However, the initial validation of such software is comparing the computational result with experimental data. These can provide a valuable reference point to check the validity of CFD models with the final validation coming in full-scale testing.

Regardless of the types of CFD software used, the main principle of simulation are the same. Formulating the governing equations is the precondition of CFD modeling; mass, momentum and energy conservation equation are the three basis governing equations to be solved iteratively [**16**]. Meanwhile, boundary conditions are decided for the flow conditions and mesh is created in order to form the grid. The basic element of the grid is the cell in structured or unstructured grid.

The three numerical methods used in the CFD solver to discretize the governing equations are Finite Different Method (FDM), Finite Element Method (FEM) and Finite Volume Method (FVM). FVM is widely used in CFD simulation software which is easily formulated for both structured and unstructured meshes **[7].**

Computational fluid dynamics (CFD), simulate the motion of a fluid within a given domain by discretizing the governing Navier-Stokes equations (NSE) and solving the resulting set of algebraic equations **[26].** Navier-Stokes equations provide the basis for theoretically solving many aerodynamic problems. One numerical technique which has revolutionized the solution of aerodynamics problem is computational fluid dynamics (CFD). When solving an aerodynamic problem with CFD there are three important phases of the problem analysis **[7].**

3.4.3.1 Pre -processor

In this phase, the physical problem is implemented into the mathematical model and creating a computational domain for the physical surface to be analysed e.g. an airfoil. This is usually performed using a meshing tool called GAMBIT, where the domain is split into a number of finite elements (cell) to create grid .The fluid properties and the boundary conditions are set. Since the CFD solution of a fluid dynamic problem is given locally, for well-defined positions within computational grid. The global accuracy strongly depends on the total number of mesh elements. The larger is the number of elements the better is the solution accuracy, even though CPU effort and the total time of convergence will be higher as well. Consequently, the optimal grid should not be uniform, but finer where higher are the variables gradients and coarser in the region characterized by smooth changes in the flow. The final success of a CFD simulation strongly depends on the preprocessing and therefore a special attention is required to the choice of the mesh and of boundary conditions.

3.4.3.2 Solver

The numerical solution algorithm is one of the most important structures in a CFD code. Most CFD solvers work with the following procedure:

- Modelling the problem unknowns by means of simple analytical functions;
- Discretizing the governing equations for the fluid flows and substituted into the governing equations;
- Solving the algebraic system of equations. Most of the commercial CFD codes such as FLUENT are based on a finite volume discretization and perform these operations; and
- Integrating the governing equations over each control volume within the computational domain is applied which usually involves iterating the set of equations.

3.4.3.3 Post-processing

This structural phase includes the solution analysis. The Solver output is a set of solution variables, associated to the given grid nodes. These data must be collected, elaborated in the most suitable way for the analysis, in order to produce a physical representation of the solution. Some CFD software package like FLUENT contain a post-processing section. Generally, one might be able to do the following post-processing operations:

- Assign a number of variables like a value of velocity or static pressure to the grid.
- Produce contour plots of velocity, pressure, turbulence etc.; and
- Analyse the result of the solution to observe the variation in these variables over the complete solved flow field. This can be performed within a complete CFD package in this case FLUENT.

The accuracy and reliability of simulations is largely dependent on the numerical methods used. The selection of the appropriate spatial and temporal discretization scheme, turbulence model and computational grid types can have a significant influence on the final simulation results. Each choice of a methodology aspect can have advantages and disadvantages **[27].** For instance, a high-order scheme is theoretically expected to give more accurate predictions; however, it may be more unstable compared to a low-order scheme. Also, one- and two-equation turbulence models are preferred over algebraic models in terms of accuracy but it takes more time to solve the problem. With respect to grid types, a structured grid has better accuracy and is first chosen in the boundary layer region along the airfoil surface; however unstructured grids require fewer grid points outside the boundary layer region. Considering irregular geometry i.e. airfoil, unstructured grids are simple to generate and also are more easily adapted to flow gradients. But structured grids allow efficient computation results. In addition, the structured grid type is more practically used in the industry. In this study, a structured Navier-Stokes equation solver is primarily applied. A commercial software package, FLUENT, which works on both structured and unstructured grids, is applied here to simulate results. Figure 3-7 below shows the road map of a typical two - dimensional CFD modelling process.

3.4.4 Two-Dimensional CFD Modeling Process Flowchart

There is no clearly stated ways of analysing air flow over an airfoil using FLUENT, therefore the user model their own methodology. There are practiced ways and hints in many literatures and these were followed for guidance. Figure 3-7 shows road map when using CFD to reproduce airfoil characteristics.

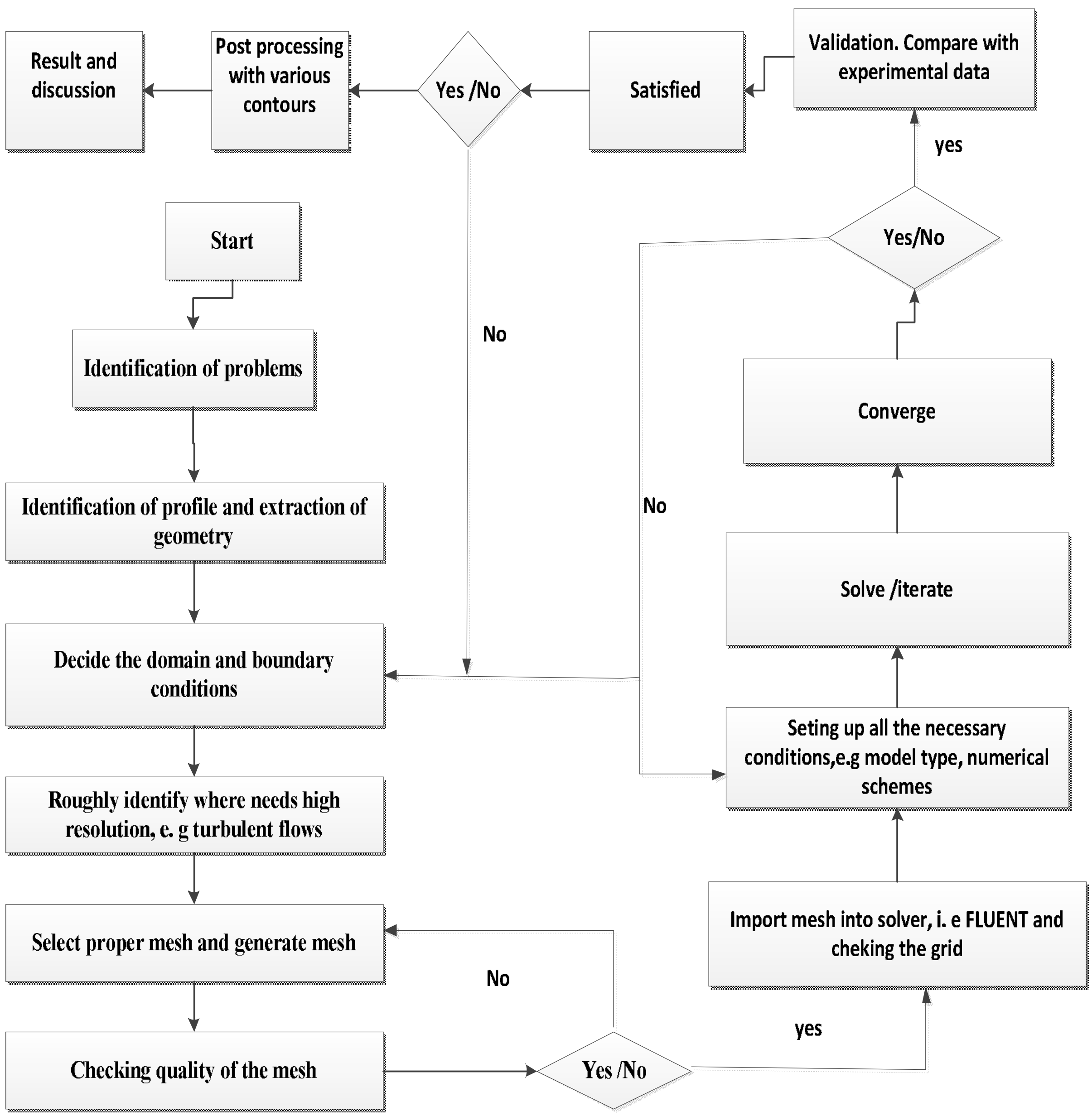

Figure 3-7: Flowchart of typical two-dimensional CFD modeling process

3.5 Mathematical Formulation and Turbulence Modeling

3.5.1 Mathematical Formulation

The characteristics of aerodynamic flow fields are represented by equations that describe the basic equation of physical fundamentals which are powerful enough to illustrate the flow physics. However, the equations by themselves are not adequate, but must be supplemented by experimental results. Various combinations of body shapes and flow conditions need to be integrated to obtain the results. The governing equations of aerodynamics such as the continuity, momentum and energy equations are highly nonlinear, partial differential, or integral equations. Accurate analytical solution to these equations does not exist. CFD approach facilitates a solution to the governing equations **[28].**

For all flows, the solver solves conservation equations for mass and momentum. Additional transport equations are also solved when the flow is turbulent. The equation for conservation of mass or continuity equation can be written as follows **[17] [29].**

$$\frac{d\rho}{dt} + \nabla.(\rho\vec{u}) = s_m \qquad \textbf{(3.10)}$$

This is a general equation for conservation of mass and is valid for both incompressible as well as compressible flows. The source S_m is the mass added to the continuous phase from the dispersed second phase and which is user-defined sources **[17].**

Conservation of momentum equation is described as:-

$$\frac{\partial(\varrho\vec{u})}{\partial x} + \nabla.(\varrho\vec{u}\vec{u}) = -\nabla \mathrm{p} + \nabla.(\bar{\bar{\tau}}) + \rho\vec{g} + \vec{F} \qquad \textbf{(3.11)}$$

In the equation p is the static pressure, τ is the stress tensor, g is the gravitational body force and F is external body force which arises from interaction with the dispersed phase, respectively. The equation also contains other model-dependent source terms such as porous-media and user-defined sources **[8].** The stress tensor τ is given by:

$$\bar{\bar{\tau}} = \left[(\nabla \vec{u}) + \nabla\vec{u}^{T} - \frac{2}{3}\right] \nabla.\vec{u}I \quad \textbf{(3.12)}$$

In the above equation is the molecular viscosity, I is the unit tensor, and the second term on the right hand side is the effect of volume dilation **[17].**

For the 2-D, steady and incompressible flow the continuity equation is:

$$\frac{\partial u}{\partial x} + \frac{\partial v}{\partial y} = 0 \quad \textbf{(3.13)}$$

x and y directions momentum equations for viscous flow are given below, respectively

$$\frac{\rho Du}{Dt} = -\frac{\partial P}{\partial x} + \frac{\partial \tau_{xx}}{\partial x} + \frac{\partial \tau_{yx}}{\partial y} + \rho f_x \quad \textbf{(3.14)}$$

$$\frac{\rho Dv}{Dt} = -\frac{\partial P}{\partial y} + \frac{\partial \tau_{xy}}{\partial x} + \frac{\partial \tau_{yy}}{\partial y} + \rho f_y \quad \textbf{(3.15)}$$

Since the flows considered have 2-D characteristics the term in the Z direction from the continuity equation $\frac{\partial w}{\partial z}$ and from momentum equation $\frac{\partial \tau_{zx}}{\partial z}$ and $\frac{\partial \tau_{yxy}}{\partial z}$ are neglected **[17] [29].**

3.5.2 Turbulence Models

The purpose of this section is to give an overview of issues related to the turbulence models provided in **FLUENT**. Categorically it is not a clear-cut to state which model is best for a specific application. There is no single turbulence model which is universally accepted as being superior for all classes of flow problems. The choice of turbulence model will depend on many factors, such as: the physics encompassed in the flow, the established practice for a specific class of problem, the level of accuracy required, the available computational resources, and the amount of time available for the simulation. To make the most appropriate choice of model for specific problem understanding the capabilities and limitations of the various options are very important **[30] [31]**. A number of different turbulence models were suitable candidates for modeling the flow over airfoil surface.

Out of many turbulence model available in FLUENT, in this study, two turbulence models are selected to assess the prediction capability. It is only stated that the model is chosen because of the very promising results for 2D flow problems without disregarding other models that may be suitable for the purpose of the this study [**32**]. Turbulence models are necessary because high capacity computers cannot be afforded to directly capture every scale of motion. Users of CFD typically want a steady-state solution with all the unsteady fluctuations averaged out rather than a detailed time-accurate one that captures every little vortex. As a result, there are turbulent motions affecting the flow that cannot be resolved directly; they must therefore be modeled **[17] [33].** In some cases, the turbulence model can have a huge effect on the results obtain from CFD software.

Turbulence models are generally classified according to which governing equations apply to like that Reynolds-averaged Navier-Stokes or Large Eddy Simulation equations **[16] [17]**. Within these broader categories, they are further broken down by the number of additional transport equations. In this work Reynolds-averaged Navier-Stokes (RANS) equations are considered, the incompressible Navier–Stokes equations are a suitable model to describe the aerodynamics of wind turbine; these are the models that are used for most aerodynamic applications **[16].**

Reynolds averaging or Reynolds decomposition is the process of dividing turbulent terms into average and instantaneous components. For example horizontal wind speed U is divided into $\overline{U}$ average and u fluctuating **[1].**

$$U = \overline{U} + u \qquad \textbf{(3.16)}$$

Reynolds averaging is used by standard CFD turbulence models for any random flux variable like velocity. Computational models are typically referred to as RANS models. The RANS equations set below include average and fluctuating variables for velocity, u, pressure, p, density, ρ, viscosity, μ, etc.

The equation of Reynolds-averaged Navier-Stokes (RANS) is defined as:

$$\rho \frac{DU_t}{D_t} = \frac{\partial P}{\partial X_i} + \frac{\partial}{\partial X_i}\left[\left(\frac{DU_t}{\partial x_j} + \frac{DU_j}{\partial x_i}\right) - \rho\overline{\acute{u_i}u_j} \right] \qquad \textbf{(3.17)}$$

It is the oldest and most common approach to turbulence modeling; the left hand side of the equation describes the change in mean momentum of fluid element and the right hand side of the equation is the assumption of mean body force and divergence stress. $\rho\overline{\acute{u_i}u_j}$ is an unknown term called Reynolds stresses **[7].**

Before describing the details of the flow simulation around the airfoil, the basic notions underlying the turbulence models used in this thesis are discussed. The turbulence models used in the flow solver are described in this section. Two models are discussed in detail: the SST k−ω (Shear-Stress-Transport k−ω) model and SA (Spalart-Allmaras) model. To compare the prediction capability of the models with each other and experimental data, the most suitable model for the main objective of this study is selected.

3.5.2.1 Spalart - Allmaras One-Equation Models (SA)

According to Spalart and Allmaras, (1992) Spalart - Allmaras (SA) turbulence modeling is a one-equation modeling **[16] [17] [31].** This solves a single transport equation for a quantity which is used to obtain the turbulent viscosity. This embodies a relatively new class of one-equation models in which it is not necessary to calculate a length scale related to the local shear layer thickness. The Spalart-Allmaras model was designed specifically for aerospace applications involving wall-bounded flows and has been shown to give good results for boundary layers subjected to adverse pressure gradients. It is also gaining popularity for turbo machinery applications.

In its original form, the Spalart-Allmaras model is effectively a low-Reynolds-number model, requiring the viscous-affected region of the boundary layer to be properly resolved. In FLUENT, however, the Spalart-Allmaras model has been implemented to use wall functions when the mesh resolution is not sufficiently fine. This might make the model less sensitive to numerical error **[30]**. In terms of computation, the Spalart-Allmaras model is the least expensive turbulence model of the options provided in FLUENT, since only one turbulence transport equation is solved. In the turbulence model of Spalart-Allmaras the transport equation can be written as shown below, in the form of the operating parameter $\tilde{\nu}$ which is referred to as the Spalart-Allmaras variable **[16] [17] [31].**

$$\frac{D\tilde{v}}{Dt} = c_{b1}(1 - f_{t2})\tilde{S}\,\tilde{v} + \frac{1}{\sigma}\left[\nabla.\left((v + \tilde{v})\right)\nabla\tilde{v} + c_{b2}(\nabla\tilde{v})^2\right] - \left(c_{w1}f_w - \frac{c_{b1}}{k^2}f_{t2}\right)\left(\frac{\tilde{v}}{d}\right)^2 + \quad f_{wt1}\Delta U^2 \tag{3.18}$$

From the above general equation $\mathbf{v}$ is molecular viscosity calculated by the Sutherland's (1893) law. The four terms on the right hand side correspond to production, diffusion, dissipation and transition, respectively. Each variable in the production term is defined as:

$$\tilde{S} \equiv S + \frac{\tilde{v}}{K^2 d^2}\left[1 - \left(\frac{\tilde{v}}{v}\right)\left(1 + \frac{(\frac{\tilde{v}}{v})^4}{(\frac{\tilde{v}}{v})^3 + C_{v1}{}^3}\right)^{-1}\right] \quad \textbf{(3.19)}$$

$$f_w = \frac{\tilde{v}}{\tilde{S}K^2 d^2}\left[1 + c_{w2}\left(\left(\frac{\tilde{v}}{\tilde{S}K^2 d^2}\right)^5 - 1\right)\right](1 + c_{w3}{}^6)^{\frac{1}{6}}\left\{\left[1 + c_{w2}\left(\left(\frac{\tilde{v}}{\tilde{S}K^2 d^2}\right)^5 - 1\right)\right]^6 + c_{w3}{}^6\right\}^{\frac{-1}{6}}$$

(3.20)

$$f_{t1} = C_{t1} g_t \exp\left[-C_{t2}\ \frac{\omega_t{}^2}{\Delta U^2}\left(d^2 + g_t{}^2 d_t{}^2\right)\right] \quad \textbf{(3.21)}$$

$$f_{t2} = C_{t3}\exp\left[-C_{t4}\left(\frac{\tilde{v}}{v}\right)^2\right] \quad \textbf{(3.22)}$$

where S is the magnitude of the vortices, d is the distance to the closest wall, d_t is the distance from the point in the flow field to the trip on the wall, ω_t is the wall vortices at the trip, $\Delta \boldsymbol{U}$ is the difference between velocity at the field point and that at the trip, $g_t = \min\left(0.1, \frac{\Delta U}{\omega_t \Delta x_t}\right)$ where Δx_t is the grid spacing along the wall at the trip. The empirical constants of the Spalart-Allmaras model available in FLUENT are **[16] [31] [8]:**

$$c_{b1} = 0.1355, \quad \sigma = \frac{2}{3}, \quad c_{b2} = 0.622, k = 0.4187, \quad c_{w1} = 3.239,$$

$$c_{w2} = 0.3, c_{w3} = 2.0, C_{v1} = 7.1, C_{t1} = 1, C_{t2} = 2, C_{t3} = 1.2, C_{t4} = 0.5$$

3.5.2.2 Two-Equation Shear-Stress-Transport k−ω Models (SST k- ω)

Two equation turbulence models are one of the most common types of turbulence models. Models like the k-epsilon and the k-omega model have become industry standard models and are commonly used for most types of engineering problems. By definition, two equation models include two extra transport equations to represent the turbulent properties of the flow. Most often one of the transported variables is the turbulent kinetic energy k. The second variable varies depending on what type of two-equation model it is. Common choices are the turbulent dissipation, or the specific dissipation. The second variable can be thought of as the variable that determines the scale of the turbulence (length-scale or time-scale), whereas the first variable k, determines the energy in the turbulence **[40].**

The shear-stress transport (SST) k- ω model was developed by Menter to effectively blend the robust and accurate formulation of the standard k- ω model in the near-wall region with the free-stream independence of the k- ε model in the far field. This blending makes the k- ω SST model valid for a wide range of flows and is recommended for airfoils **[42].** Along with the Spalart-Allmaras model, two-equation models make up the bulk of the turbulence models used for CFD **[16].** When using this model, the flow is assumed to be turbulent everywhere, and does not provide a transition from laminar to turbulent flow. This assumption has the potential of causing some error between the computational and experimental data. A turbulent boundary layer plays a significant role in the formulation of drag, thus the error can be most noticed in the comparison of drag forces **[42].**

SST k- ω model is however, more accurate and reliable for a wider class of flows (e.g., adverse pressure gradient flows, airfoils) than the standard k- ω model. Other modifications include the addition of a cross-diffusion term in the ω equation and a blending function to ensure that the model equations behave appropriately in both the near-wall and far-field zones.

The turbulence kinetic energy, k, and the specific dissipation rate, ω, are obtained from the following transport equations **[16] [17] [8].**

$$\frac{\partial}{\partial t}(\rho k) + \frac{\partial}{\partial x}(\rho k u_i) = \frac{\partial}{\partial_{xi}}\left(\Gamma_k \frac{\partial k}{\partial xi}\right) + G_K - Y_K + S_K \tag{3.23}$$

$$\frac{\partial}{\partial t}(\rho \omega) + \frac{\partial}{\partial x}(\rho \omega u_i) = \frac{\partial}{\partial_{xi}}\left(\Gamma_\omega \frac{\partial \omega}{\partial xi}\right) + G_\omega - Y_\omega + S_\omega \tag{3.24}$$

In the above expression, G_k represents the generation of turbulence kinetic energy due to mean velocity gradients. G_ω represents the generation of ω. Γ_ω and Γ_k represent the effective diffusivity of ω and k, respectively. Y_k and Y_ω represent the dissipation of k and ω due to turbulence. S_k and S_ω are user-defined source terms **[8].** All of the above terms are calculated and described in reference **[31] [34].**

CHAPTER 4

TWO-DIMENSIONAL AIRFOIL MODELING

4.1 Objectives of the Modeling

This section is designed to become familiar with the computational tools and their various operations. In order to become familiar with the tools, a tutorial provided by the Sibley School of Mechanical and Aerospace Engineering at Cornell University was followed. The tutorial provides a step by step explanation of how to mesh an airfoil in GAMBIT and solve fluid flow over an airfoil surface in FLUENT. The full tutorial can be viewed in reference **[35].**

The other task of this section is to develop a 2-D model of the airfoil based on commercially available software such as GAMBIT and solve fluid flow over the surface of the airfoil in FLUENT in order to verify the model and validate the results. After some verification of the model and validation of the CFD results, the model is used with confidence for airfoil simulation of different cases and that the results are considered trustworthy for the specific case of this study, Adama I wind turbine blade airfoil**.**

4.2 Airfoil Modeling

The first step in the process of airfoil modeling is to import the points that make up the upper and lower surface of the airfoil. The points are created from a set of coordinate points. The coordinate points file for NACA airfoils are imported from UIUC airfoil coordinate database as dat. file **[37].** The model is set up as a two-dimensional (2D) flow problem in single phase, with the assumption that the fluid movement in the third component (z direction) is negligible. The Cartesian co-ordinate axes were fixed at the leading edge of the airfoil. This model of an airfoil section was created with the aim of calculating lift and drag data for the airfoil at varying angle of attacks (AOA). These data can give an estimation of the relative performance of wind turbine airfoil**.**

Due to large application in wind turbine industry **[44],** for this study, an airfoil whose aerodynamic characteristics are representative of horizontal axis wind turbine (HAWT) airfoils ,NACA 63-415 geometries are created and meshed using the preprocessor with geometry modeling and mesh generation software - GAMBIT. The pre-processor is software that can be employed to develop model of the airfoil in 2-D or 3-D, applying structured or unstructured meshes, which can consist of different elements such as quadrilateral, triangular or tetrahedral elements for modeling the airfoil geometry. The airfoil NACA 63-415 is 15 % thick and a schematic of the geometric model of the airfoil created in GAMBIT and used in this study is shown in Figure 4-1.

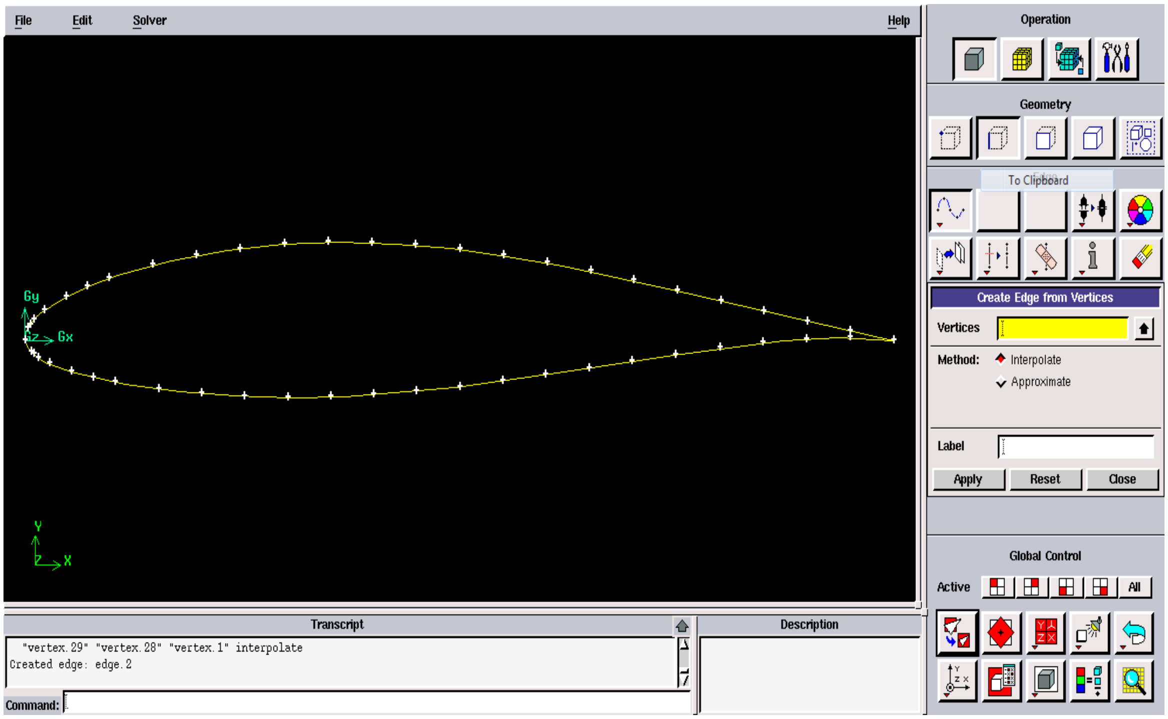

Figure 4 -1: NACA 63-415 airfoil geometry developed using the pre- processor - GAMBIT

4.2.1 Far-field Boundary Conditions

In an external flow such as over an airfoil, it is needed to define a far-field boundary and mesh the region between the airfoil geometry and the far-field boundary. The far-field boundary is placed at an arbitrary distance from the airfoil geometry since the ambient conditions to define the boundary are used at the far-field. It is known that the farther from the airfoil, the less effect it has on the flow and so more accurate is the far-field boundary condition. The flow is 2D and the computational domain used is a C-type far field in GAMBIT, which is commonly used for structured meshes **[7].** To allow the air to be fully expanded, the length of computational domain is determined at 32.5 times that of chord length, the width is determined at 25 times that of chord length as indicated in Figure 4-2 below. These are recommended values used in several studies in the literatures **[7] [16] [17] [35].** Accordingly, creating this geometry ensures the far field boundary conditions are not affected by the flow around the airfoil.

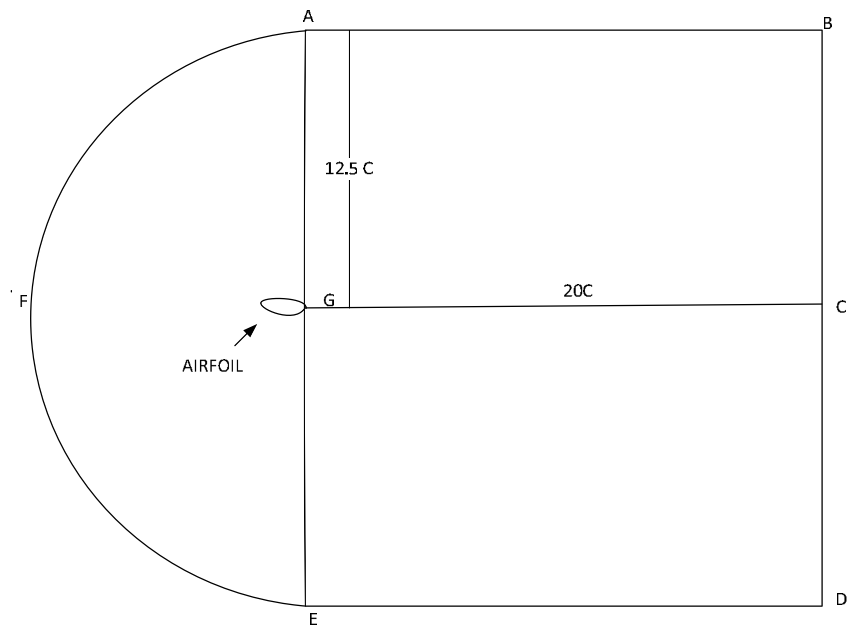

Figure 4-2: Generation of far field boundary from corner point and the length of computational domain

From Figure 4-2, the domain consists of four edges, a curved edge in front of the leading edge of the airfoil, top and bottom edges that are parallel to the chord line of the airfoil, and a vertical edge behind the trailing edge. The generation of these edges comes from first defining corner points and then connecting them with either an arc or straight edges. The top and bottom edges are connected with the curved edge to form an inlet part, and the vertical edge forms the outlet part. The grouping of these edges into parts is important for the boundary condition definition phase.

4.2.2 Boundary Conditions

Three boundaries types are set for the far-field condition: the velocity inlet, airfoil and pressure outlet. The velocity inlet describes the boundary for the flow approaching the airfoil which includes the top, bottom and left side of the domain. The airfoil describes the boundary for the airfoil itself and is defined as a wall with no slip boundary condition and the pressure outlet described the boundary for the flow leaving the airfoil and is defined as a pressure outlet. The final domain constructed on GAMBIT with specified boundary conditions is shown in Figure 4-3 below.

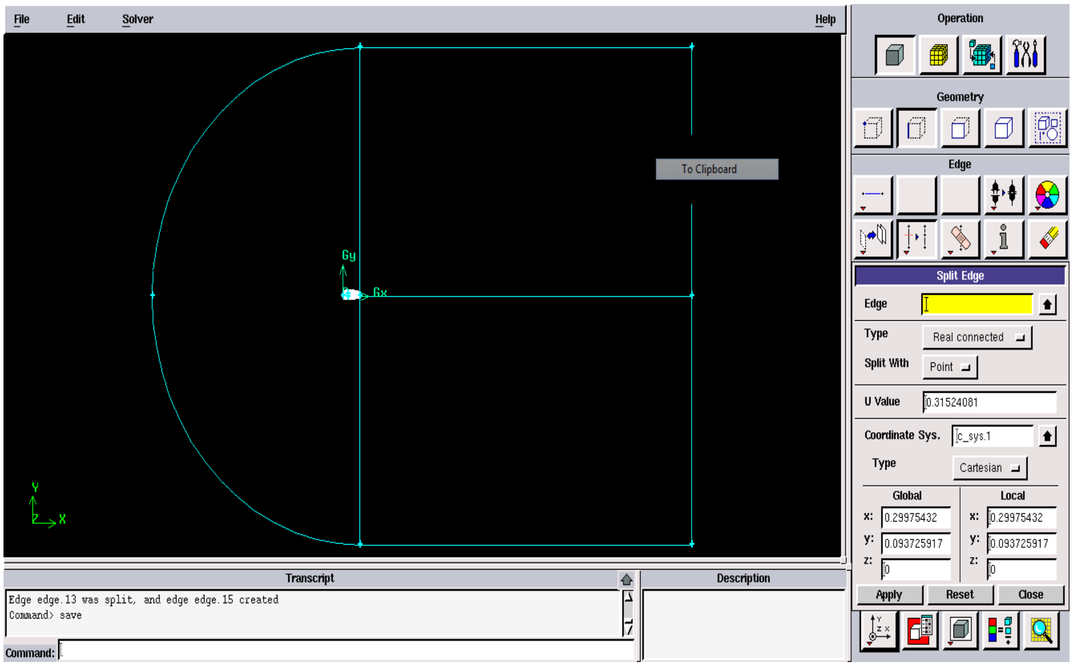

Figure 4-3: Far field boundary and the length of computational domain developed on GAMBIT

4.2.3 Grid Generation

To conduct numerical simulation the computational domain shown in Figure 4-3 is meshed with control volume built around each grid using GAMBIT, which is the preprocessor for FLUENT.

In order to save the computational space and time available for the simulation, this study utilized structured quadrilateral mesh type. Since closer to the airfoil surface large gradients in flow variables (pressure, velocity) dominate the flow. As a result, in meshing the model the most resolution is needed close to the surface near the leading and trailing edges of the airfoil since these are critical areas with the steepest gradients. Cluster points are made near the airfoil since this is where the flow is modified the most. The mesh consists of 12,195 quadrilateral cells, of which 151 are on the airfoil. Model grid distributions for all faces and close to the airfoil are given in Figure 4-4.

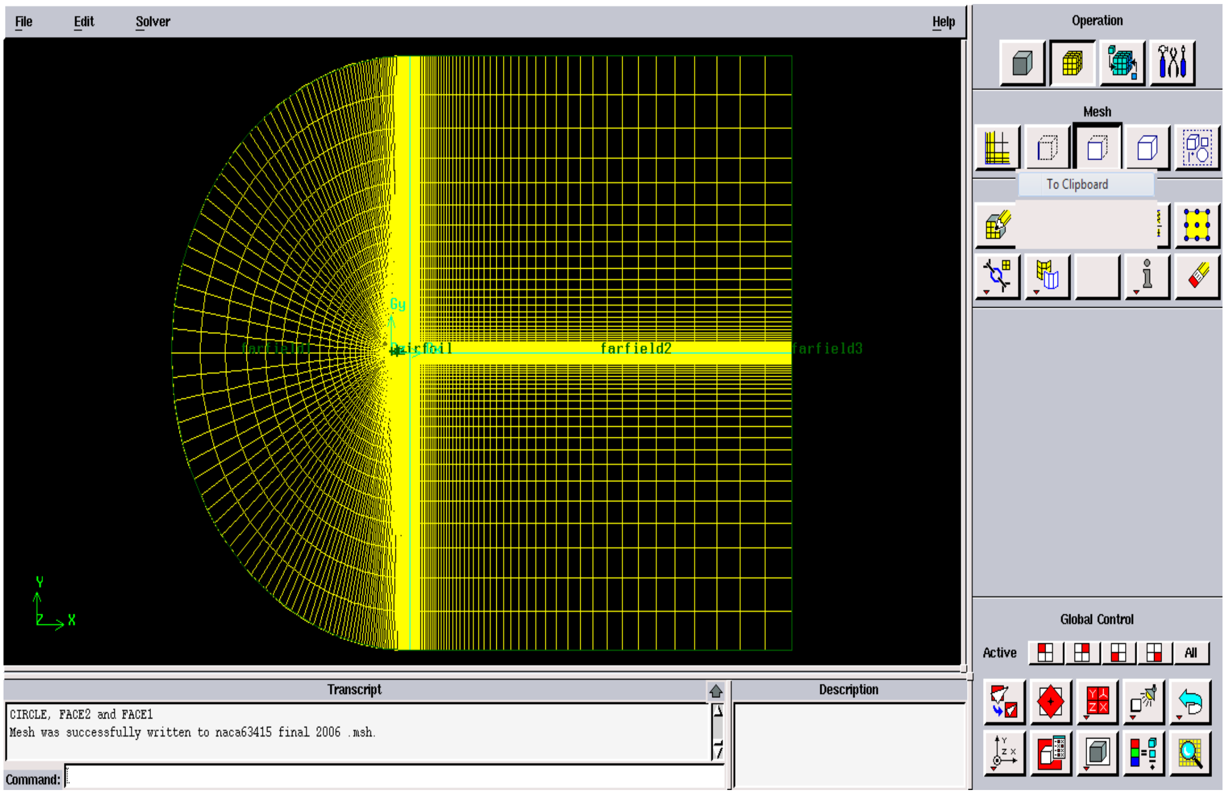

Figure 4-4: Computational domain meshing by using structured grid over the system using GAMBIT

Figure 4-5, shows structured mesh near the airfoil leading and trailing edges, the most critical areas with the steepest gradients.

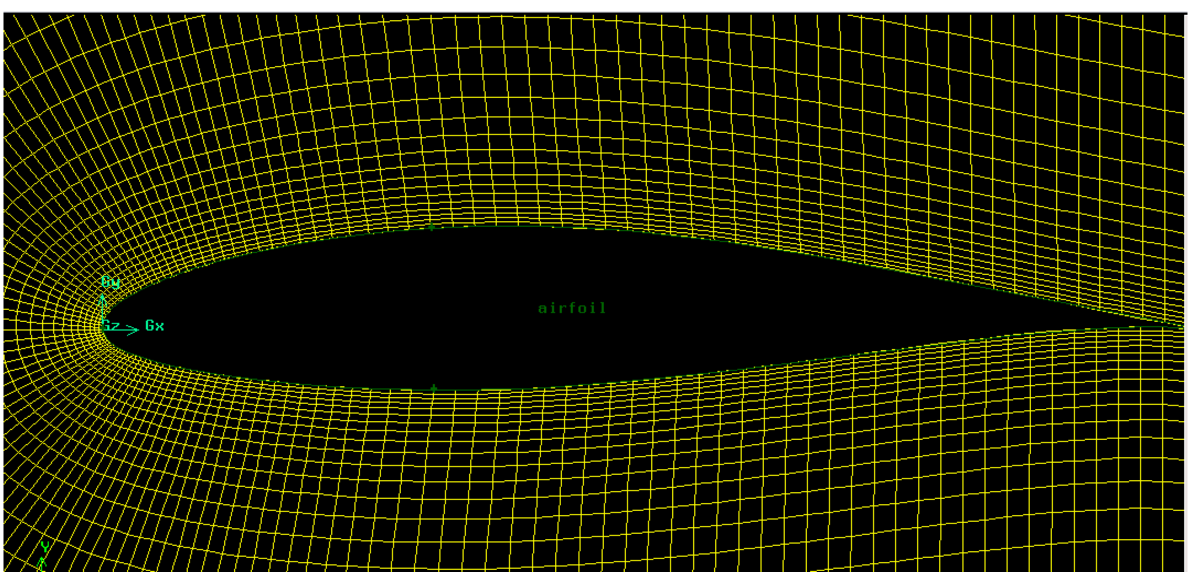

Figure 4-5: Mesh around NACA 63-415 airfoil using structured grid on GAMBIT

4.2.4 Solution Methods

Once a good quality mesh has been generated throughout the entire domain and around the airfoil, the mesh file is imported into the CFD solver, FLUENT. Before the governing equations could be solved, the appropriate settings are first enabled throughout solver interface and the correct boundary conditions are specified to accurately match the conditions in which the calculations are performed. Table 4-1 shows the list of typical solver settings and boundary conditions used for this simulation. To more accurately match the experimental conditions, the simulation is performed under the same conditions with the experimental data.

A CFD solver generally requires setting boundary conditions, defining fluid properties, performing simulation and post processing the results. FLUENT 6.3.26, 2ddp (two-dimensional with double precision) flow solver is employed, which implements 2-D Reynolds averaged Navier-Stokes (RANS) equations using a finite volume- solver. The numerical method employed is the pressure-based solver (PBS). Since PBS is developed for low speed incompressible flows, in the present study which involves incompressible flow and separation is caused by adverse pressure gradients, thus the pressure - based approach is preferred. In this approach the governing equations are nonlinear and coupled to one another. In order to solve the set of governing equations, several iterations of the solution must be performed before a converged solution is obtained. In this study a segregated pressure–based solver (SPBS) algorithm has been used. Using segregated approach, the governing equations are solved sequentially (i.e. segregated from one another). Because the algorithms are memory efficient and discretized the equations need only to be stored in the memory one at a time. However the solution convergence is relatively slow **[31]**. Each iteration consists of the steps illustrated in Figure 4-6.

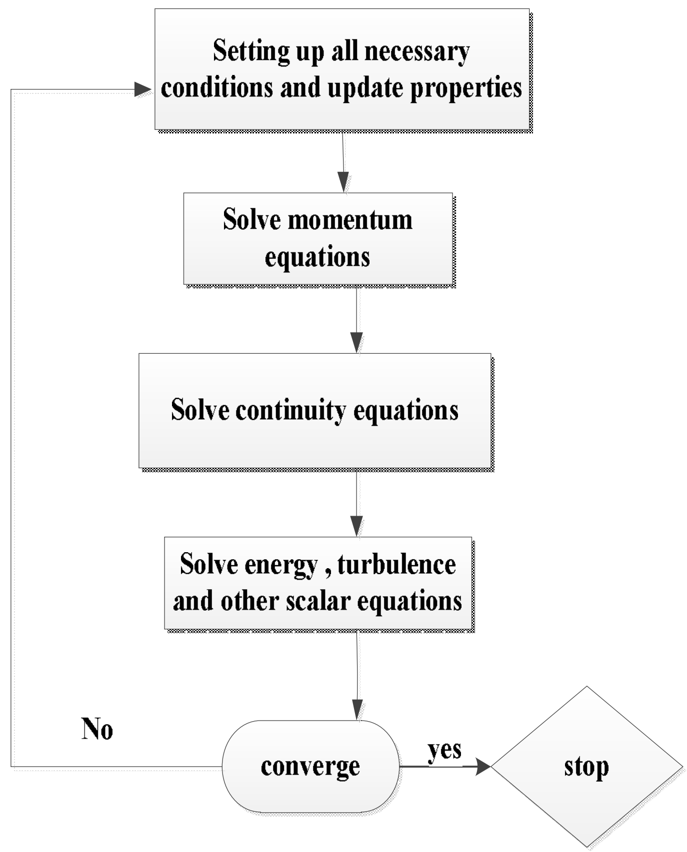

Figure 4-6: Overview of the segregated solution method

4.2.5 Interpolating Scheme

The spatial discretization of all the transport equations is set to second order upwind scheme. Fluid flow over the surface of the airfoil is not always aligned with the grid. Hence, the second-order-upwind interpolation schemes for the convection terms are used for all nodes. FLUENT recommends this second order scheme to decrease the numerical diffusion error that is more likely to occur with a first order scheme **[30] [31].** The computational expense of second order methods is more expensive per grid point than first order schemes, but the computational accuracy per overall cost of this higher order method is much greater. Stopping criteria for iterative calculations is based on monitoring both the residual history and the lift and drag coefficients. The convergence of the segregated solution is achieved when the sum of the absolute differences of the solution variables between two successive iterations falls below a pre-specified small number, which is chosen as 10^{-6} in this study. Figure 4-7 represents a convergence history of NACA 63-415 airfoil for 5^0 angles of attack (AOA).

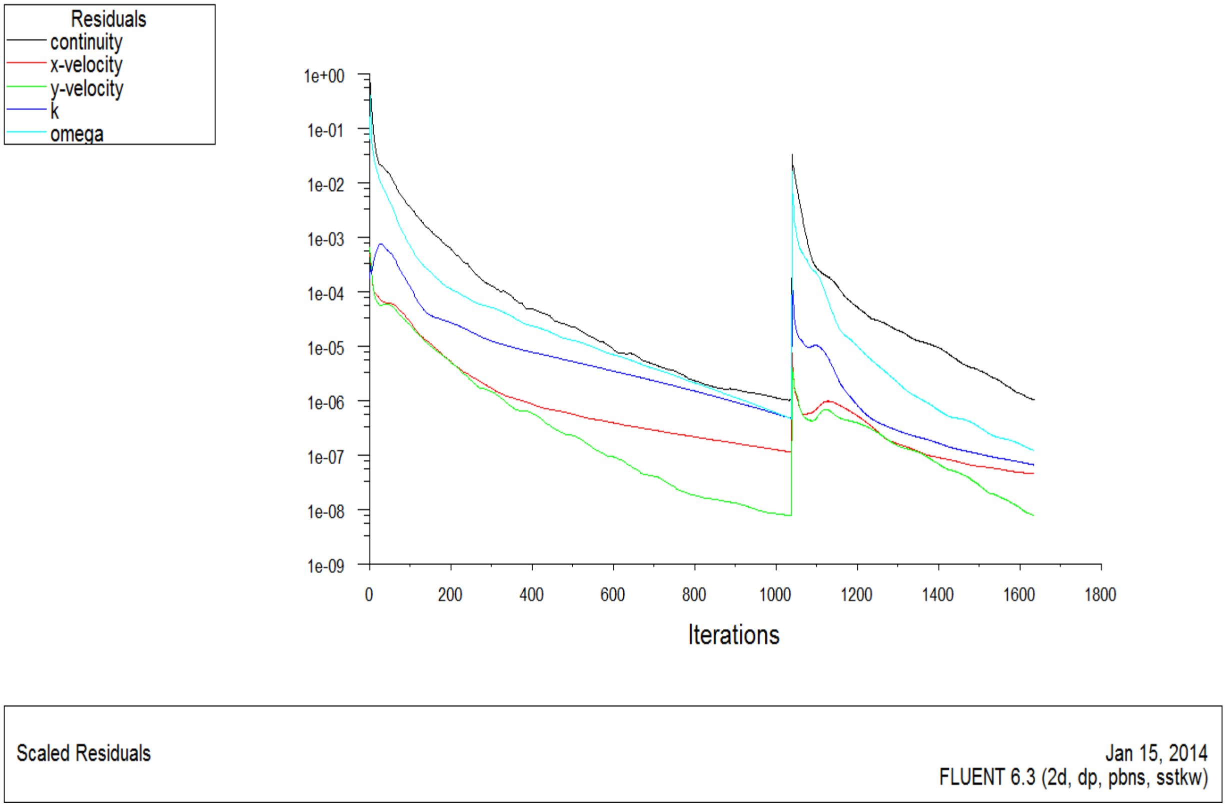

Figure 4-7: Residuals plot with convergence criterion set to 10^{-6} at AOA 5^{0}.

Figure 4-7 shows the status of residual values. It also shows the residuals of x, y velocities and k, omega and their convergence. Y axis shows the residuals levels and X axis is the number of iterations.

4.2.6 Fluid Properties

The working fluid for the simulation is air with density equal to the reference value in the experimental data which is 1.225 kg /m^3 **[36].** A maximum wind speed profile of 40 m/s is taken at the entrance of the domain as boundary condition with fixed turbulence intensity of 1% and turbulence viscosity of 1.789 x10-5 kg / m .s is considered and the Reynolds number for the simulation is about 1.6 $x10^6$ **[36].** For these conditions the flow can be described as incompressible. This is an assumption close to reality and it is not necessary to resolve the energy equation. The simulation is done for these flows ensuring in the process that the computations are numerically reliable. Operating pressure is taken as 101325 Pa. Far-field in the backside of the airfoil is set as pressure outlet with a gauge pressure of zero **[36]**.

After specifying the physical models and boundary conditions, the calculation starts from arbitrary initial conditions and converges to the correct solution after performing a number of iterations. For different angle of attacks and different velocity components are set as velocity inlets and lift and drag coefficients are monitored.

The simulation is, therefore, run with an inlet velocity of 40 m/s over a range of different angles of attack. The x and y components of the velocity are controlled by modifying the angle of attack appropriately.

$$Vx = V\cos\alpha \quad , \quad Vy = V\sin\alpha \qquad \textbf{(4.1)}$$

To control the AOA of the validation cases, the velocity magnitude are split into the corresponding X and Y components. These velocity components are shown in Table 4-1.

Table 4-1: Validation Velocity Components

Velocity (V) = 40 m/s				
AOA (degree)	X component	Y component	Vx	Vy
-5	0.9962	-0.0872	39.85	-3.49
0	1	0	40	0
5	0.9962	0.0872	39.85	3.49
10	0.9848	0.1736	39.39	6.95
15	0.9659	0.2588	38.63	10.35
20	0.9397	0.3420	37.59	13.68

Having the lift and drag coefficients output to the display window, the values are recorded and plotted with the corresponding angles of attack using MATLAB.

4.2.7 Fluent Analysis Parameters

Table 4-2: Computational conditions of two-dimensional simulation

Parameter	Value
Fluent Version	2ddp
Solver	Pressure based / segregated solution algorithm
Simulation type	Steady simulation
Formulation	Implicit
Turbulence Model	One equation SA and two equation SST k-w model
Airfoil profile	NACA 63-415
Fluid material	Air
Flow type	Incompressible flow
Temperature	300 k
Kinematic Viscosity	1.789 x 10 -5 kg /m-s
Density	1.225 kg/m^3
Reynolds Number	1.6 x10^6
Pressure	101325 Pa
Wind Speed	40 m/s
CFD algorithm	SIMPLEC
Interpolating scheme	Pressure (Standard) Momentum (Second Order Upwind) Modified turbulent viscosity (Second Order Upwind)
Boundary condition	Velocity inlet and pressure outlet Stationary wall with no slip condition
Initialization	Inlet values
Force Monitors	Lift and drag coefficient
Reference Values	Inlet values
Convergence Limit	10^{-6}

CHAPTER 5

RESULTS AND DISCUSSION

5.1 Experimental Comparison: Two-Dimensional CFD Validation

In this section, the computational results and available experimental measurement data are compared for NACA 63-415 airfoil. The validation process is performed to show the level of accuracy of the CFD code and the computational model and methodologies provided accurate results. These methodologies and settings could then be applied for special cases such as the case study of this thesis.

The NACA 63-415 is chosen for the initial validation for it has widely available experimental data to compare with computational results. This is accomplished by plotting the performance parameters, the lift, drag and lift to drag coefficients of the airfoil with AOAs. These data which are available experimentally are conveniently reproduced to numerical data. As discussed in section 4.2.6, the simulation is performed using the same ambient and fluid flow conditions as the experiment. The experiment was carried out in the VELUX wind tunnel at the Technical University of Denmark and RISO National Laboratory; the tested airfoils were manufactured by LM Glasfiber A, Denmark which is found in reference **[36]**. The most significant results are discussed and results are presented in graphical and tabular form for selected values of angle of attacks.

5.1.1 Results

In this subsection, the aerodynamic analysis of airfoil NACA 63-415 is conducted in two – dimensional simulation using two turbulence model in FLUENT and the results are compared with experimental data to find out the model which has a better accuracy in predicting the parameters.

Table 5-1 and Table 5-2 show comparison of simulation results obtained from CFD solver and experimental values of force coefficients (lift and drag) over a range of AOAs using the two turbulence models S-A and SST k- ω. A percentage (%) error is also included in the comparison to determine the deviation of the CFD results from experimental values.

Figure 5-1 and Figure 5-2 show polar curves of experimental measurement data and computed results of lift and drag coefficients verses AOA, respectively. The results obtained from both turbulence models are in good agreement with experimental values in the simulation of lift coefficient. Figure 5-1 shows the lift coefficient comparison of experimental measurement values with the numerical simulation results for both S-A and SST k- ω models.

The predictive capabilities of the models are compared with maximum percentage errors. The error lies within maximum of 12% in the S-A model as compared to the experimental values, whilst maximum of 9% in the SST k- ω for the calculation of lift coefficients. However, the corresponding errors for the drag show 16 % for the S-A model and 12 % for the SST k- ω model. As many literatures reported **[45],** this deviation is expected in the simulation of drag coefficients because in the actual airfoil the flow is mostly dominated by laminar flow. The turbulence models in the solver S-A and SST k- ω however, assume the flow as fully turbulent, which results in higher drag prediction.

Accordingly, comparison of the results of S-A and SST k- ω model with VELUX wind tunnel experimental values, the SST k- ω model most accurately determines the lift and drag characteristics of the airfoil.

Table 5-1: Comparisons of aerodynamic coefficient using S-A model with experimental values: NACA 63-415

AOA (α)	C_l				C_d			C_l / C_d	C_l / C_d
	EXP	CFD S-A	% Error		EXP	CFD S-A	% Error	EXP	S-A
-5	-0.25	-0.228	9.649		0.015	0.01413	6.157	-16.667	-16.135
0	0.3	0.3415	12.152		0.01	0.01083	7.664	30.00	31.533
5	0.8	0.8808	9.173		0.015	0.01625	7.692	53.333	54.203
10	1.25	1.3288	5.930		0.03	0.02776	8.038	41.667	47.854
15	1.35	1.4751	8.481		0.08	0.06896	16.009	16.875	21.391
20	1.125	1.072	4.944		0.23	0.24612	6.549	4.891	4.356

Table 5-2: Comparisons of aerodynamic coefficient using SST k- ω model with experimental values: NACA 63-415

AOA (α)	C_l				C_d			C_l / C_d EXP	C_l / C_d SST k- ω
	EXP	CFD SST k-ω	% Error		EXP	CFD SST k- ω	% Error		
-5	-0.25	-0.2326	7.480		0.015	0.0149	0.671	-16.667	-15.6107
0	0.3	0.3297	9.028		0.01	0.01139	12.203	30.00	28.95259
5	0.8	0.8691	7.951		0.015	0.01581	5.123	53.33	54.97154
10	1.25	1.2486	0.112		0.03	0.03148	4.701	41.667	39.66328
15	1.35	1.4524	7.050		0.08	0.08028	0.349	16.875	18.09168
20	1.125	1.1658	3.499		0.23	0.23062	0.269	4.782	5.055069

5.1.2 Discussion

A convenient way of validating the CFD results with the corresponding experimental data is to plot the values of lift and drag coefficients against AOAs. The lift coefficient comparisons are performed on the variation of lift with respect to AOA. Figure 5-1 clearly shows the increment in lift with increasing AOA. For all the AOAs considered good agreement between the CFD results and an existing experimental measurement are observed especially for angle of attack prior to stall. An increasing trend of lift coefficient curve with AOA up to an angle of 15^0 is observed, after which the lift coefficient curve decreases. Since the airfoil section is cambered the lift coefficient is not zero at zero angle of attack. The zero lift coefficient lies between -3^0 to -2^0.

Comparison of the results of the turbulence models S-A and SST k- ω with experimental measurement, the SST k- ω model most accurately determines the lift and drag characteristics of the airfoil, NACA 63-415. Figure 5-1 also shows how the S-A model and SST k- ω model both give fairly similar trend for the lift coefficient prior to stall angle. With regards to the drag coefficient Figure 5-2 clearly shows that the SST k- ω model also gives a better match to the experimental measurement. As a result, the SST k- ω turbulence model has been chosen for the main analysis.

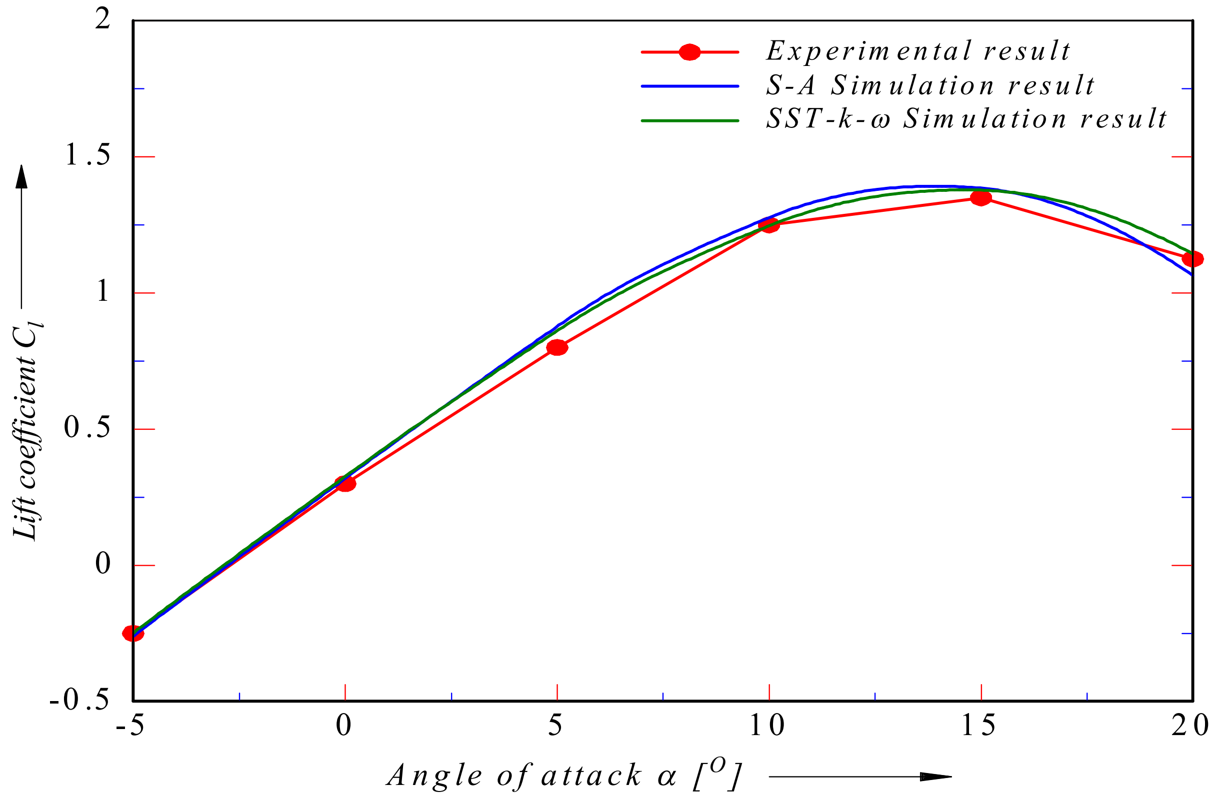

Figure 5-1: Comparison of experimental and computed results of lift coefficient.

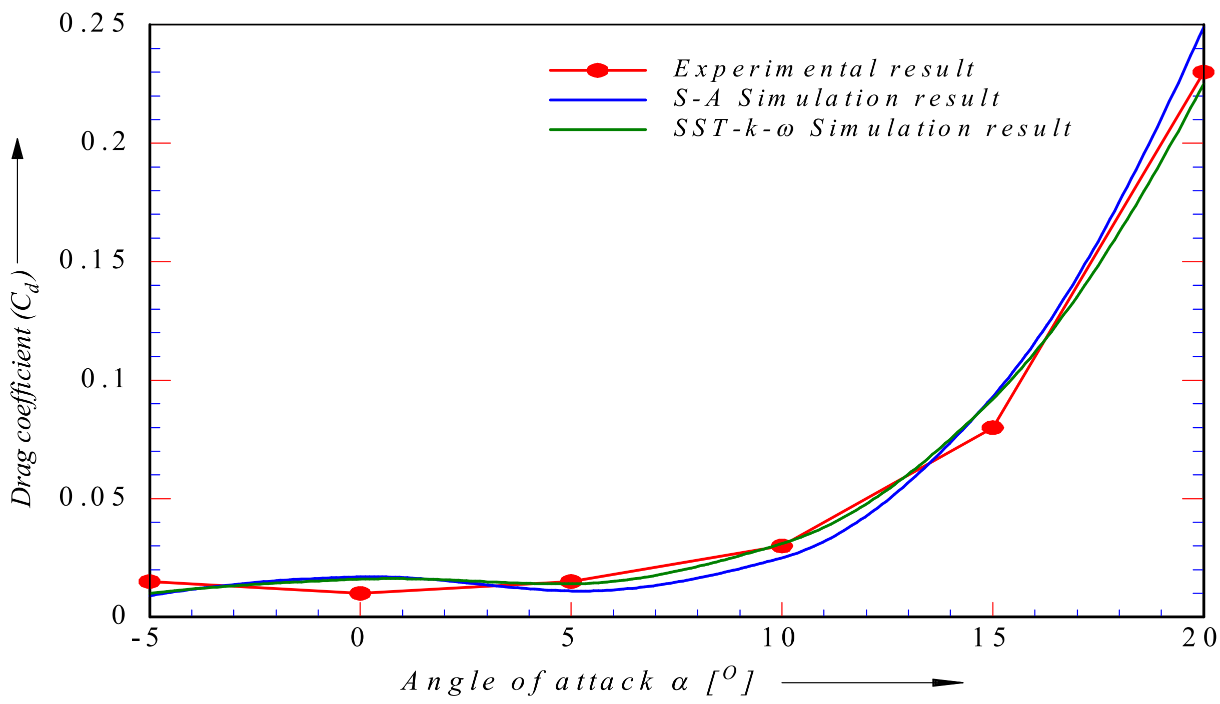

Figure 5-2: Comparison of experimental and computed results of drag coefficient.

The other way of validating the numerical result is plotting the lift to drag (C_l/C_d) ratio, which is shown in Figure 5-3. This ratio increases from zero at around -3^0 to a maximum value at a moderate AOA and then decreases relatively as the angle of attack is further increased. The maximum C_l/C_d value of around 5^0 is derived from the lift and drag characteristics as shown in the Figure 5-3. This is the optimal relationship between lift and drag and the most efficient lift generation for an airfoil is possible. Here, the maximum C_l/C_d ratio is around 54.203 in S-A model while it is around 55 in the SST k- ω model and this value is around 53.33 in the experimental measurement case.

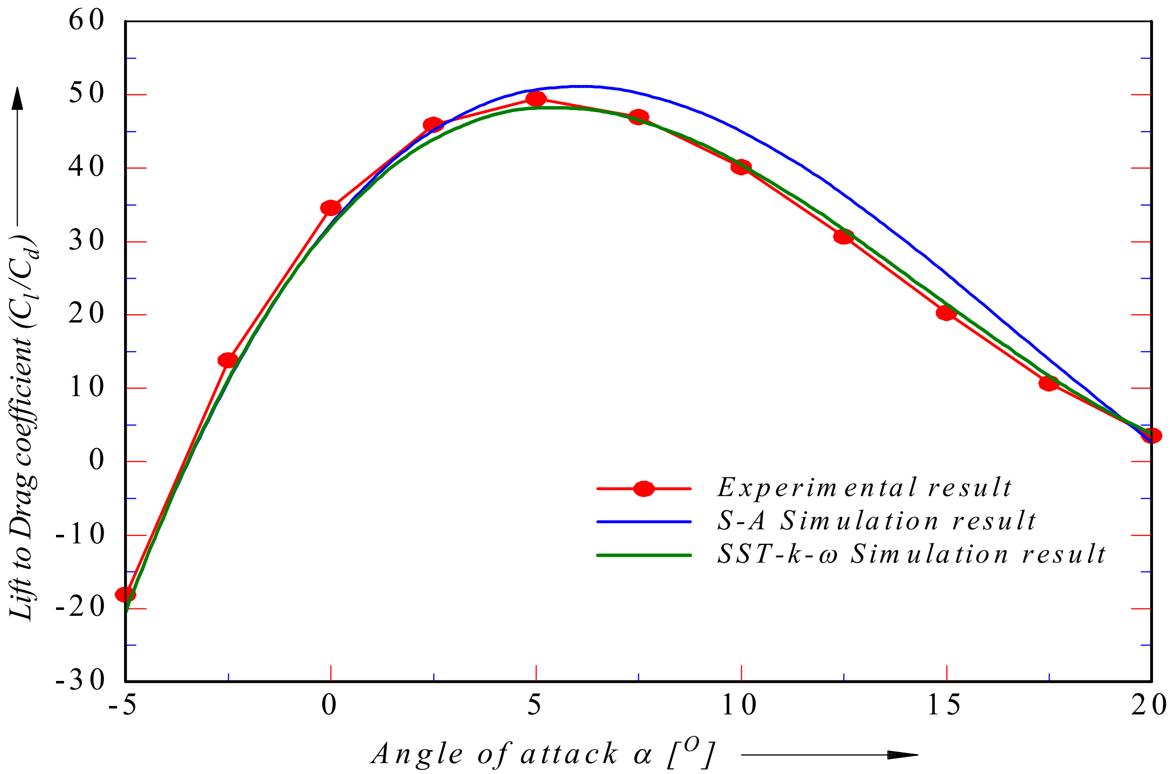

Figure 5-3: Comparison of experimental and CFD result of lift to drag ratio

The deviation of the experimental values and accuracy of the computed lift and drag coefficients are validated against the corresponding experimental values and verified in terms of their percentage deviation. The majority of the deviations are considerably less than 12 % in both S-A and SST k- ω models in the calculation of lift coefficient. However, some important discrepancies are also observed in the calculation of drag coefficient. In the SST k- ω model the maximum deviation observed is less than 12% which is less than 16 % in the S-A model. These differences between the results are likely a result of the turbulence model used in the solver. The other factor responsible for the discrepancy for the result is probably the flow region which is not properly resolved with the RANS approximation, inappropriate boundary layer mesh. Figure 5-4 and Figure 5-5 show the maximum percentage deviation of the models in the calculation of lift and drag coefficients respectively.

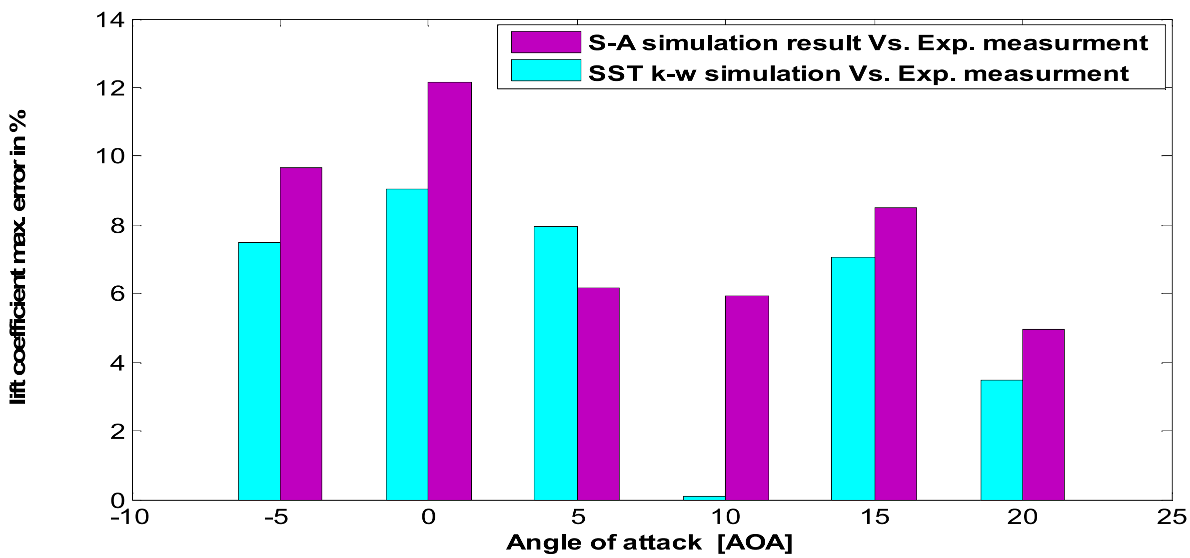

Figure 5-4: S-A and SST k- ω model with experimental result max. Error in % for lift

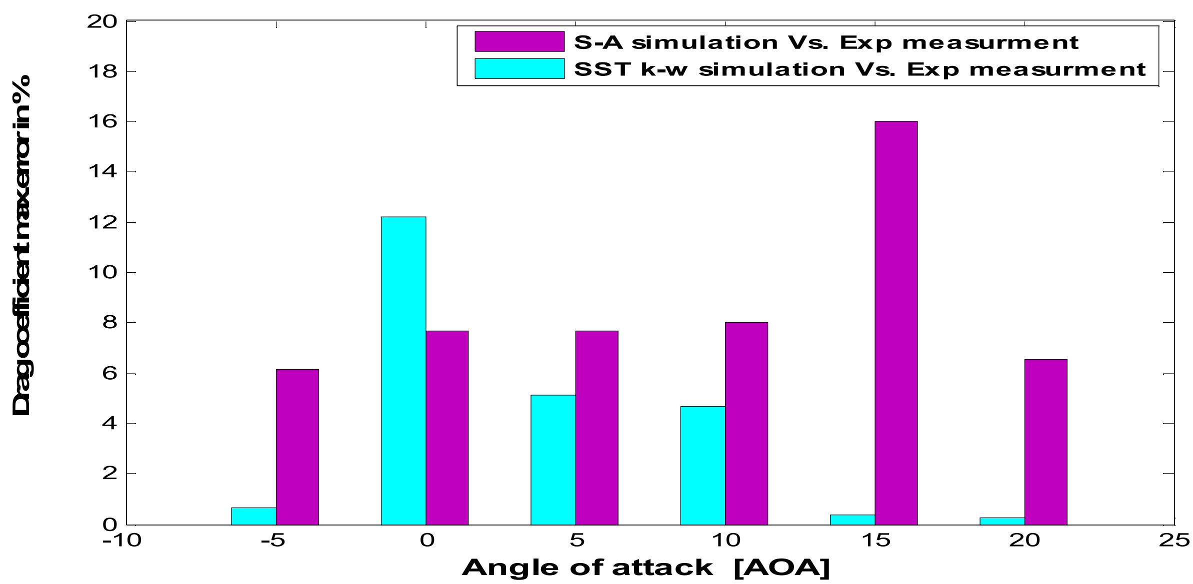

Figure 5-5: S-A and SST k- model with experimental result max. Error in % for drag

5.1.3 Analysis

Figure 5-1 and Figure 5-2 show the lift and drag coefficients. At this range of angle of attacks, calculation was done using two turbulence models S-A and SST k- ω and results are compared with experimental data for the validation of the numerical results.

From Figure 5-1, the lift curve obtained from the simulation is fairly close to the experimental data. At small AOA from -5^0 to 5^0 both curves are almost on top of each other. As AOA increases greater than 5^0, the differences between the curves are beings to grow. However the curve shows a steeper linear increase in both cases. The computed result also show that the airfoil has reached its stall point around 15^0 with maximum lift coefficient (Cl_{max}) value of 1.475 in the S-A turbulence model while it's around 1.45 in the SST k- ω. As far as the experimental data is concerned, the airfoil stalled at earlier AOA of 14^0 and recording a slightly lower Cl_{max} of 1.35. Thus the result from turbulence models shows small over prediction in the calculation of lift coefficients at stall point.

Overall both turbulence models had good agreement with experimental data at angle of attack even at small negative angles, the same trend of curve was observed at all angle of attack. However, small discrepancy was observed between the CFD curve and the experiment. It's a well-known fact that lift coefficient are reduced and drag coefficients increased as angle of attack increased above stall point, as shown in Figure 5-1 and Figure 5-2. Accordingly the determined drag coefficients were show an error of 16 % in the S-A and 12 % in SST k- ω than the experiment. The discrepancy in the drag coefficient, obtained from simulation is due to the fact that the flow over the actual airfoil is mostly dominated by laminar flow. However, the turbulent models S-A and SST k- ω is assumed the flow as fully turbulent over the surface of the airfoil and does not provide a transition from laminar to turbulent flow. This assumption has the potential of causing some error between the simulation result and experimental data. A turbulent boundary plays a substantial effect in the prediction of drag coefficients, thus the error between the simulation and the experiment can be noticed in the comparison of drag coefficient.

In conclusion, by comparing the simulation results and available experimental data for the force coefficients (lift and drag) values through Figure 5-1 and Figure 5-2, it can be concluded that the CFD solution is providing sufficiently accurate results for a majority of the AOAs. The discrepancy in calculating in lift and drag values comes from limitations in the turbulence model behavior and the majority of the lift and drag curves match the experimental data in both models. However, the most well agreed model was the SST k- ω model. As a result, the SST k- ω turbulence model has been chosen for the main analysis of the case study discuss below.

5.2 Case Study of Adama I Wind Turbine Airfoil

The case study discussed here is to predict aerodynamic performance parameters of wind turbine airfoil that all the major technical specification is given in Table 5.4 below.

5.2.1 Project Description

The physical model taken for this numerical calculation is the Adama wind farm project which has capacity of generating 51 MW, 3 blades and 34 sets of 1500kW GOLDWIND (GW) horizontal axis upwind wind turbines , located in the middle part of Ethiopia, about 3.91 Km North West of Nazareth. The project was constructed and starts operation in year 2011/ 2012. The objective of the project is utilizing the wind power to generate electricity, which had connected to the national grid in order to add 162.7MWh energy per year **[6].**

5.2.2 Manufacturer Technical Specifications of GW77/1.5 Wind Turbine

Table 5-3: Technical specifications for GW 77 /1.5 wind turbine **[6]**

Parameters	**GW77**	
	IEC class	**IIA**
Operational parameters	Rated power	1500kW
	Cut in wind speed	3m/s
	Rated wind speed	11.1 m/s
	Cut out wind speed(10min)	22m/s
	Survival wind speed (3min)	59.5m/s
	Design life time	≥ 20 years
	Operating ambient temperature	-30° C to +40° C
	Stand by ambient temperature	-40° C to +50° C
Rotor	Nominal diameter	77m
	Number of blades	3
	Blade airfoil type	LM 37.3P or similar
	Aerodynamic profile, modified NACA and others	NACA 63-4xx and fx 77/79

	Blade length ,nominal	37.25m
	Root chord /max. chord	3097mm
	Twist at root chord	11.4^0
	Center line	30%

According to the feasibility report of Adama Wind Park the design average wind speed of the site at the WTG hub height of 65m is 9.56 m/s. However, the extreme wind speed with a return period of 50 years is extrapolated to the hub height are 31.39 m/s. The calculated long term average temperature is 21.2^0C and the atmospheric pressure of the site is 853.3hPa (85330Pa), the air density of the site at hub height range from 0.959- 0.973 kg/m^3. However, for this simulation 0.97 kg/m^3 is considered **[6] [38].**

The present study utilized CFD solver; FLUENT to predict the aerodynamic performance parameters while fluid with density of 0.97 kg /m^3 flows over the horizontal axis wind turbine (HAWT) airfoil. The aerodynamic performance parameters of the airfoil for average wind speed of 9.56 m/s (corresponding to Reynolds number of 6.1 x 10^5 and Mach number of 0 .028) were predicted. The aerodynamic profile of the airfoil from UIUC Airfoil Coordinates Database NACA 63-415 airfoil is considered. These coordinates point are given on Appendix A.

The model used for this case study is the same as the validation described in the above sections in all the way. The FLUENT solution set up was also identical, however the only difference in the solution set up is the input parameters such as velocity, temperature, pressure, and density etc. Since there is no experimental data available with the same conditions as the selected site, validation of the CFD results and verification of model for different conditions for the NACA 63-415 is required. The conditions for the simulations as well as associated properties are given in Table 5-4.The calculations were all done with average speed of 9.56m/s flow with SST k-w two equations turbulence model.

An evaluation scheme is presented to compute the airfoil lift, drag and pitching moment for the range of angles of attack in order to predict the parameters.

5.2.3 Fluent Analysis Parameters

Table 5-4: Computational conditions of two-dimensional simulation

Parameter	Value
Fluent Version	2ddp
Solver	Pressure based / segregated solution
Simulation type	Steady simulation
Formulation	Implicit
Turbulence model	SST k-w
Airfoil profile	NACA 63-415
Fluid material	Air
Flow type	Incompressible flow
Temperature	294.2 k
Kinematic viscosity	1.52 x 10 -5 Kg /m.s
Density	0.97 kg/m^3
Pressure	85330 pa
Average wind speed	9.56 m/s
Reynolds number	6.1×10^5
Mach number	0 .028
CFD algorithm	SIMPLEC
Interpolating scheme	Pressure (Standard) Momentum (Second Order Upwind) Modified Turbulent Viscosity (Second Order Upwind)
Boundary condition	Velocity Inlet and Pressure Outlet Stationary wall with no slip condition
Initialization	Inlet Values
Force monitors	Lift , Drag and moment coefficients
Reference values	Inlet Values
Convergence limit	10^{-6}

5.2.4 Results and Discussion

All the information gathered in terms of the lift, drag and moment characteristics results from the pressure and velocity distributions over the surface of the airfoil at a given set of operating conditions are discussed. An angle of attack range from -5^0 to $20^{\ 0}$ is selected, with an interval of 5^0 between each simulation. The computed results and the NACA 63-415 findings at the given conditions are compiled.

Figure 5-6 to Figure 5-9 has four plots showing the lift, drag, moment and lift to drag coefficients curves plotted. Generally, the lift and moment coefficients are plotted as function of angle of attack, while the drag coefficients are plotted as a function of lift coefficients. However, all the performance coefficients in this report are plotted as a function of angle of attack. In Table 5.5, the results obtained from the simulation are tabulated.

Table 5- 5: Simulation result of NACA 63-415 airfoil using SST k- ω model at average wind speed of 9.56 m/s

α	C_l	C_d	C_m	C_l/ C_d
-5	-0.2285	0.02815	0.07941	-8.1172
0	0.2942	0.0256	0.0605	11.4921
5	0.8026	0.03549	0.03925	22.6148
10	1.241	0.05587	0.01356	20.2123
15	1.3596	0.15456	0.021229	8.7965
20	0.8877	0.27912	0.00799	3.1803

The plot in Figure 5-6 shows the variation of lift coefficient with AOAs. There is a range of angle of attack where the lift coefficient varies linearly. The lift coefficient is negative at negative angle of attack until it achieves the zero angle of attack and then increases with increasing AOA. The lift coefficient is zero when angle of attack at around -3^0. The lift coefficient keeps increasing until it reaches the critical angle of attack, point at which maximum lift coefficient attain. The critical angle of attack is around 15^0 and the maximum lift coefficient recorded at this angle of attack is around 1.3596. A further increase in AOAs beyond these AOA causes a decrease in the lift coefficient.

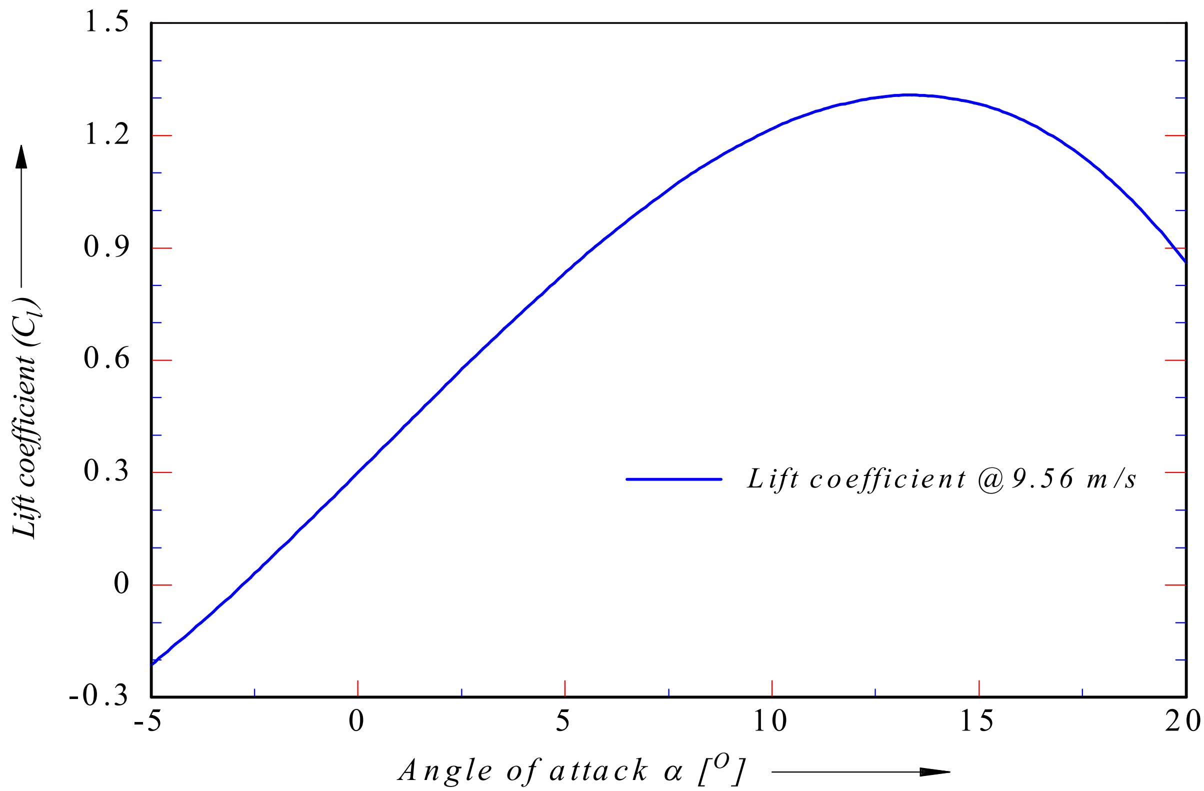

Figure 5-6: CFD result of C_l vs. AOA for - NACA 63-415 @ 9.56 m/s

Figure 5-7 shows the variation of drag coefficient with AOAs. The values of drag coefficient increase with the angle of attack. However, the drag coefficient values are in a low for the angle of attack from -5^0 to 10^0 before it rises exponentially. In the same way, before the airfoil achieves the critical angle of attack the lift coefficient values are rises linearly then after the lift coefficient achieves its maximum value and then after this point the airfoil is called stalled.

Figure 5-8 shows the variation of pitching moment coefficient which is almost always decreasing as the angle of attack increases. Rapid change occurs in this coefficient at stall region. A negative pitching moment coefficient corresponds to a nose down force acting on the airfoil while a positive pitching moment corresponding to a nose up force.

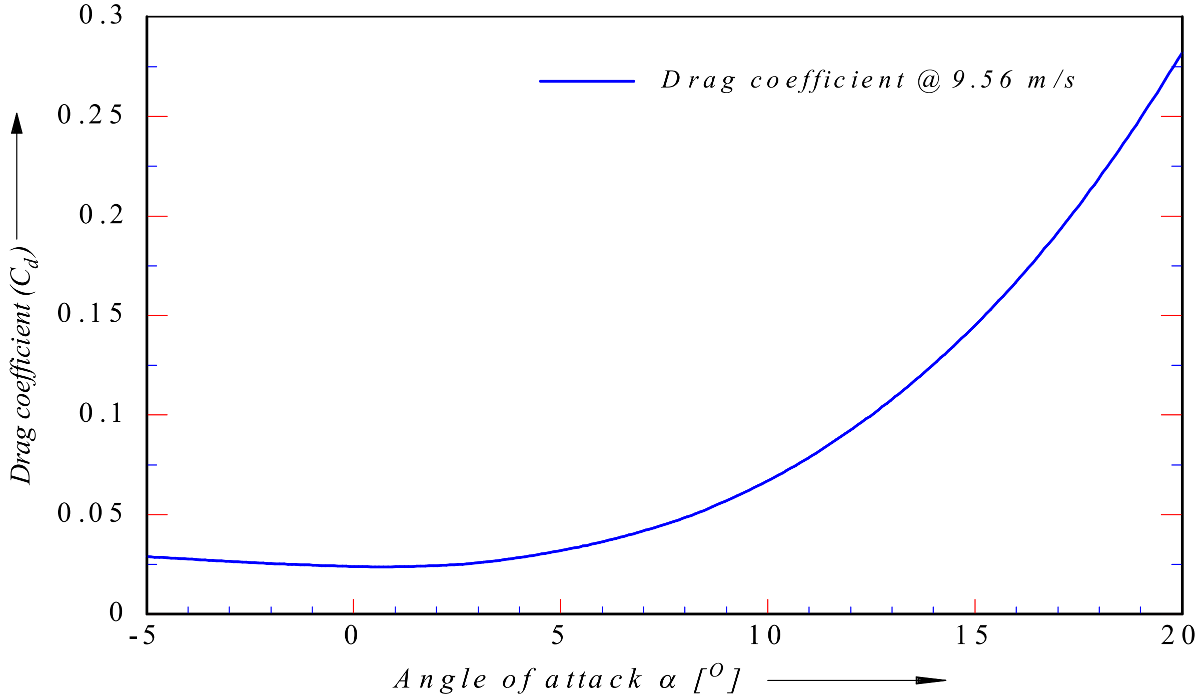

Figure 5-7: CFD result of C_d vs. AOA for - NACA 63-415 @ 9.56 m/s

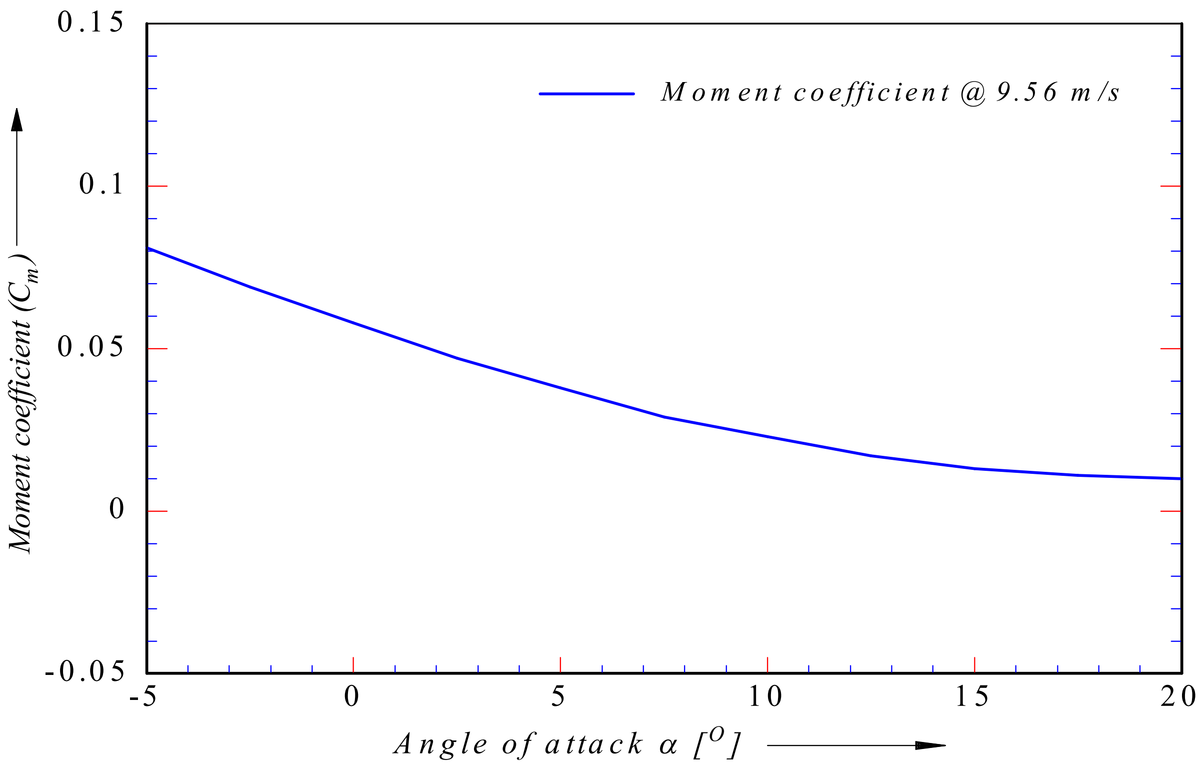

Figure 5-8: CFD result of C_m vs. AOA for - NACA 63-415 @ 9.56 m/s

The maximum lift to drag ratio of an airfoil is another important performance parameter to characterize the airfoil. The optimum angle of attack is where lift to drag (C_l/C_d) coefficient has the maximum value. Figure 5-9 shows the lift to drag ratio plot obtained from the lift and drag data, for angle of attack ranging from -5^0 to 20^0. From the curve the optimum angle of attack of the airfoil is around 5^0. At this point lift to drag ratio value is 22.

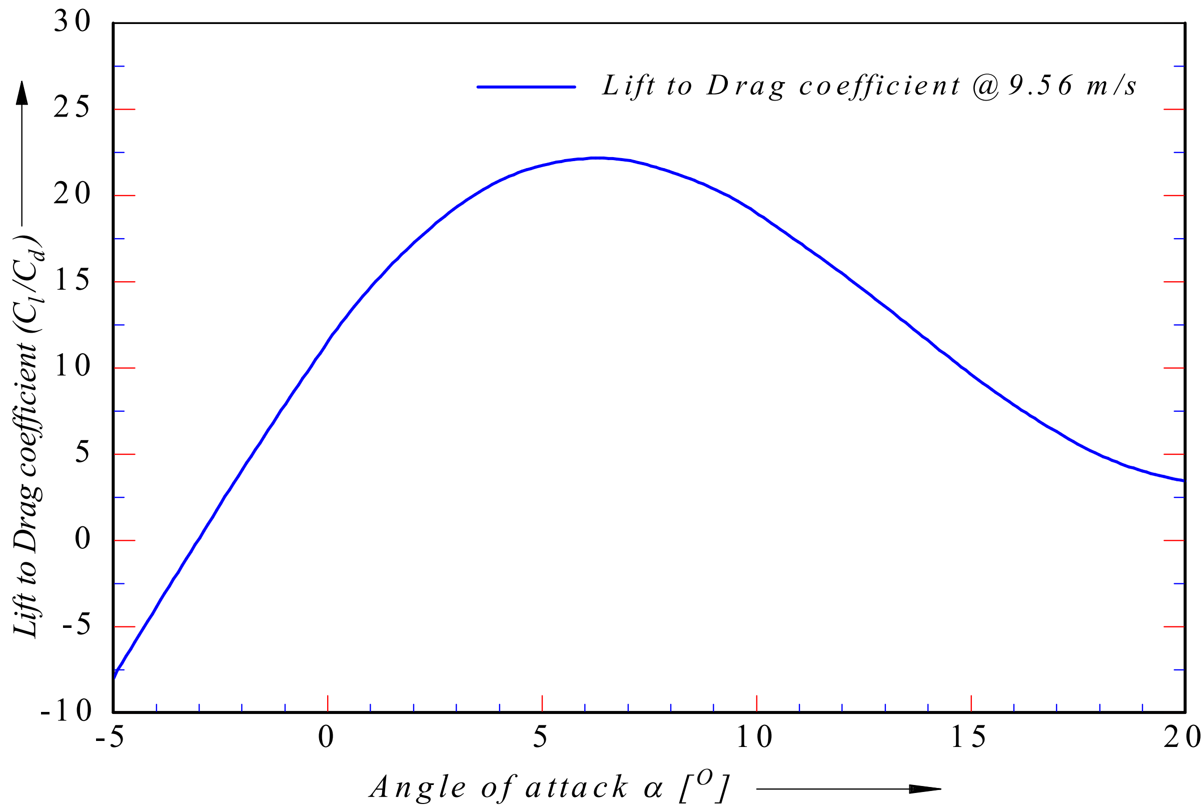

Figure 5-9: CFD result of C_l/C_d vs. AOA for - NACA 63-415 @ 9.56 m/s

5.2.5 Post – processing Results

Flow passing over an airfoil surface is not always the same. Related to the effect such as velocity flow over the surface, air ambient pressure, air density, viscosity, etc., flow has different characteristics. As a result, velocity and pressure distributions over an airfoil surface are different. When the flow passes over the upper surface of the airfoil, flow velocity is greater than the free-stream velocity; the pressure over the upper surface is negative. On the other hand, flow velocity decreases when it is passing on the lower surface of airfoil and as a result, pressure on this surface increases. Hence, both the negative pressure over the upper and the positive pressure under the lower surface contribute to the lift. Moreover, friction between air and airfoil surface exists and air flow velocity decreases when it reaches to airfoil surface.

At angle of attack between zero lift and stalling angles, the total pressure pushing down on the airfoil upper surface will always be less than the total pressure pushing up on the lower surface. The absolute pressure difference pushing up on the lower surface will increase as angle of attack increases create large region of flow separation over the upper surface causing what is known as the stall effect. Any pressure output plots over an airfoil appearing above the atmospheric static pressure regarded as a positive pressure whereas pressure below the atmospheric is a negative pressure.

5.2.5.1 Contour plot of static pressure distribution

Figure 5-10 to Figure 5-15 show pressure distribution plots. Figure 5-11 shows the result from 0^0 attack angle and it shows the stagnation point (maximum pressure) at the leading edge of the airfoil. Increasing the attack angle to 5^0, 10^0, 15^0 and 20^0 shows a dramatic change in the pressure distribution plot. It is evident from the contours plots there is region of very large low pressure on the upper surface of airfoil as compared to the bottom surface of the airfoil. The largest pressure differences from the free stream value are at the leading edge and the difference tapper off toward the trailing edge and the stagnation point has moved to the lower surface as angle of attack increased. Figure 5-10 to Figure 5-15 show the simulation results of static pressure for angles of attack -5° to 20° with 5° increments using SST k- ω model.

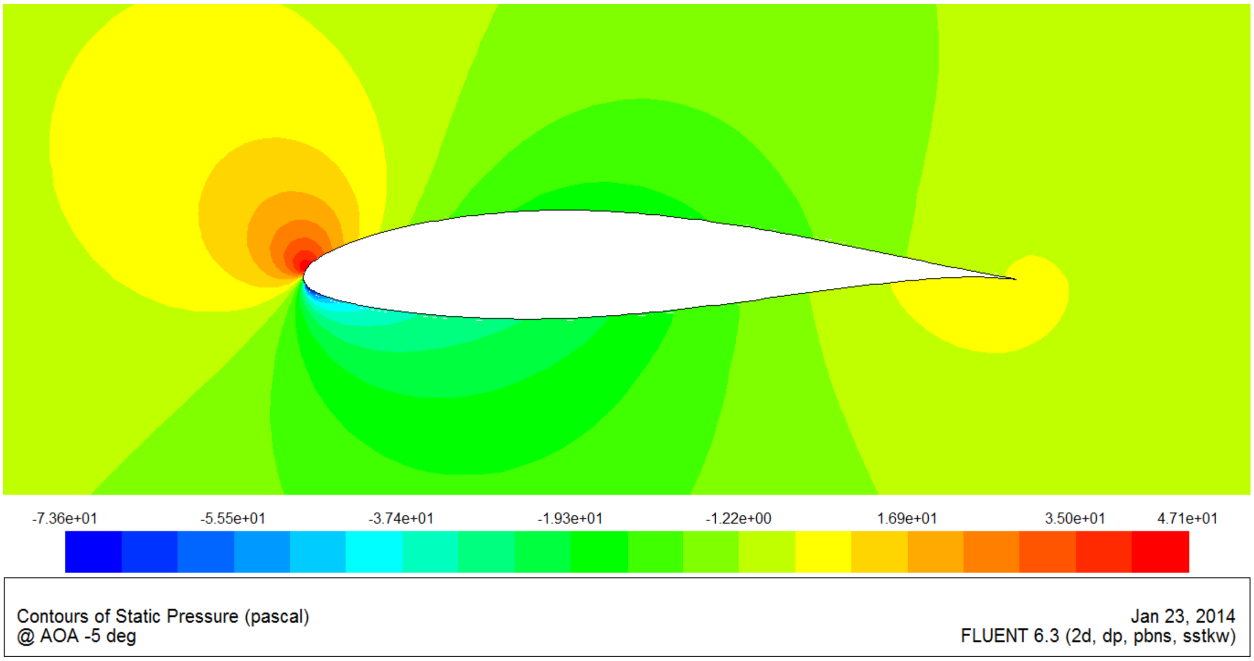

Figure 5-10: Contour of static pressure at - 5° AOA with the SST k- ω turbulence model

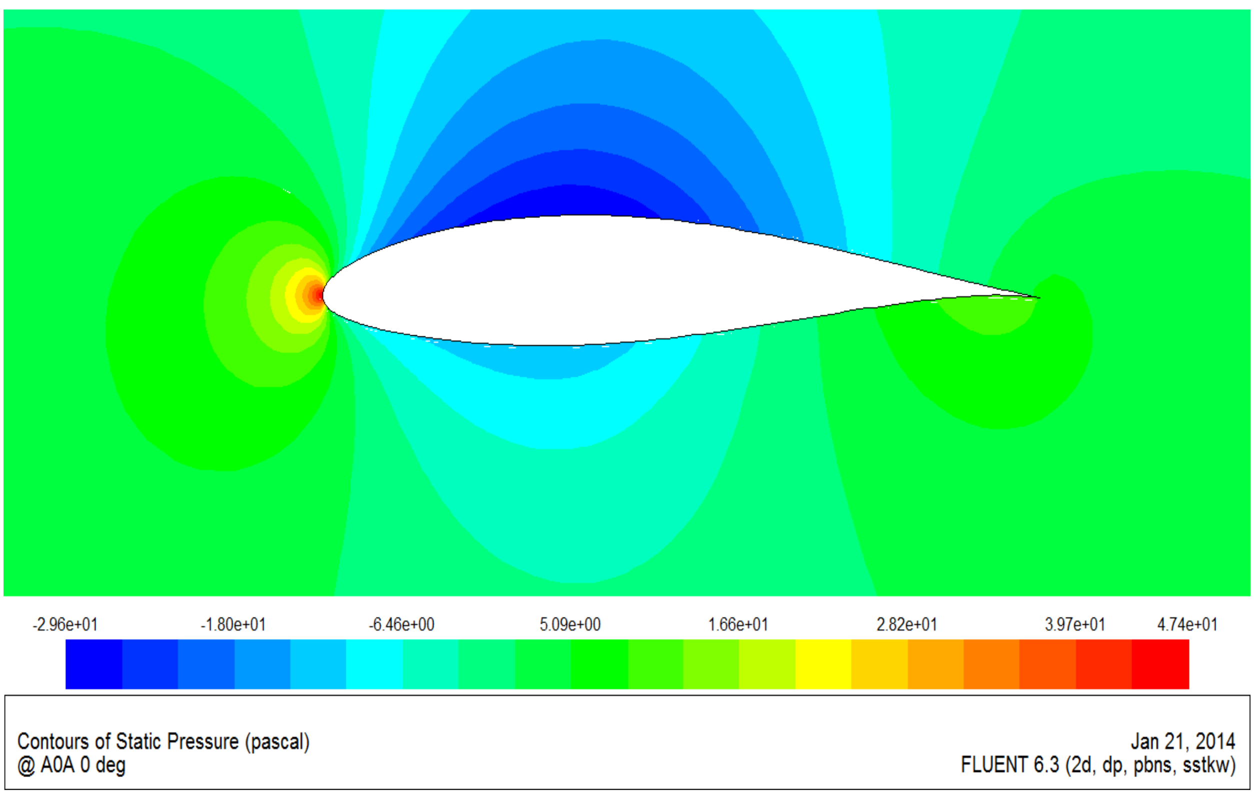

Figure 5-11: Contour plot of static pressure at 0° AOA using SST k- ω turbulence model

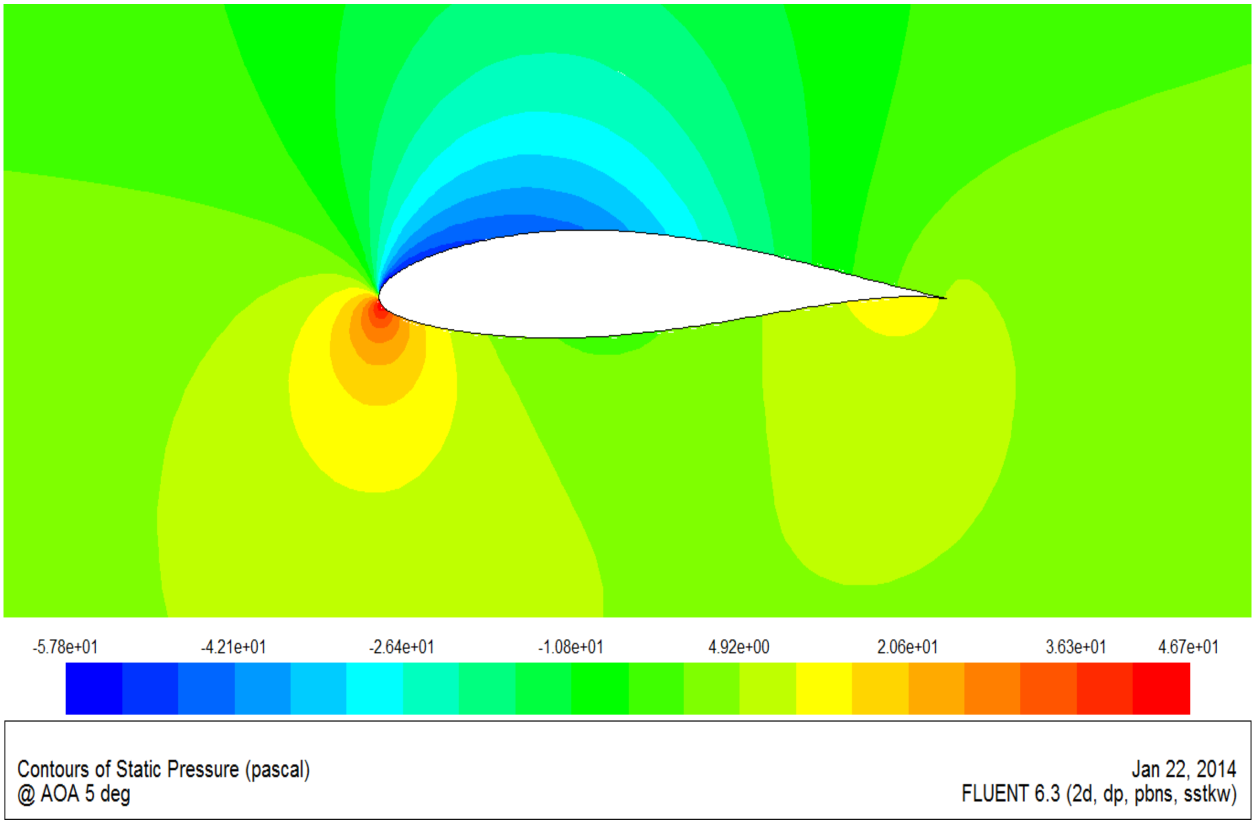

Figure 5-12: Contour of static pressure at 5° AOA with the SST k- ω turbulence model

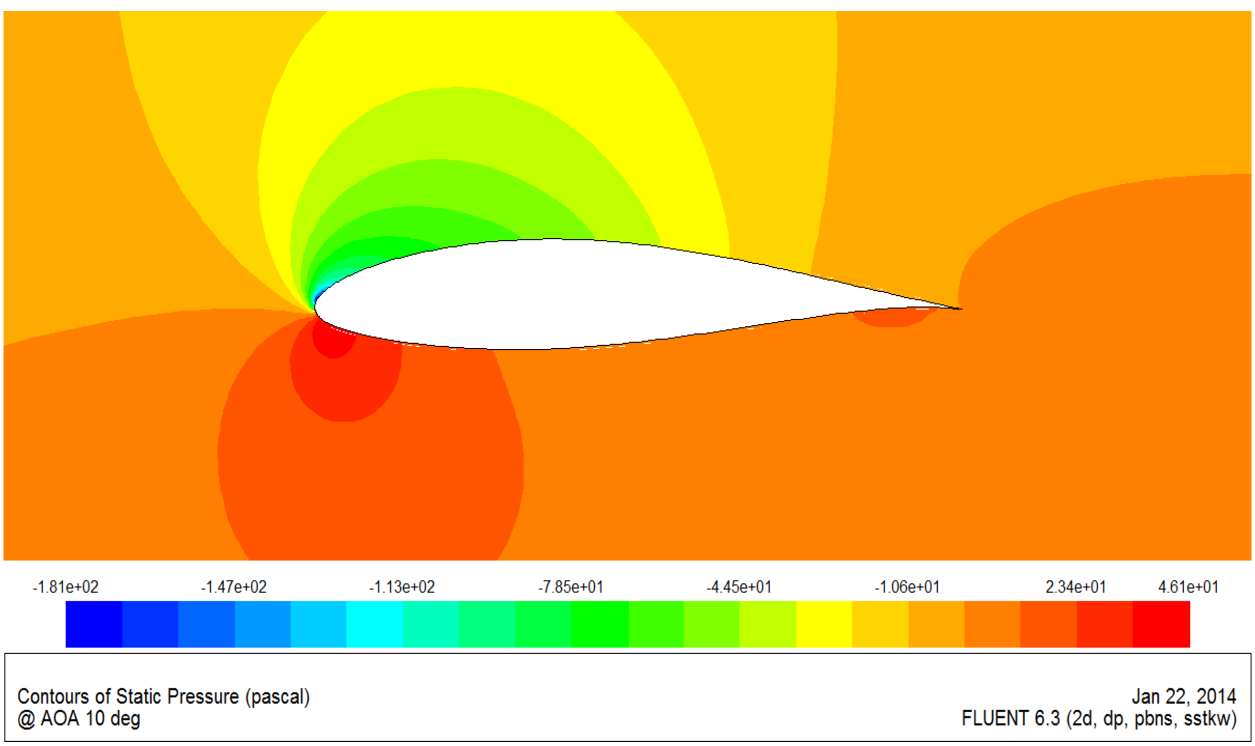

Figure 5-13: Contour of static pressure at 10° AOA with the SST k- ω turbulence model

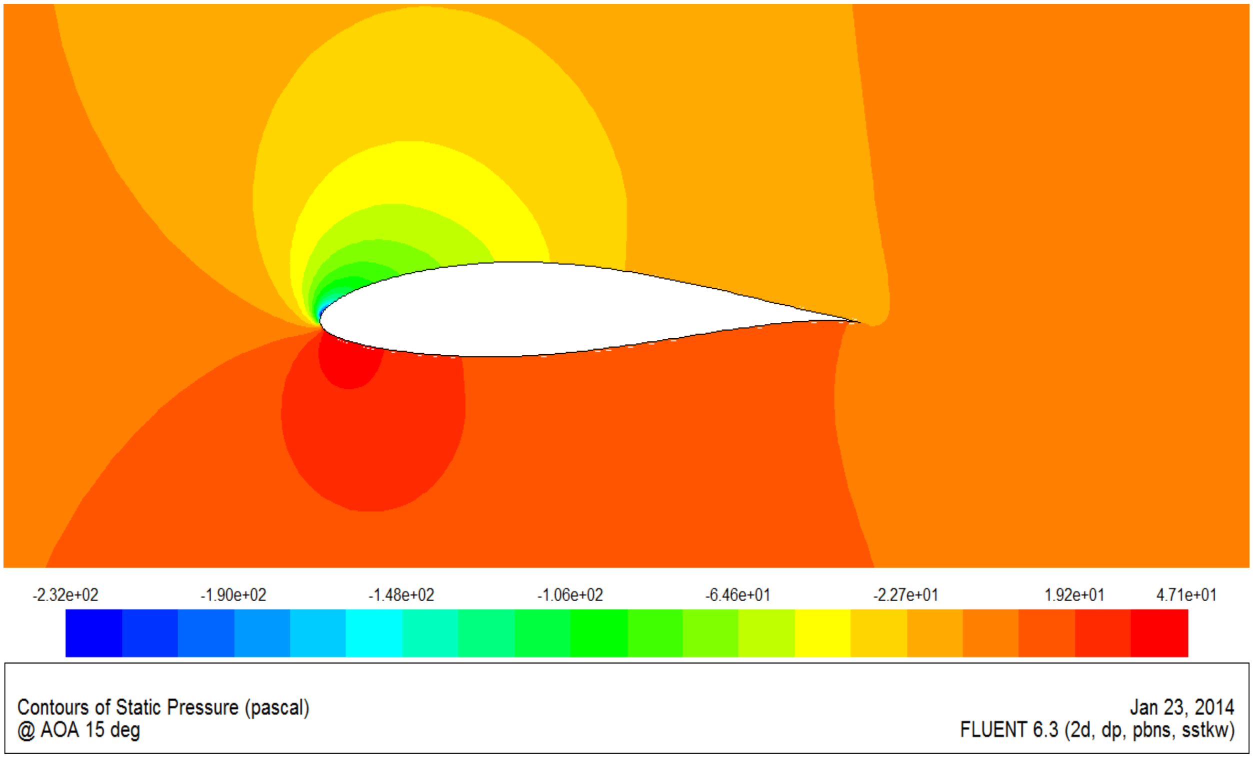

Figure 5-14: Contour of static pressure at 15° AOA with the SST k- ω turbulence model

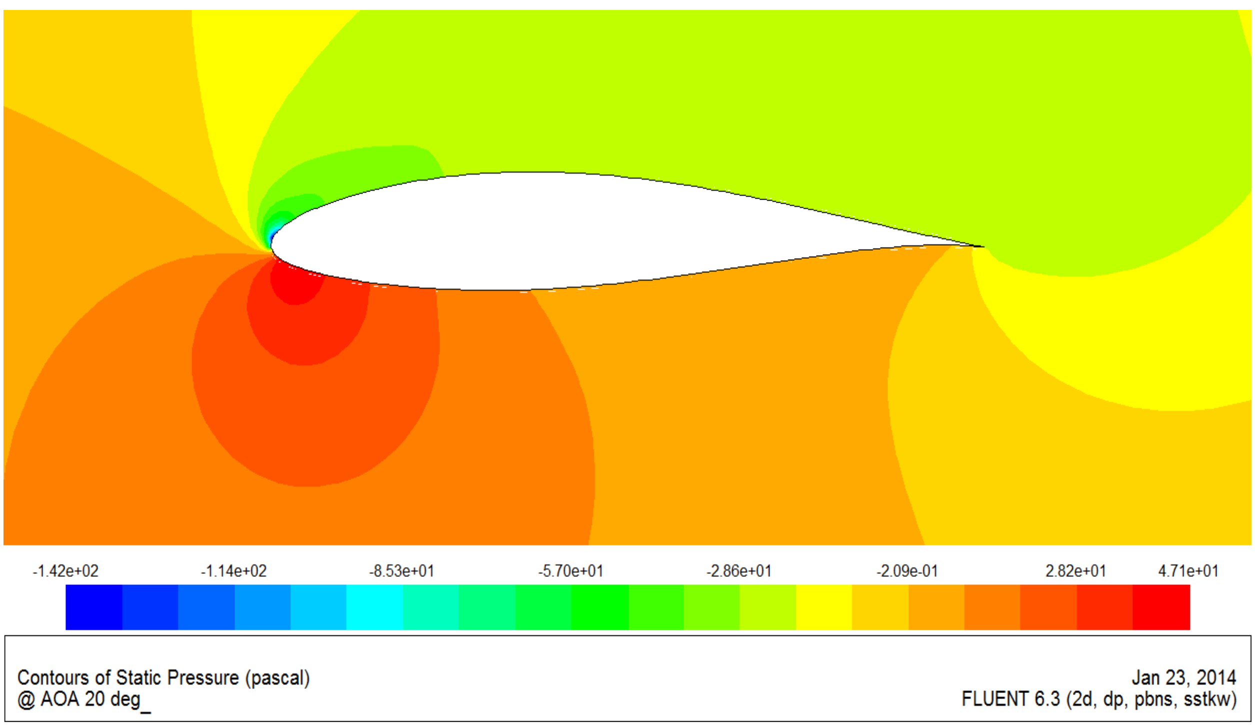

Figure 5-15: Contour of static pressure at 20°AOA with the SST k- ω turbulence model

5.2.5.2 Contour plot of velocity distribution

Figure 5-16 to Figure 5-21 show the velocity contours developed around the NACA 63-415 airfoil. As can be observed, the velocities over the upper surface of the airfoil are substantially higher than the lower surface except for negative angle of attack in this case the condition is reversed.

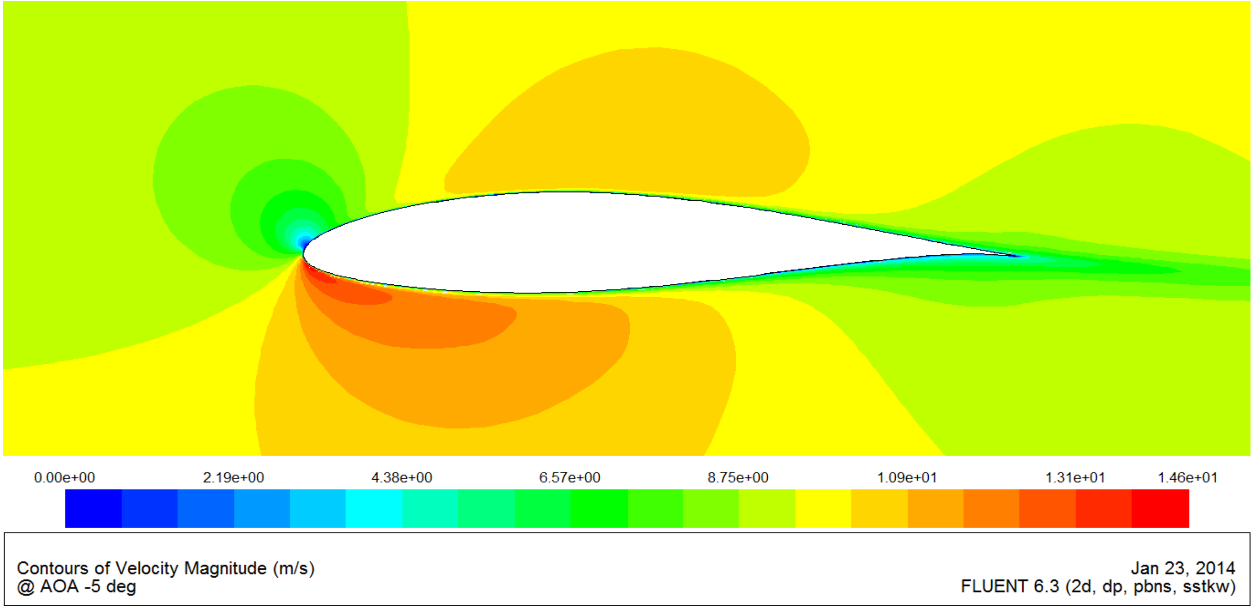

Figure 5-16: Contour of velocity magnitude at -5° AOA with the SST k-ω turbulence model

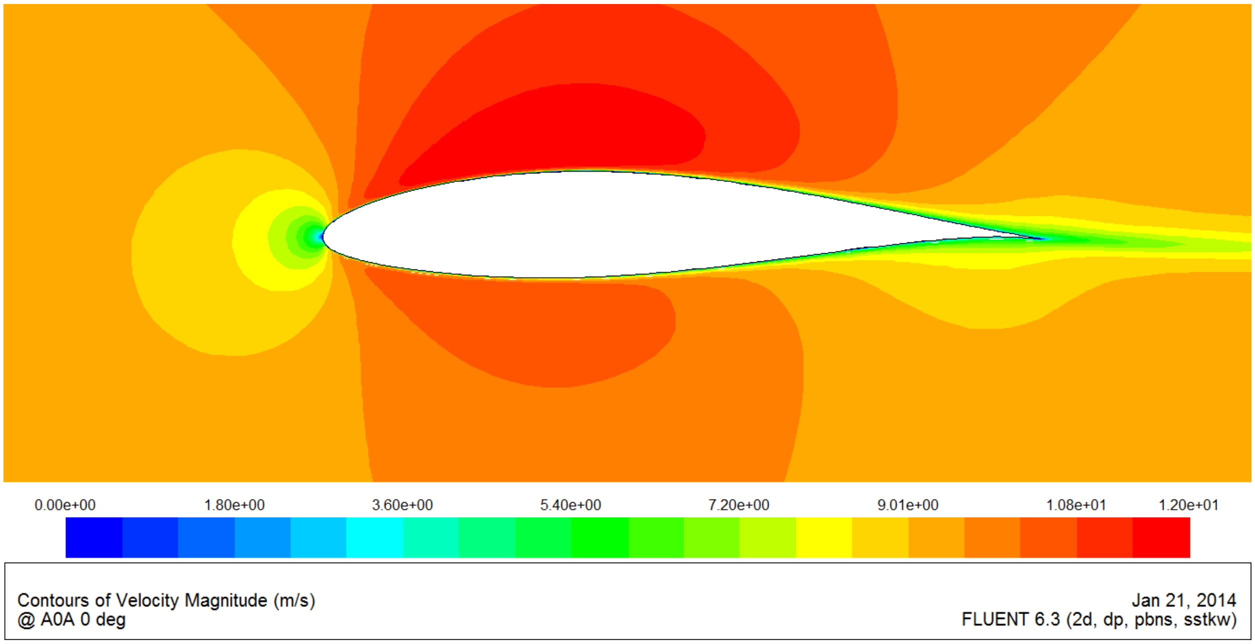

Figure 5-17: Contour of velocity magnitude at 0° AOA with the SST k- ω turbulence model

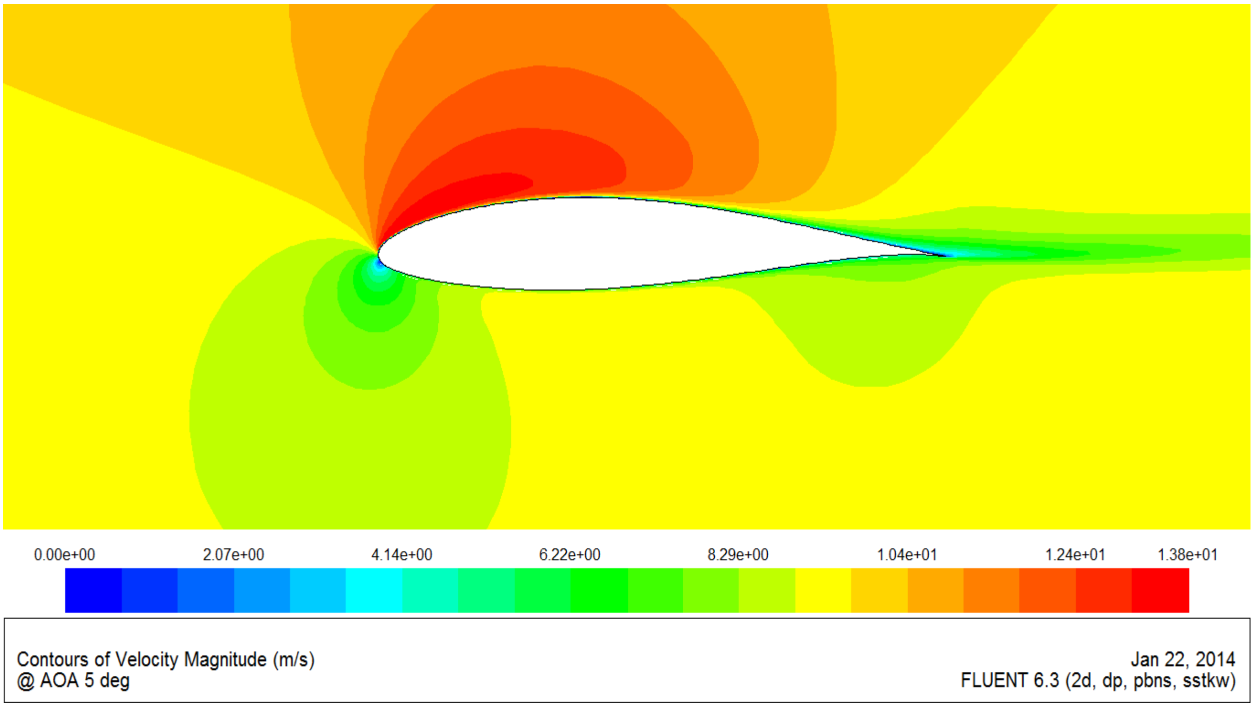

Figure 5-18: Contour of velocity magnitude at 5° AOA with the SST k- ω turbulence model

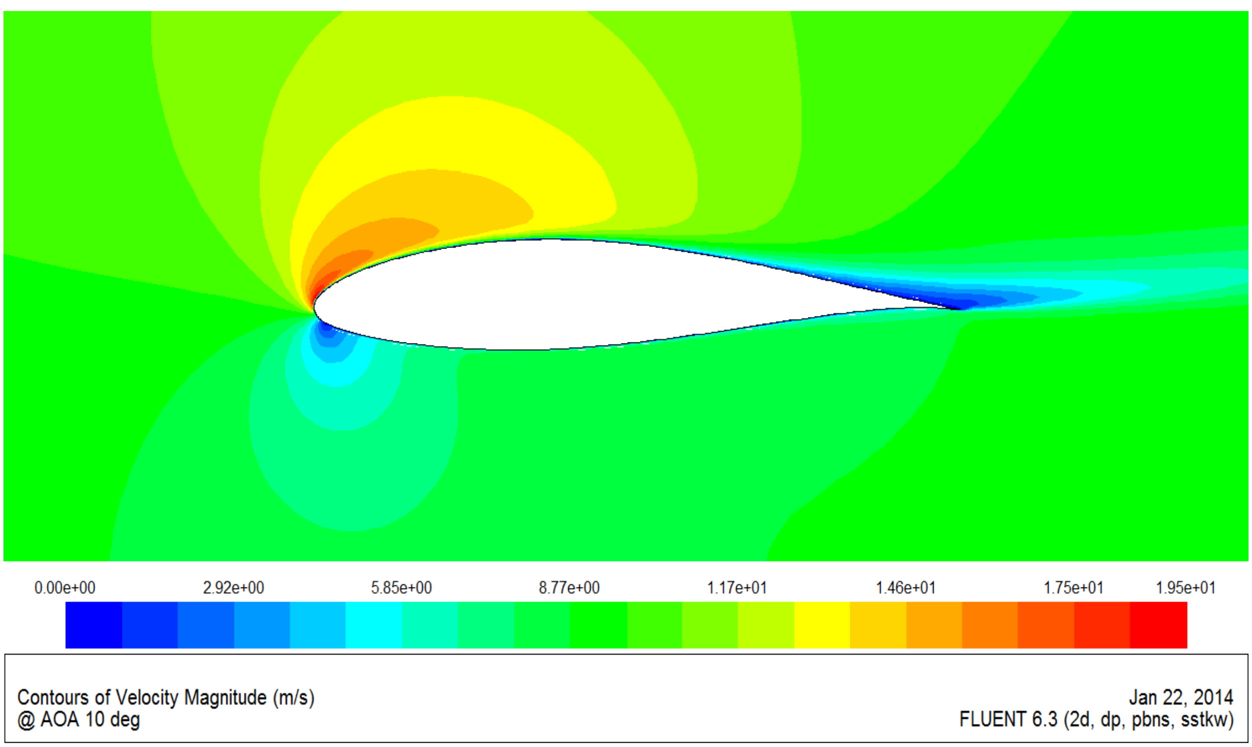

Figure 5-19: Contour of velocity magnitude at 10° AOA with the SST k- ω turbulence model

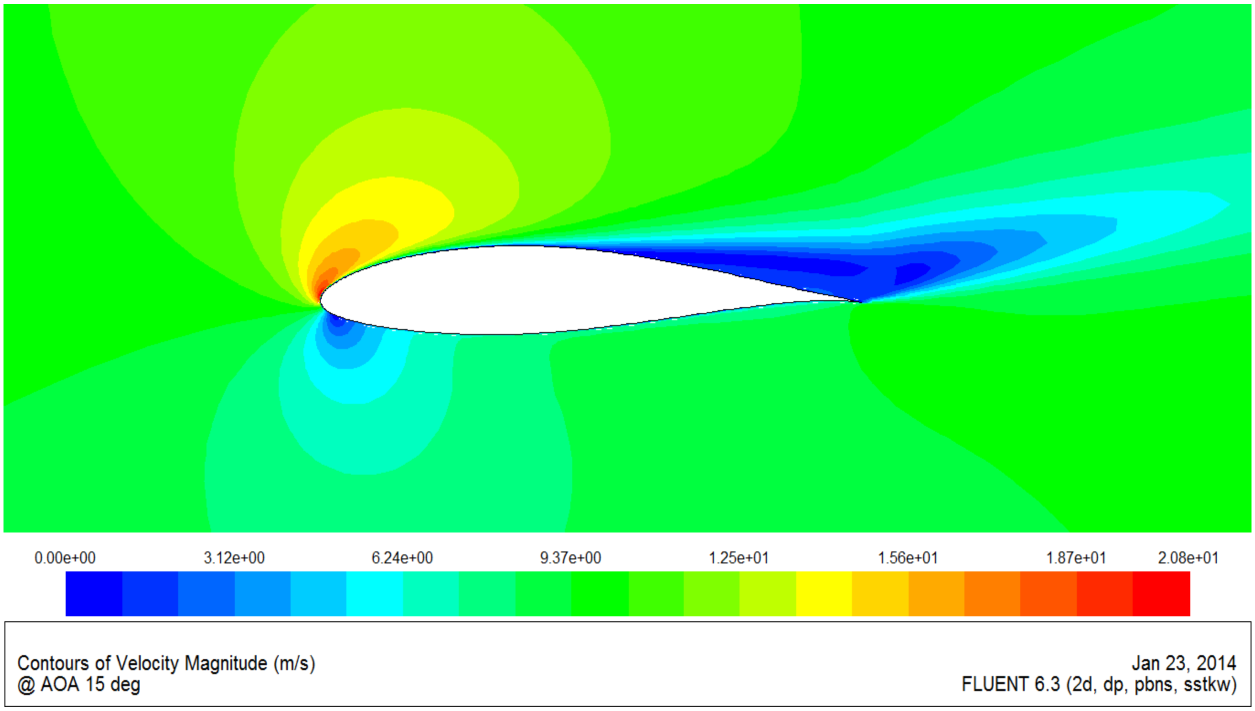

Figure 5-20: Contour of velocity magnitude at 15°AOA with the SST k- ω turbulence model

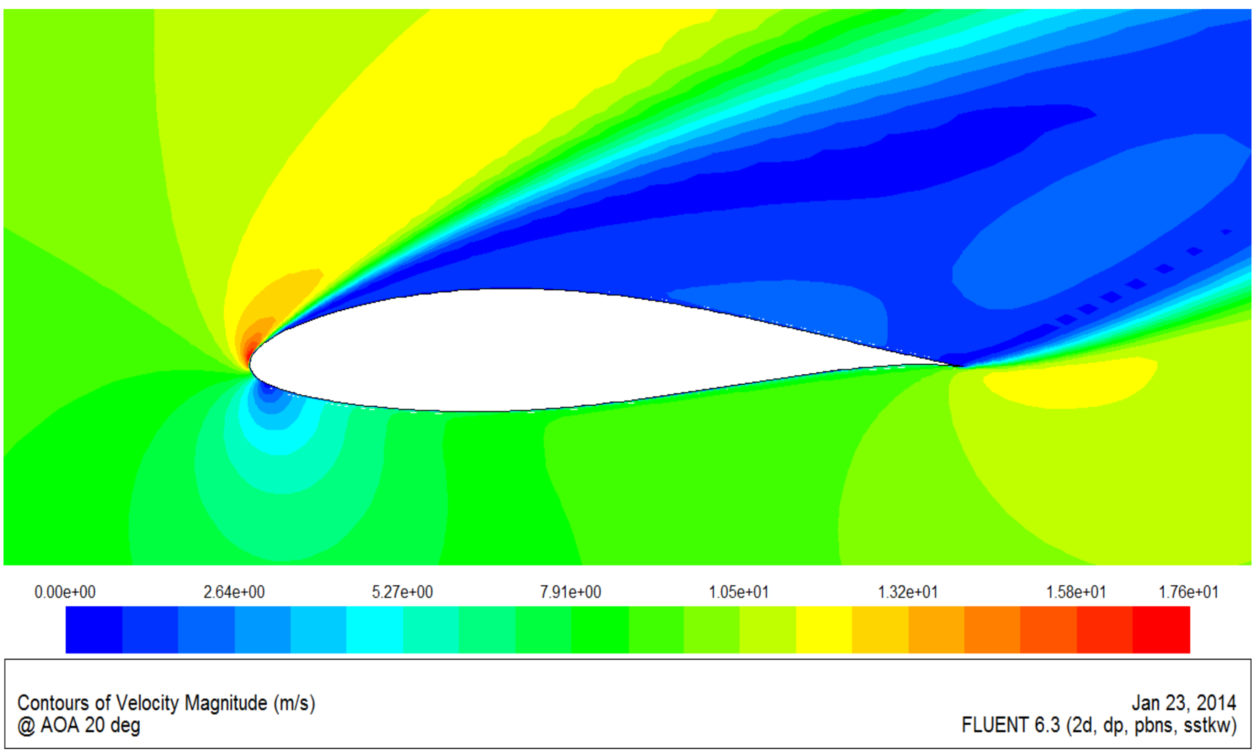

Figure 5-21: Contour of velocity magnitude at 20°AOA with the SST k- ω turbulence model

5.2.5.3 Contour plot of velocity streamlines

At small angles of attack, the boundary-layers that develop on the upper and lower surfaces of the airfoil do not separate; the flow is attached to the airfoil throughout flow. Therefore, there is a thin viscous region on the airfoil surface. An increase on the angle of attack leads to adverse pressure gradients create flow separation with a viscous region of relatively large dimension that leads to the decrease of lift coefficient. The occurrence of flow separation is related to velocity and pressure distribution over the surface of the airfoil. At large angles of attack, the airfoils develop large adverse pressure gradients that cover the complete upper surface of the airfoil. Separation appears close to the trailing edge and separation point moves upstream with the increase of the angle of attack. Figure 5-22 to Figure 5-27 show the velocity vectors, colored by velocity magnitude for different AOAs.

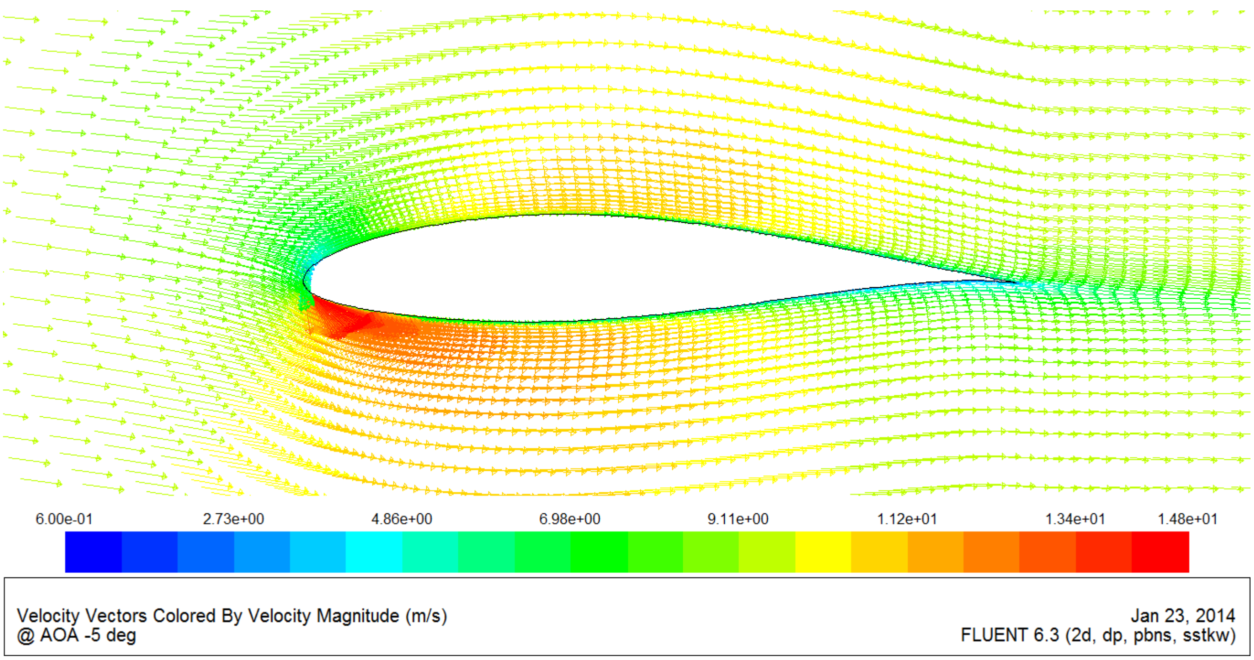

Figure5-22: Velocity vectors colored by velocity magnitude at -5° AOA with the SST k- ω model

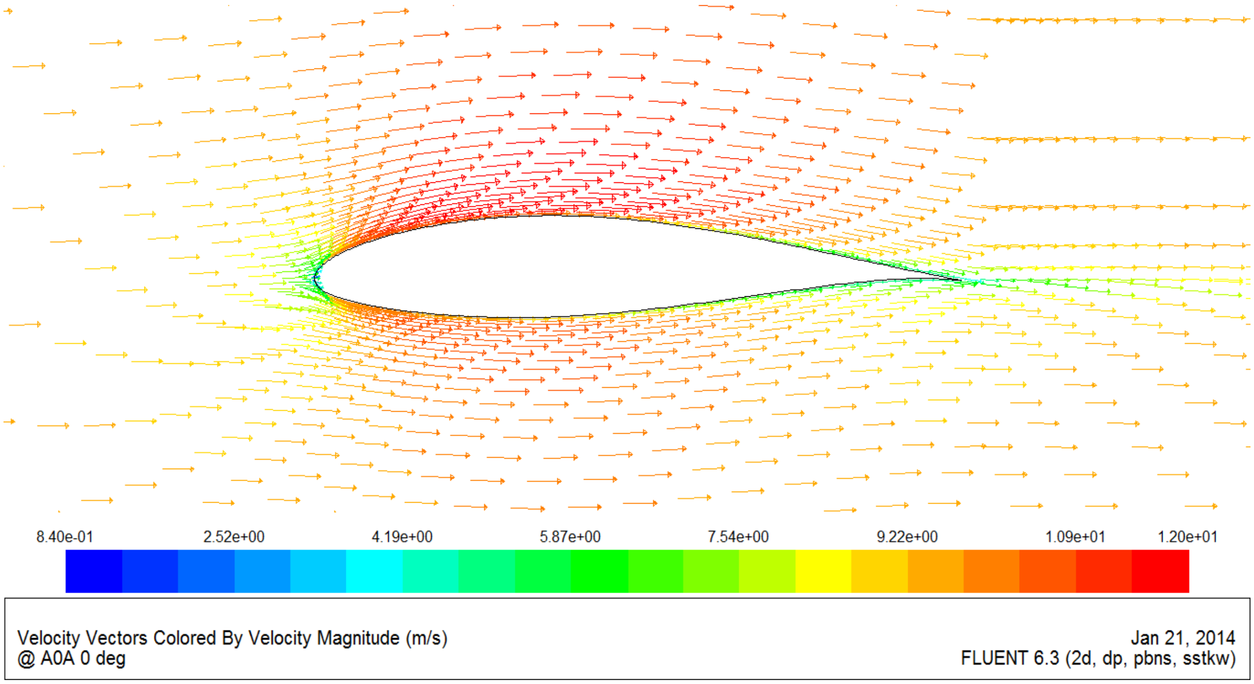

Figure 5-23: Velocity vectors colored by velocity magnitude at 0° AOA with the SST k- ω model

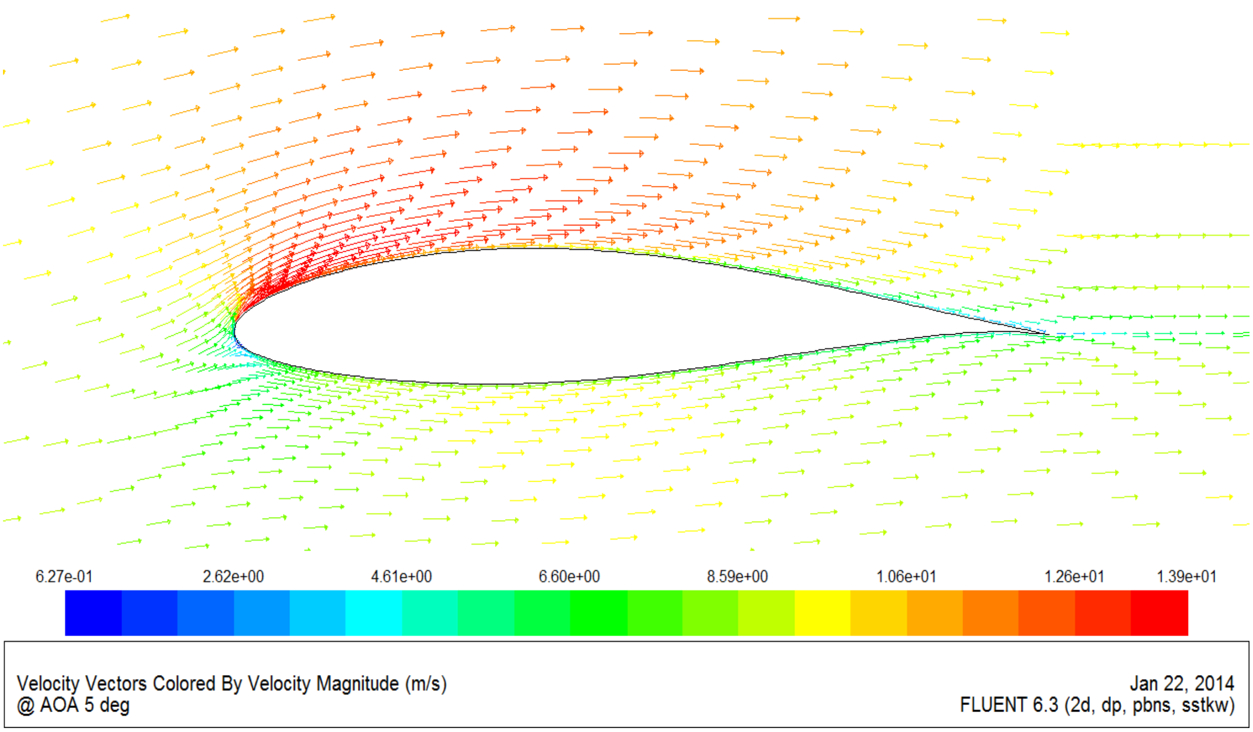

Figure 5-24: Velocity vectors colored by velocity magnitude at 5° AOA with the SST k- ω model

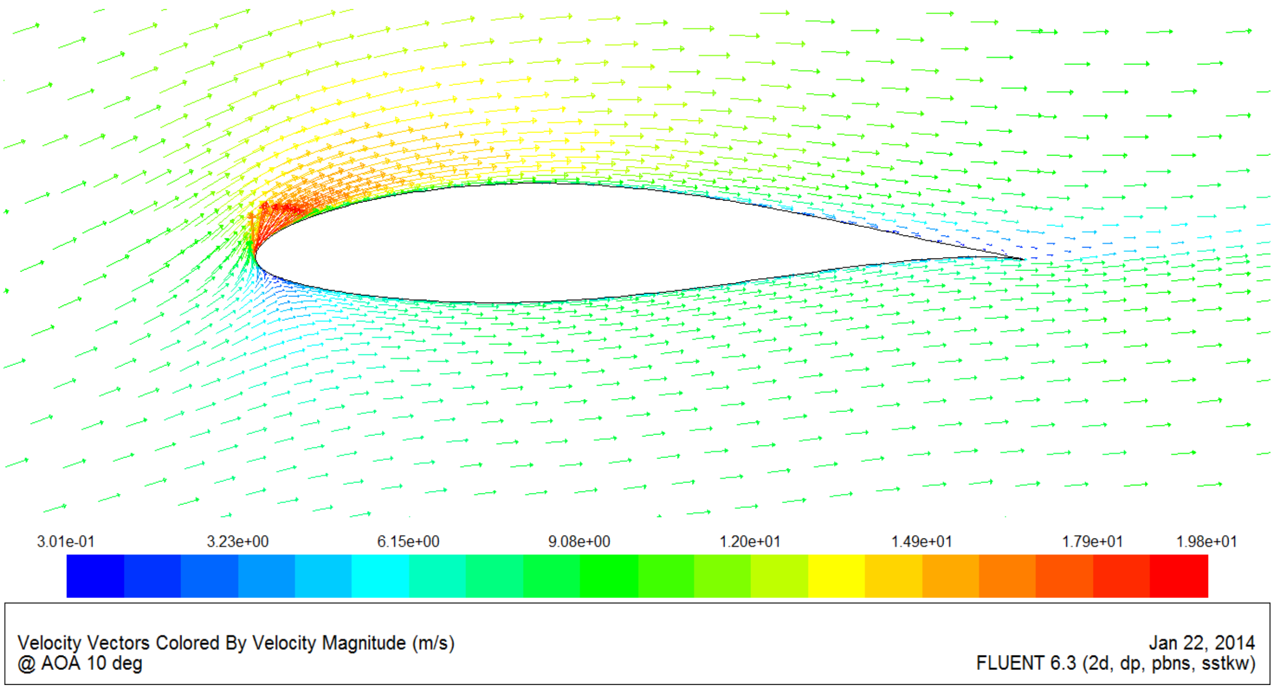

Figure 5-25: Velocity vectors colored by velocity magnitude at 10° AOA with the SST k- ω model

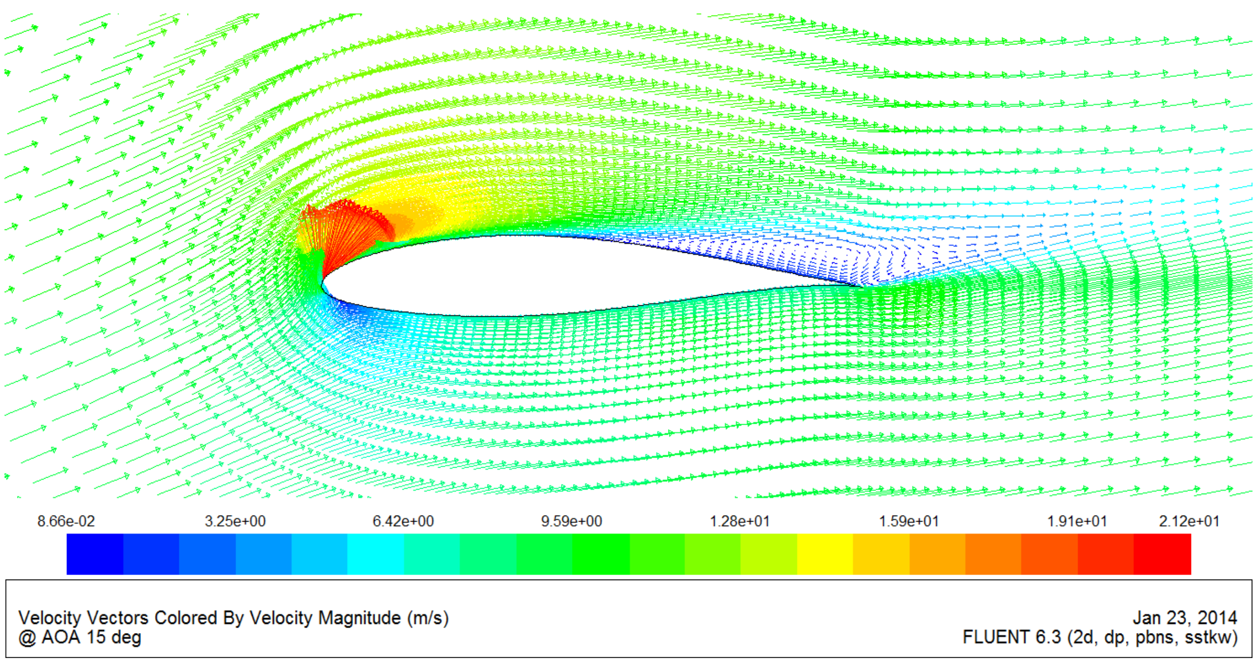

Figure5-26: Velocity vectors colored by velocity magnitude at 15° AOA with the SST k- ω model

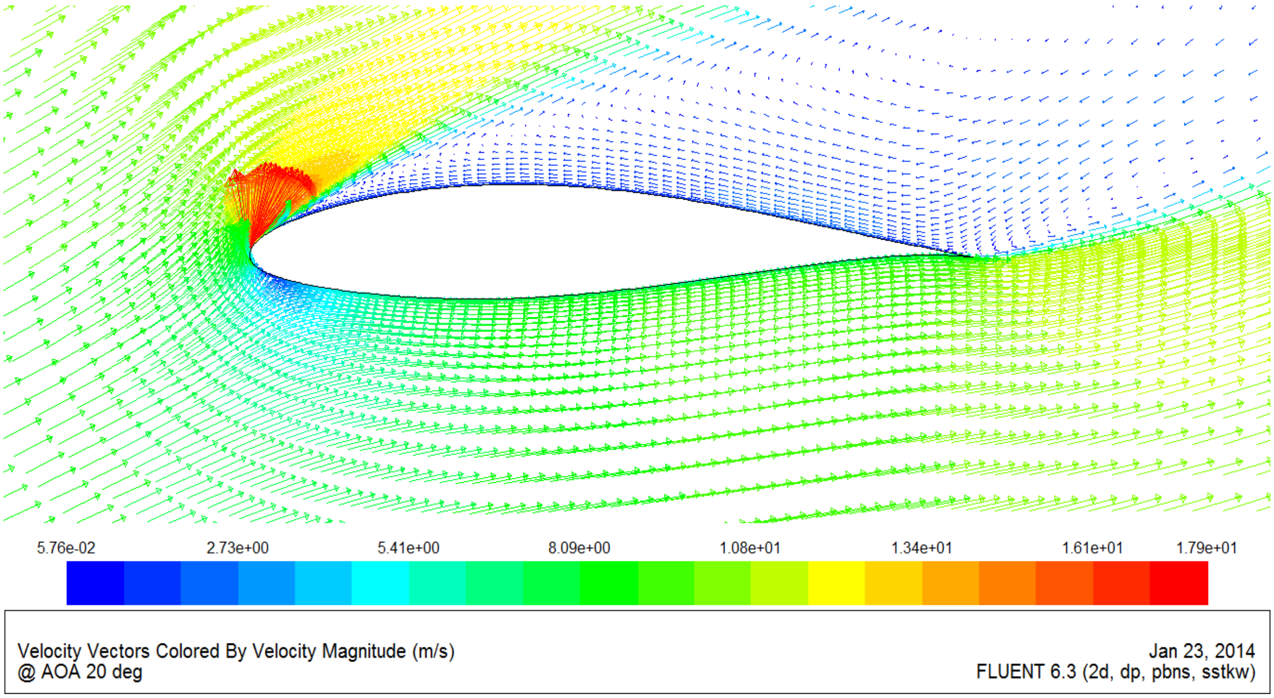

Figure 5-27: Velocity vectors colored by velocity magnitude at 20° AOA with the SST k- ω model

5.2.5.4 X_Y plot of pressure coefficients

Figure 5-28 to Figure 5-33 show the chord wise pressure distribution on an airfoil surface of NACA 63-415. The plot show negative values of C_p in the upper surface and positive values in the lower surface. A negative C_p values indicate pressure is lower than the free stream pressure and the positive values correspond to pressure higher than the free stream. The figures show the chord wise pressure distribution over the upper and lower surface of NACA 63-415airfoil at different angles of attack. The upper curve corresponds to the pressure distribution on the lower surface and vice versa.

From the figures as angle of attack increase there is a large suction peak (large negative value of C_p) is observed near the leading edge on the upper surface, whereas there is a region of increasing adverse pressure gradient (C_p values) to the trailing edge. In lower surface of the airfoil there is a stagnation point (point of maximum pressure) near the leading edge, where Cp value of nearly one (Cp= 1) is observed.

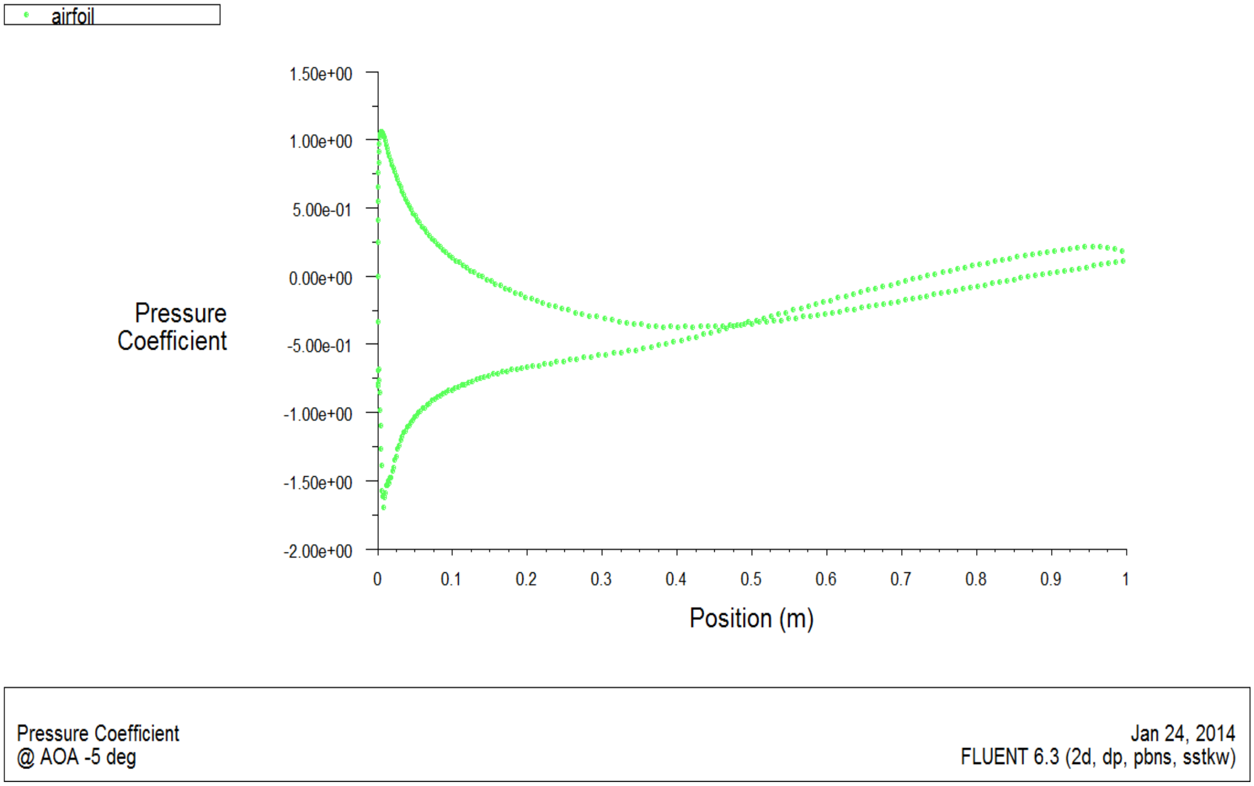

Figure 5-28: Pressure coefficient along the chord line for AOA of - 5^0 using SST k- ω model

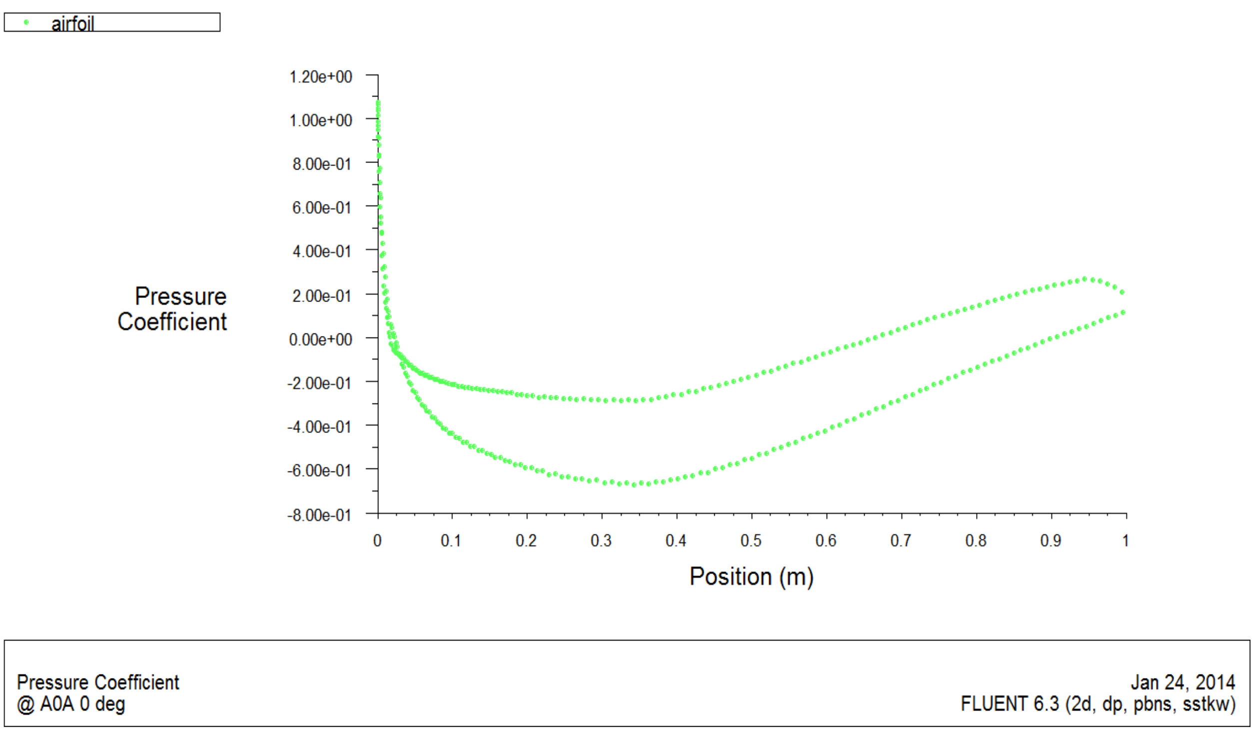

Figure 5-29: Pressure coefficient along the chord line for AOA of 0^0 using SST k- ω model

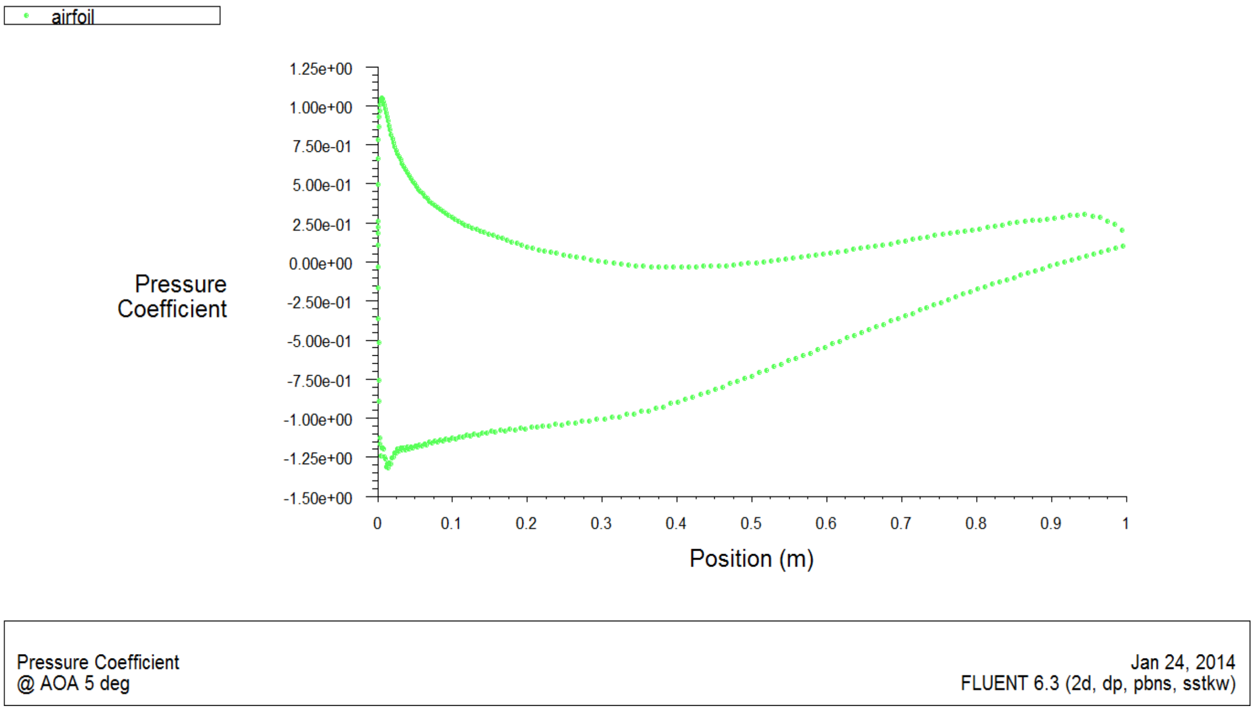

Figure 5-30: Pressure coefficient along the chord line for AOA of 5^0 using SST k- ω model

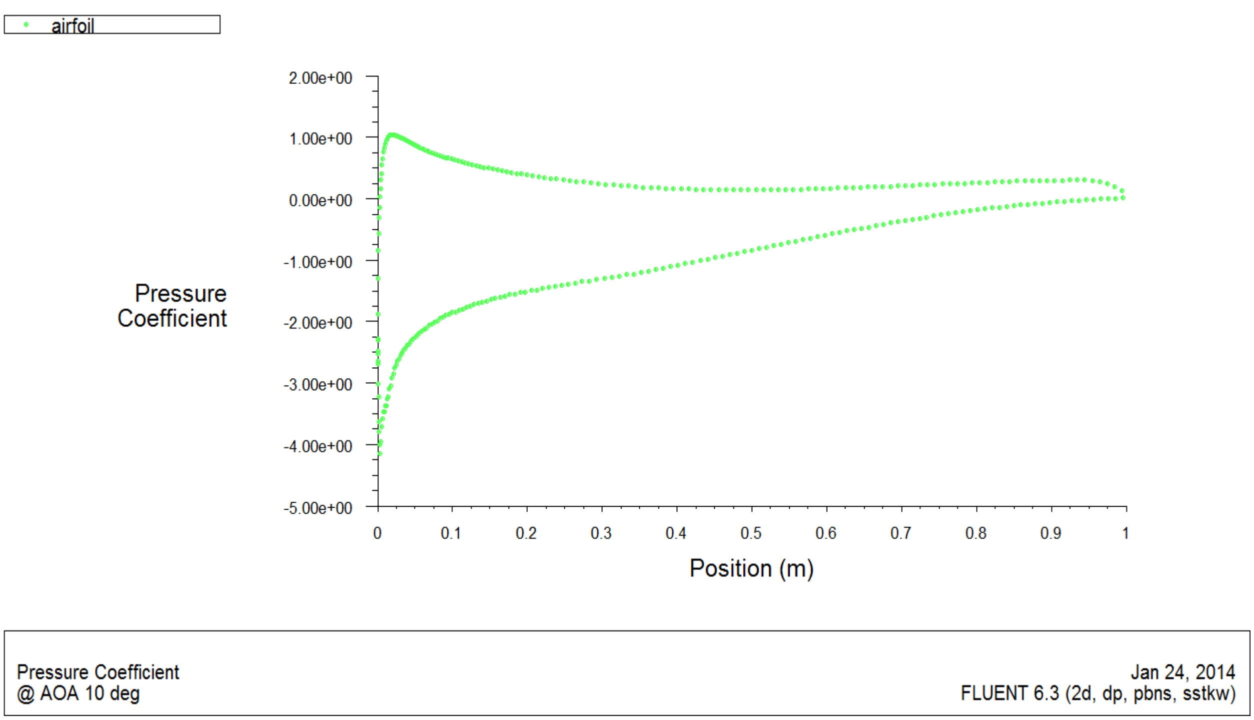

Figure 5-31: Pressure coefficient along the chord line for AOA of 10^0 using SST k- ω model

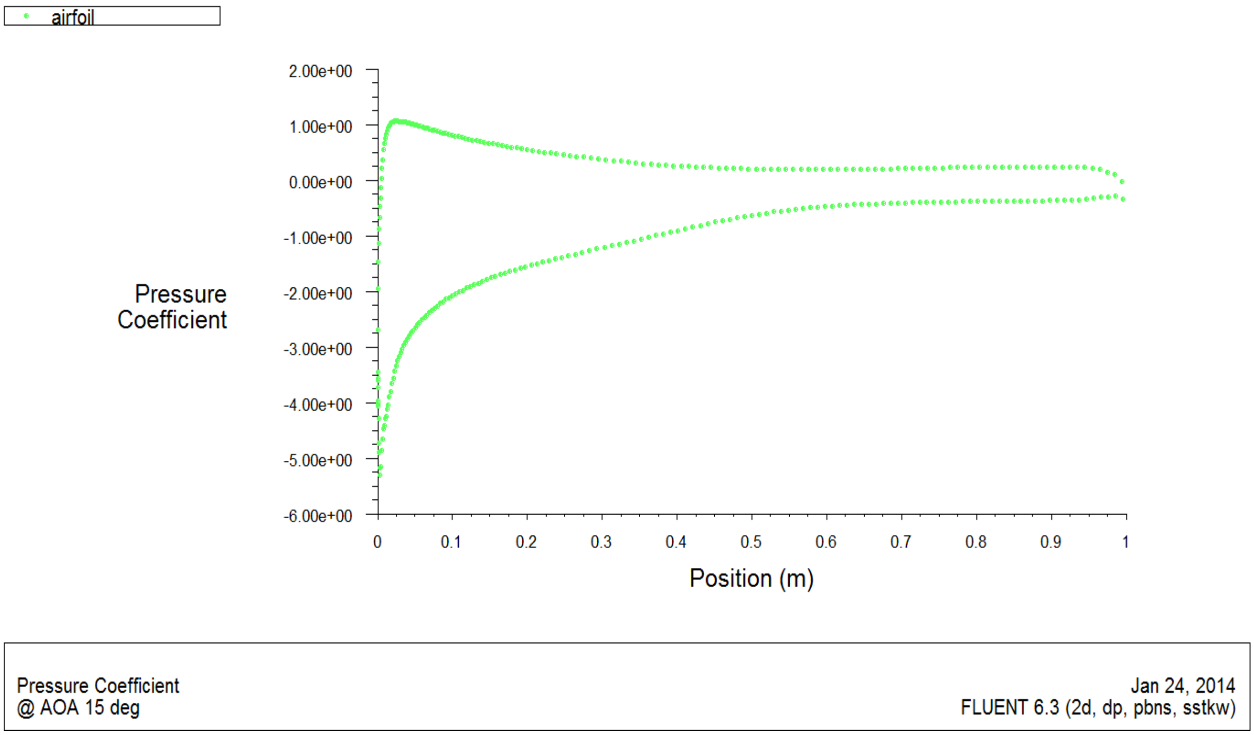

Figure 5-32: Pressure coefficient along the chord line for AOA of 15^0 using SST k- ω model

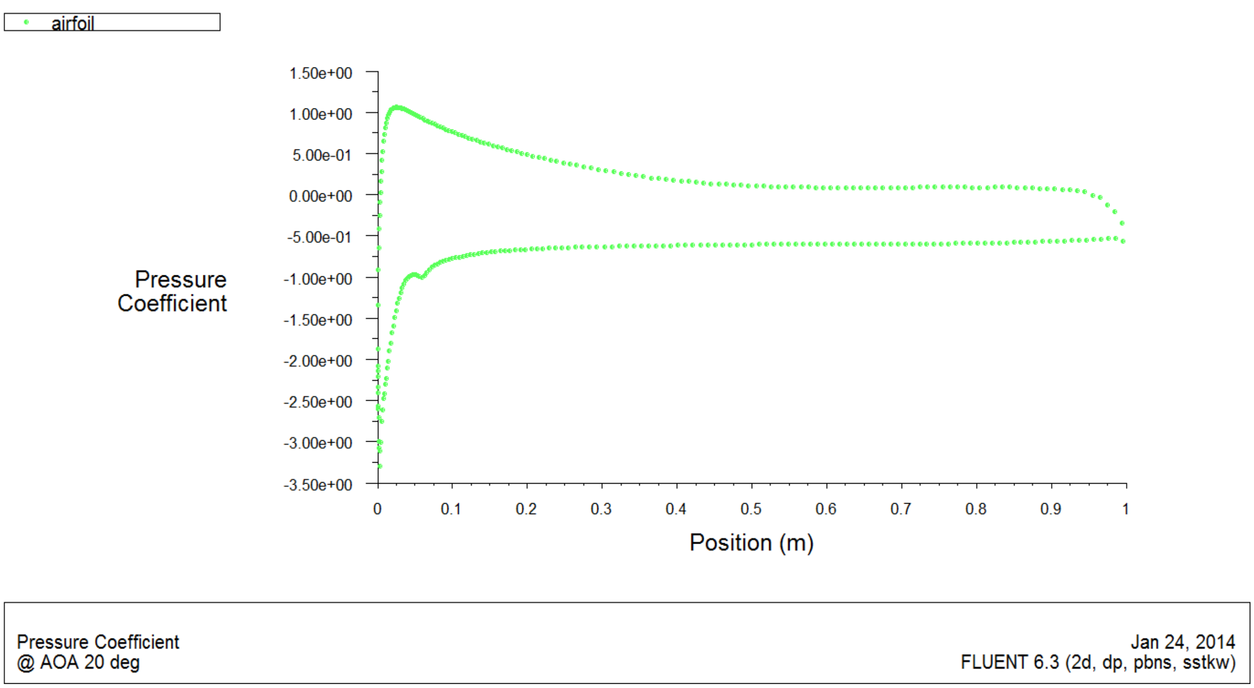

Figure 5- 33: Pressure coefficient along the chord line for AOA of 20^0 using SST k- ω model

5.2.6 The Power Coefficient (C_p) of GW 77/ 1500 Turbine Airfoil

Different wind turbines exist in different sizes. Then once the wind turbine is operating it will experience a wide range of conditions. This variability complicates the comparison of different types of turbines. The coefficient of power is the most important parameters in wind turbine aerodynamics. This parameter is directly related to efficiency, so values between zero and less than one are typical **[48].**

The graph shows a power coefficient curve for GW 77/ 1500 wind turbine. Although the average efficiency for these turbines is somewhat above 30%, the power coefficient varies very much with the wind speed. For this case the power coefficient of the turbine is about 35.3 % at a wind speed of around 9 m/s.

At small wind speed the power coefficient is not so important, because there is not much energy to produce. At high wind speed the turbine must waste any excess energy above what the turbine was designed. Power coefficient therefore matters most at the mean wind speed (9.56 m/s for the Adama) of the turbine where most of the energy is to be generated.

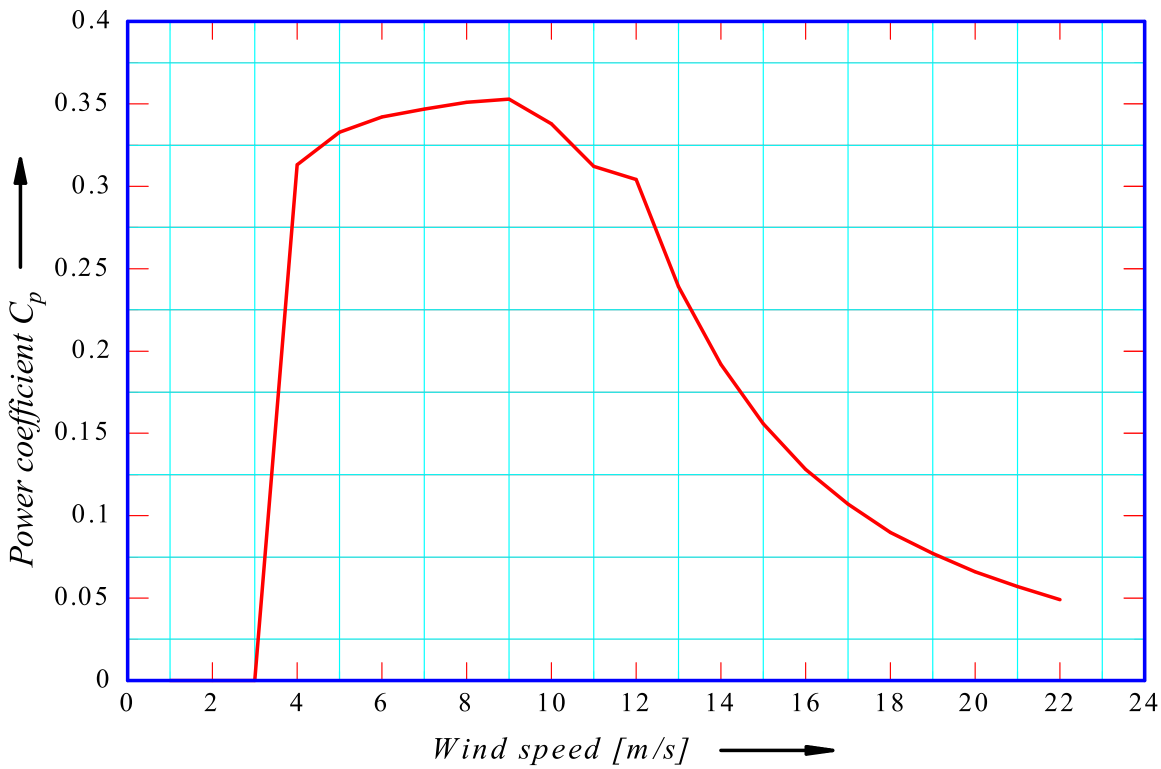

Figure 5- 34: Power Coefficient vs. Wind speed

5.2.7 Power coefficients of blade section as function of C_l/C_d, vs. tip speed ratio (λ)

Once the blade section has been designed for optimum operation at a specific design tip speed ratio, the performance of the rotor over all expected tip speed ratio needs to be determined. For each tip speed ratio, the aerodynamic conditions are predicted. From these, the performance of the total blade section can be determined. The results are usually presented as a graph of power coefficient versus tip speed ratio, called a Cp - λ curve.

Cp - λ curves can be used in wind turbine design to determine the blade power for any combination of wind and rotor speed. They provide immediate information on the maximum rotor power coefficients and optimum tip speed ratio. The data for such a relationship can be found from turbine tests or from modeling. In either case, the results depend on the lift and drag coefficients of the airfoils, which may vary as a function of the flow conditions. Variations in airfoil lift and drag coefficients, which can vary with angle of attack being considered.

The relationship between the power coefficient and the tip speed ration for different Lift to drag coefficient ratio is drawn using this formula.

$$C_{p,max} = \left(\frac{16}{27}\right)\lambda\left[\lambda + \frac{1.32\left(\frac{\lambda-8}{20}\right)^2}{B^2}\right]^{-1} - \frac{(0.57)\lambda^2}{\frac{Cl}{Cd}\left(\lambda+\frac{1}{2B}\right)} \qquad (5.1)$$

The power coefficient starts to increase as the value of tip speed increases and reaches maximum value afterwards starts to decrease as the tip speed ratio further increased. For Cd=0, the power coefficient increase to maximum value and become almost constant afterwards.

As expected, when the lift to drag ratio coefficient (C_l/C_d) becomes smaller, the power coefficient which can be achieved also decreases. When the C_l/C_d ratio and tip-speed ratio are high (C_l/C_d = 22.6), the number of rotor blades (B) has relatively little influence on the achievable Cp value, but when the C_l/C_d ratio and tip-speed ratio are low (C_l/C_d = 8.2), the number of blades apparently is of greater importance.

The effect of the lift to drag ratio on maximum achievable power coefficients for GW77/1500 turbine blade airfoil section is shown in Figure 5- 35. There is clearly a significant reduction in maximum achievable power as the airfoil drag increases. For instance, the NACA 63-415 airfoil has a maximum C_l /C_d ratio **of** 22 at an angle of attack of 5 degree at the mean wind speed of 9.56m/s.

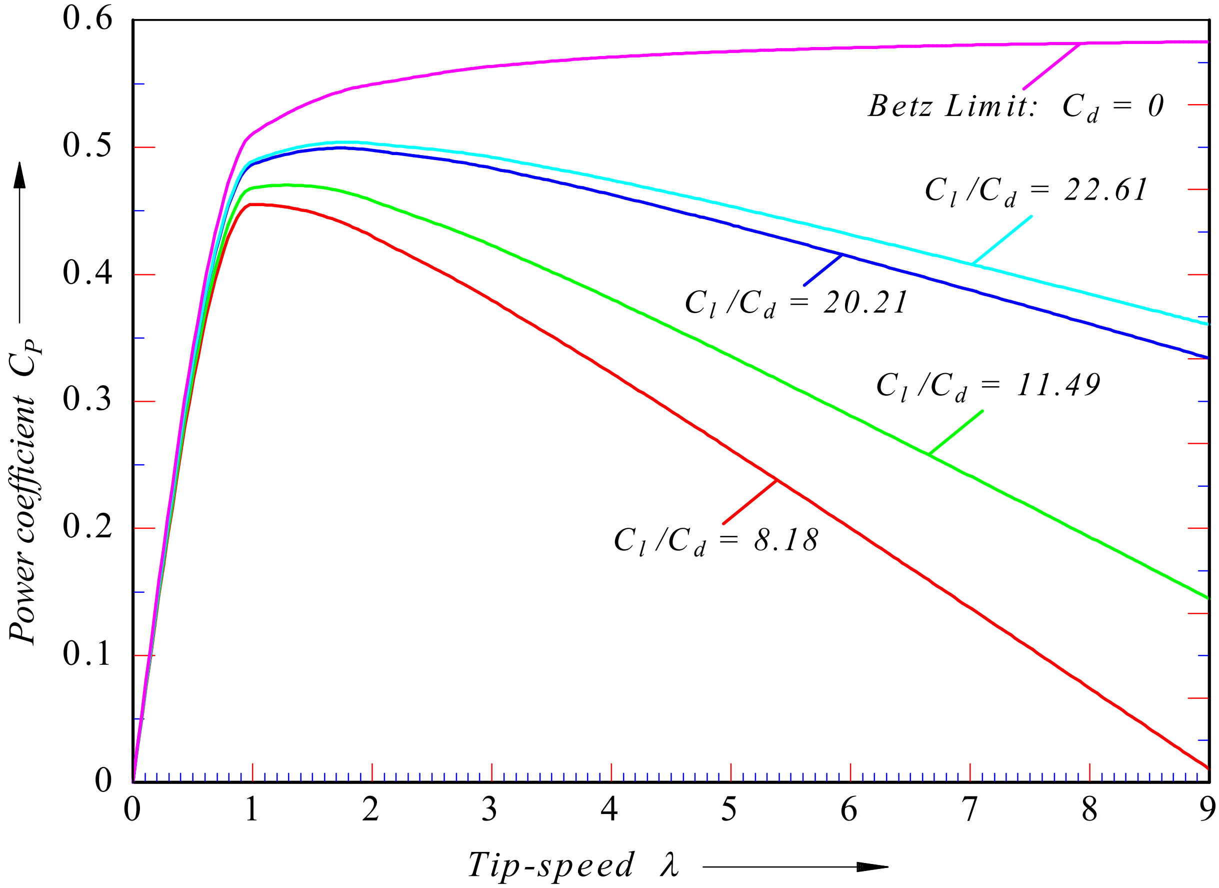

Figure 5- 35: Cp vs. λ as a function of lift to drag ratio

CHAPTER 6

CONCLUSION AND FUTURE WORKS

6.1 Conclusions

From the steps described in Chapter 4 the 2-D model of the airfoil NACA 63-415 was created. The model has generated results which are in good agreement with experimental data when run in FLUENT under the same conditions. This validates the use of a simpler CFD code for analyzing airflow over airfoils instead of the more expensive and time consuming wind tunnel experiment. However in this study it is found that the ability to successfully obtain specific aerodynamic characteristics is highly dependent on modeling the airfoil section in the preprocessor called GAMBIT and selecting appropriate turbulence model in the solver called FLUENT.

The effect of two turbulence models (S-A and SST k- ω) on the prediction of performance parameters and aerodynamic force coefficients on NACA 63-415 airfoil have been studied for a range of angle of attack conditions. It was found that the two turbulence models achieved a reasonable and a good agreement in predicting the coefficients. Among the model studied, the most appropriate turbulence model for these simulations was the SST k- ω two equation model, which is good agreement with the experimental data than S-A one equation model. As a result, it was decided to use the SST k- ω turbulence model for the main analysis.

For lift coefficient, results with less than a 12% deviation were obtained, when compared to experimental data, using both (S-A and SST k- ω) turbulence model in FLUENT, for the angles of attack considered. For the drag coefficient however, comparison of the experimental data with both models revealed, results that have a maximum of 16 % deviation in S-A model and 12 % deviation was found in SST k- ω turbulence model. These deviations are expected in the simulation of drag coefficients; in the actual airfoil, the flow is mostly dominated by laminar flow, whereas the turbulence models in the solver (S-A and SST k- ω) are assumed fully turbulent. Figure 5-1 and Figure 5-2 show a comparison of the FLUENT produced results to the experimental data as well as the variation of the turbulent model results at a given angle of attack for lift and drag coefficients values, respectively.

Comparing the numerical results and experimental data for the force coefficients (lift and drag) values in Figure 5-1 and Figure 5-2, it can be concluded that the CFD solution provides sufficiently accurate results for the majority of the AOAs. The discrepancy in calculating lift and drag values comes from limitations in the turbulence model behavior; the deviation occur at large AOAs. However, majority of the lift and drag curves match the experimental data.

6.2 Future works

In this study, due to limited resources certain issues are not discussed in detailed. This could be considered as an introductory study to illustrate the uses of computational fluid dynamic (CFD) software in simulation of fluid flow over airfoil surface with different turbulent models. Below are listed the future work in this area. This is mainly focused on improving the modeling methods for the HAWT blades and optimization of the geometry of the blade.

CFD modeling gives the possibility to visualize flow phenomena and get more detailed quantitative data of the flow through the turbine blades. Performing CFD simulation of a complete 3D HAWT is also extended as a future work in this area.

Appendix A: Airfoil Coordinates data

Coordinates points of the NACA 63-415 airfoil and chord wise dimensions, x, and thickness dimensions, y, are given in terms of the chord width, C.

Upper Surface		Lower Surface	
x/C	**y/C**	**x/C**	**y/C**
0.000000	0.000000	0.000000	0.000000
0.003000	0.012870	0.007000	-0.010870
0.005250	0.015850	0.009750	-0.013050
0.009910	0.020740	0.015090	-0.016460
0.021980	0.029640	0.028020	-0.022200
0.046600	0.042640	0.053400	-0.030000
0.071470	0.052610	0.078530	-0.035650
0.096470	0.060770	0.103530	-0.040090
0.146690	0.073480	0.153310	-0.046560
0.197050	0.082790	0.202950	-0.050950
0.247500	0.089410	0.252500	-0.053610
0.298000	0.093620	0.302000	-0.054740
0.348520	0.095590	0.351480	-0.054390
0.399050	0.095270	0.400950	-0.052430
0.449550	0.092890	0.450450	-0.049090
0.500000	0.088710	0.500000	-0.044590
0.550390	0.082980	0.549610	-0.039180
0.600700	0.075950	0.599300	-0.033110
0.650930	0.067800	0.649070	-0.026600
0.701060	0.058770	0.698940	-0.019890
0.751090	0.049070	0.748910	-0.013270
0.801020	0.039000	0.799890	-0.007160
0.850850	0.028850	0.849150	-0.001930
0.900590	0.018840	0.899410	0.001840
0.950280	0.009310	0.949720	0.003330
1.000000	0.000000	1.000000	0.000000

Reference

[1] Wei Tong. (2010). *Wind Power Generation and Wind Turbine Design.* Radford, Virginia, USA.

[2] Robert Y. Redlinger. (2002). *Wind Energy in the 21st Century: Economics, Policy, Technology and the Changing Electricity Industry.*

[3] GWEC*, (2012). Global Wind Power Cumulative Capacity*. [Online] available at: <http://en.wikipedia.org/wiki/File:GlobalWindPowerCumulativeCapacity.png>[accessed may 15, 2012].

[4] *"Wind Energy Statistics (2012)" Report.* Global Wind Energy Council. February 2013. Retrieved 11-February-2013.

[5] GWEC. *Global wind energy outlook.* November (2012).

[6] *"Feasibility Study for Ethiopia Adama (Nazret) Wind Park" report*. Hydro china Corporation, (2009).

[7] Kay, A. W. (2010). *Evaluating the Performance of Commercially Available Computational Codes for Determining the Aerodynamic Characteristics of Wind Turbine Airfoils.* University of Strathclyde Engineering.

[8] Ece Sagol, Marcelo Reggio, and Adrian Ilinca,. (2012). Assessment of Two-Equation Turbulence Models and Validation of the Performance Characteristics of an Experimental Wind Turbine by CFD. *International Scholarly Research Network*, *ISRN Mechanical Engineering Volume (2012*), Article ID 428671, 10 pages.

[9] Patel, M. B. (2012). A Review on Aerodynamic Analysis of Wind Turbine Blade Using CFD Technique. *International Journal of Engineering Research & Technology (IJERT) Vol., 1* Issue 10, ISSN: 2278-0181.

[10] Cao, H. (2011). *Aerodynamics Analysis of Small Horizontal Axis Wind Turbine Blades by Using 2D and 3D CFD Modelling.* University of central Lancashire.

[11] Manwell, J.F., Rogers, A.L, McGowan, J.G., (2009). *Wind Energy Explained: Theory, Design and Application,* (2nd Ed.). Amherst.

[12] Hau, E. (2005). *Wind Turbines: Fundamentals, Technologies, Application, Economics.* (2nd Ed.).

[13] Tony Burton, David Sharpe, Nick Jenkins and Ervin Bossanyi. (2001). *Wind Energy Handbook.* Wiley & sons, Ltd.

[14] Jha, A. R. (2011). *Wind turbine technology.* Boca Raton, FL: CRC Press, pp. 9 - 15.

[15] National Research Council. (2007). *"Environmental Impacts of Wind-Energy Projects,"* the U.S. National Academies, the National Academies Press, Washington, D.C, U.S.A.

[16] Douvi C. Eleni, Tsavalos I. Athanasios and Margaris P. Dionissios. (2012 ,March). Evaluation of the Turbulence Models for the Simulation of the Flow over a National Advisory Committee for Aeronautics (NACA) 0012 Airfoil. *Journal of Mechanical Engineering Research Vol. 4(3),* pp. 100-111.

[17] Amit Kumar Saraf, Manvijay Singh, Ajay Kumar. (2012, August). Analysis of the Spalart-Allmaras and k-ω standard models for the simulation of the flow over a National Advisory Committee for Aeronautics (NACA) 4412 airfoil. *International Journal of Scientific & Engineering Research,* Vol *3*(8), ISSN 2229-5518.

[18] Walter P. Wolfe. (1997, September). *Predicting Aerodynamic Characteristics of Typical Wind Turbine Airfoils Using CFD.* SAND96-2345 UC-261.

[19] C. Rajendran. (2010). Aerodynamic Performance Analysis of Horizontal Axis Wind Turbine Using CFD Technique. *European Journal of Scientific Research*, ISSN 1450-216X Vol.65 No.1 (2011), pp. 28-37.

[20] L. X. Zhang, Y. B Lian, X. H. Liu, Q. F. Jiao and J. Guo. (2013). Aerodynamic Performance Prediction of Straight-bladed Vertical Axis Wind Turbine Based on CFD. *Advances in Mechanical Engineering* Volume 2013 (2013), Article ID 905379, 11 pages http://dx.doi.org/10.1155/2013/905379.

[21] Davis, C. J. (2012). *Computational Modelling of Wind Turbine Wake Interactions.* Colorado State University.

[22] *"Basic renewable energy and wind turbines" 2012. http://www.eere.energy.gov/.*

[23] Spera, D. A. (2009). *Wind Turbine Technology: Fundamental Concepts of Wind turbine engineering.* (2nd Ed.).

[24] Arnab Roy., (2012). *A First course on Aerodynamics.* Aps .ISBN 978-87-7681-926-2.

[25] Anil W. (2005). *Introduction to Computational Fluid Dynamics.* Indian Institute of Technology, Bombay.

[26] Sumner, J.; Watters, C.S.; Masson, C. (2010). CFD in Wind Energy: The Virtual, Multiscale Wind Tunnel. *Energies 2010,* 3*, 989-1013.*

[27] Jianping Pan and Eric Loth. (2003). *Effect of Airfoil Geometry on Performance with Simulated Ice Accretions.* Volume 2: numerical investigation .University of Illinois at Urbana-Champaign 104 S. Wright Street Urbana, IL 61801.

[28] M. Senthil Kumar and K. Naveen Kumar. (2013, June). Design and Computational Studies on Plain Flaps. *International Journal of Industrial Engineering and Management Science,* Vol. 3, No. 2.

[29] Spalart, P. R. and Allmaras, S. R., (1992). A One-Equation Turbulence Model for Aerodynamic Flows. *AIAA* Paper 92-0439.

[30] *Fluent 6.2 User's Guide © Fluent Inc., 2005.*

[31] *FLUENT 6.3 User's Guide © Fluent Inc. 2006-09-20.*

[32] Christian Bak, Peter Fuglsang, Niels N. Sørensen, Helge Aagaard Madsen. (1999). *Airfoil Characteristics for Wind Turbines*. Risø-R-1065(EN).

[33] *"Mathematical formulation and turbulence modelling" 2012.* [online] available at: <http://www.innovative-cfd.com/turbulence-models.html> [accessed may 24,2012]

[34] Fernando Villalpando and Marcelo Reggio. Assessment of turbulence models for flow simulation around a wind turbine airfoils. *Advances in Computational Fluid Dynamics and Its Applications.*

[35] Sibly School of Mechanical and Aerospace Engineering. *FLUENT Tutorials – Flow over an Airfoil.* Cornel University. [Online] available at: http://courses.cit.cornell.edu/fluent/index.htm [Accessed June 2013].

[36] Christian Bak, Peter Fuglsang, Jeppe Johansen, Ioannis Antoniou. (2000). *Wind Tunnel Tests of the NACA 63-415 and a Modified NACA 63-415 Airfoils*. Risø National Laboratory, Roskilde, Denmark.

[37] *Anon. UIUC Airfoil Coordinate Database. Available from: http://www.ae.illinois.edu/m-selig/ads/coord_database.html*.

[38] *"Proposal for Engineering, procurement and Construction of Adama Wind farm",* volume 2 technical offer, HYDROCHINA &CGCOC joint venture November, 2009.

[39] M. Senthil Kumar and K. Naveen Kumar. (2013, June). Design and Computational Studies on Plain Flaps. *International Journal of Industrial Engineering and Management Science,* Vol. 3, No. 2.

[40] Md. Hasanuzzaman and Mohammad Mashud. (2013, may 16**)**. Effect of Reynolds Number on Aerodynamic Characteristics of an Airfoil with Flap. *Annals of Pure and Applied Mathematics*, Vol. 3, No. 1, 27-40 ISSN: 2279-087X (P), 2279-0888 (online) www.researchmathsci.org.

[41] S.Kandwal1, Dr. S. Singh. (2012, September). Computational Fluid Dynamics Study of Fluid Flow and Aerodynamic Forces on an Airfoil. *International Journal of Engineering Research & Technology (IJERT)* Vol. 1 Issue 7, ISSN: 2278-0181.

[42] Radermacher, Ryne Derrick. (2012). "*Computational Analysis of a Wing Oscillator*". Western Michigan University: Available at. http://scholarworks.wmich.edu/masters_theses.

[43] Mohammad A. Hossain, Ziaul Huque, Raghava R. Kammalapati, Shubarna Khan. (2013, February). Numeric Investigation of Compressible Flow over NREL Phase VI Airfoil. *International Journal of Engineering Research & Technology (IJERT)* Vol. 2 Issue 2, ISSN: 2278-0181.

[44] W.Z. Wan Omar, M.M.A. Rahim, T. Mat Lazim. (2013). A CFD Study of NACA 63415 with deployment of leading edge and trailing edge surface**,** *2nd International Conference on Mechanical, Automotive and Aerospace Engineering (ICMAAE 2013)*, 2-4 July 2013, Kuala Lumpur.

[45] Ravi.H.C, Madhukeshwara.N, S.Kumarappa. (2013). Numerical Investigation of Flow Transition for NACA-4412 Airfoil Using Computational Fluid Dynamics. *International Journal of Innovative Research in Science, Engineering and Technology* Vol. 2, Issue 7, ISSN: 2319-8753.

[46] Gaurav saxena and Mahendra agrawal. (2013). Aerodynamic analysis of NACA 4412 airfoil using CFD. *International Journal of Emerging Trends in Engineering and Development*. Issue 3, Vol.4, ISSN 2249-6149.

[47] Kevadiya, M. M. (2013, May). CFD Analysis of Pressure Coefficient for NACA 4412. *International Journal of Engineering Trends and Technology (IJETT), Volume 4* (Issue 5).

[48] "*Guided Tour on Wind Energy 2002*". http://www.windpower.org